

Exploration Implications of Multiple Formation Environments of Advanced Argillic Minerals

Jeffrey W. Hedenquist^{1,†} and Antonio Arribas²

¹*Department of Earth and Environmental Sciences, University of Ottawa, Ontario K1N 6N5, Canada*

²*Department of Geological Sciences, The University of Texas at El Paso, Texas 79968, USA*

Abstract

Advanced argillic minerals, as defined, include alunite and anhydrite, aluminosilicates (kaolinite, halloysite, dickite, pyrophyllite, andalusite, zunyite, and topaz), and diaspore. One or more of these minerals form in five distinctly different geologic environments of hydrolytic alteration, with pH 4–5 to <1, most at depths <500 m. (1) Where an intrusion-related hydrothermal system, typical of that associated with porphyry Cu ± Au deposits, evolves to white-mica stability, continued ascent and cooling of the white-mica-stable liquid results in pyrophyllite (± diaspore) becoming stable near the base of the lithocap. (2) A well-understood hypogene environment of formation is vapor condensation near volcanic vents, where magmatic SO₂ and HCl condense into local groundwater to produce H₂SO₄ and HCl-rich solutions with a pH of 1–1.5. Close to isochemical dissolution of the host rock occurs because of the high solubility of Al and Fe hydroxides at pH <2, except for the SiO₂ component, which remains as a siliceous residue because of the relatively low solubility of SiO₂. This residual quartz, commonly with a vuggy texture, is largely barren of metals because of the low metal content in high-temperature but low-pressure volcanic vapor. Rock dissolution causes the pH of the acidic solution to increase, such that alunite and kaolinite (or dickite or pyrophyllite at higher temperatures) become stable, forming a halo to the residual quartz. This initially barren residual quartz, which forms a lithocap horizon where permeable lithologic units are intersected by the feeder structure, may become mineralized if a subsequent white-mica-stable liquid ascends to this level and precipitates copper and gold. (3) Boiling of a hydrothermal liquid generates vapor with CO₂ and H₂S. Where the vapor condenses above the water table, atmospheric O₂ in the vadose (unsaturated) zone causes oxidation of H₂S to sulfuric acid, forming a steam-heated acid-sulfate solution with pH of 2–3. In this environment, kaolinite and alunite form in horizons above the water table at <100°C. Silica derived within the vadose zone will precipitate as amorphous silica at the water table, as the condensate follows the hydraulic gradient, causing opal replacement above and at the aquifer. (4) By contrast, where condensation of this vapor occurs below the water table, the CO₂ in solution forms carbonic acid (H₂CO₃), leading to a pH of 4–5. This marginal carapace of condensate, with temperatures up to 150°–170°C, commonly acts as a diluent of the ascending parental NaCl liquid. This steam-heated liquid forms intermediate argillic alteration of clays, kaolinite, and Fe-Mn carbonates; this kaolinite, which can be present at depths of several hundreds of meters, can potentially be mistaken as having been caused by a steam-heated acid-sulfate or supergene overprint. (5) The final setting is supergene, caused by posthydrothermal weathering and oxidation of mainly pyrite, locally creating pH <1 liquid because of high concentrations of H₂SO₄ within the vadose zone and forming kaolinite, alunite, and Fe oxyhydroxides.

This genetic framework of formation environments of advanced (and intermediate) argillic alteration provides the basis to interpret alteration mineralogy, in combination with alteration textures and morphology plus zonation, including the overprint of one alteration style on another. This framework can be used to help focus exploration for and assessment of hydrothermal ore deposits, including epithermal, porphyry, and volcanic-hosted massive sulfide.

Introduction

Hydrothermal ore deposits are typically characterized in part by a description of the associated alteration minerals. One alteration type, termed “advanced argillic,” occurs in relatively shallow geologic environments where sulfate-bearing and/or aluminosilicate minerals such as alunite, kaolinite, dickite, and pyrophyllite indicate formation by reactive fluids. Advanced argillic alteration was defined by Meyer and Hemley (1967, p. 171), with the term now in wide use to refer to hydrothermal alteration that may include “dickite, kaolinite, pyrophyllite, usually with sericite, quartz, and frequently alunite, pyrite, tourmaline, topaz, zunyite, and amorphous

clays”; sericite¹ is a typically alkali-deficient and silica-rich white mica. Andalusite and corundum may also be included in this association (Hemley et al., 1980). Some of these minerals are also part of other alteration associations², including the kaolinite, dickite, and halloysite clays of the argillic term, as

¹ “The name ‘sericite’ began as a field term to designate fine-grained white mica associated with ore deposits. As such it has survived many attempts to abandon it and redefine it. It probably still has merit as a general designation, though more explicit structural or compositional refinement should be a goal of every study of wall rock alteration where white mica appears as a phase” Meyer and Hemley (1967, p. 172).

² We use the term “association” to refer to a mineral grouping, rather than assemblage, as the latter connotes equilibrium (Einaudi et al., 2003); all minerals included in the term “advanced argillic” are unlikely to occur together, certainly not at equilibrium, as their temperature stabilities (see below) do not all overlap.

[†]Corresponding author: e-mail, jhedenquist@gmail.com

defined by Hemley and Jones (1964) and modified to “intermediate argillic” by Meyer and Hemley (1967). These terms are useful when considering the chemical processes of formation. However, the wide and often cursory use of advanced argillic and other general alteration terms during mapping and logging detracts from the abundant information that the specific mineralogy, coupled with textures and alteration zone morphology, can provide on the environment of formation and the relationship to the location of potential ore.

Hemley and Jones (1964) referred to the process of advanced argillic alteration as advanced hydrolytic decomposition (hydrogen metasomatism) and noted that many occurrences of pyrophyllite and other fine-grained minerals may have been overlooked because of ambiguity of microscopic determination. Since most of these minerals (with hydroxyl or sulfate bonds) are near- and short-wave infrared (NIR-SWIR) active, they can now be reliably identified in the laboratory and field with portable SWIR spectrometers. In part for this reason, the recognition and interpretation of advanced argillic minerals have increased during mineral exploration over the past two decades (Thompson et al., 1999; Simpson and Christie, 2016). This marked increase in readily available information on mineralogy from widespread and varied hydrothermal settings (subaerial to submarine, ~1+ km depth to the surface, and ~350°C to ambient temperature) provides the opportunity to interpret which minerals, assemblages, and associations are diagnostic of and useful for determining the

environment of formation and the relationship of alteration mineralogy to the location of a potential mineral deposit.

Based largely on the early experimental work by J. Julian Hemley, now augmented with the insight from more recent studies of active hydrothermal systems (e.g., Hedenquist et al., 2018), we provide here a field-based interpretive scheme for minerals of hydrolytic alteration, including the advanced and intermediate argillic groups, that form in distinctly different geologic environments, particularly those relevant to the exploration for and assessment of porphyry, epithermal, and related ore deposits (Fig. 1; modified from Sillitoe, 2010). This genetic and spatial framework can be used to confidently interpret alteration assemblages (particularly advanced argillic), textures, and morphologies of distribution, based on geologic observation plus careful use of a 20× hand lens, supported by analytical equipment such as SWIR, to assist exploration efforts as well as studies of alteration mineralogy.

Mineral Stability Framework

Aluminosilicate and sulfate minerals

Several seminal experimental studies relevant to the minerals considered here were conducted by Hemley and coworkers from 1959 through 1992. The catalyst for some of this early research was Hemley's employment with the Anaconda Copper Mining Co. Research Laboratory in the 1960s, which provided him the opportunity to examine mineral assemblages

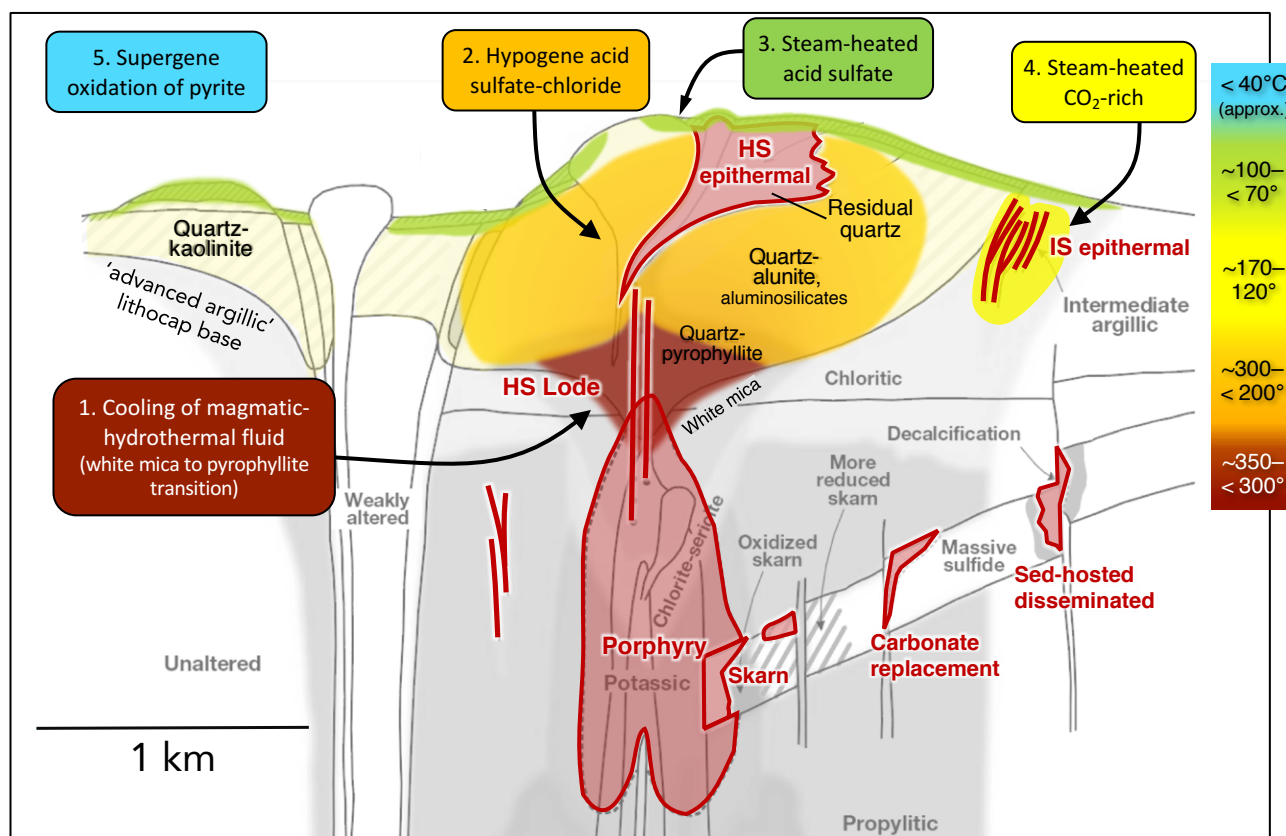


Fig. 1. Schematic porphyry Cu system showing associated ore deposit types (modified from Sillitoe, 2010). The five formation environments of hydrolytic alteration discussed in the text are noted (color coded for later figures), with indicative temperature range. HS = high sulfidation, IS = intermediate sulfidation.

in the field and understand their intimate relationship to ore mineralization (such as muscovite, andalusite, diaspore, and pyrophyllite relationships at the El Salvador porphyry copper deposit in Chile; Gustafson and Hunt, 1975).

Hemley (1959) studied the stability of minerals common in hydrothermal systems, including K-feldspar, white mica, pyrophyllite, and kaolin-group minerals (kaolinite and dickite plus nacrite and halloysite). He recognized that the most important controls on the stability fields of these minerals are the activity ratio of K^+/H^+ and temperature (Fig. 2). These relationships were subsequently refined by Hemley and Jones

(1964), Montoya and Hemley (1975), and Sverjensky et al. (1991). The original kaolin-group and white-mica fields can be divided into kaolinite and dickite, and illite and muscovite, respectively, based on more recent observations of the thermal stabilities of these minerals (Figs. 2, 3). The isochemical transition of kaolinite to dickite in active geothermal systems occurs at about 200°C (Reyes, 1990), consistent with experimental results (Zotov et al., 1998). The white-mica group includes illite and muscovite; illite is deficient in K and Al but has more Si than muscovite (Al/Si 1:1). Higher temperature leads to silica loss (van de Kamp, 2008) and increased

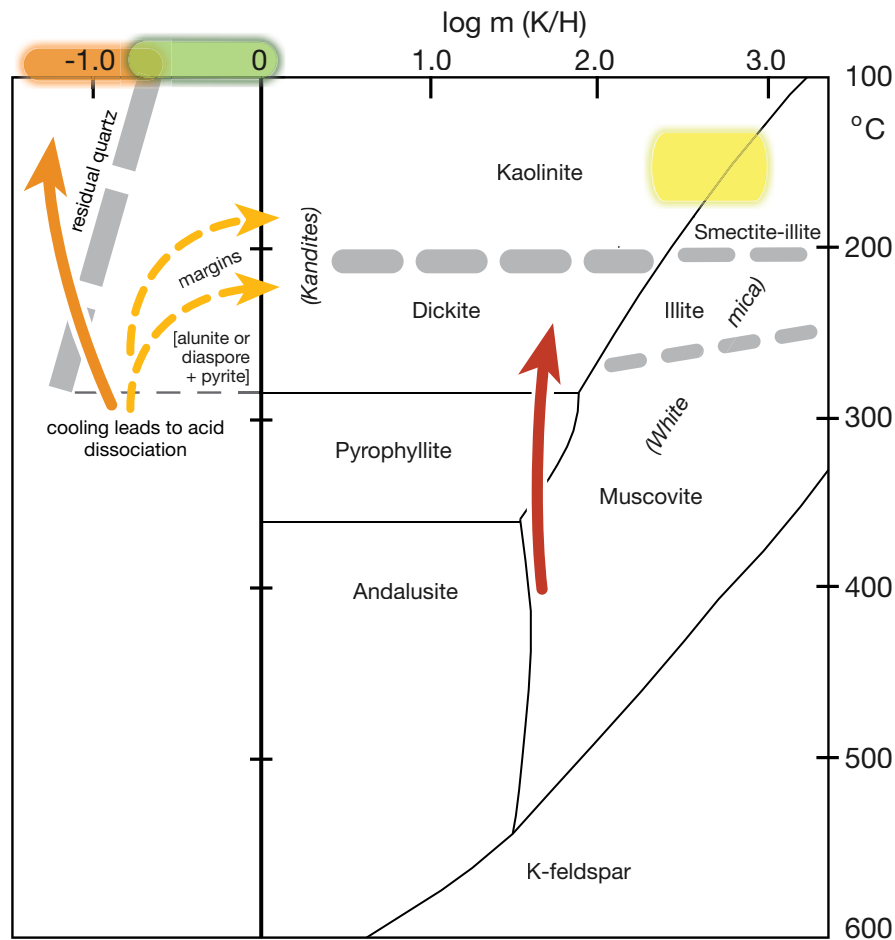


Fig. 2. Temperature versus $\log m (K/H)$ diagram based on experimental results of Hemley and Jones (1964) and Montoya and Hemley (1975), refined by Sverjensky et al. (1991); boundaries at 1 kbar, adjusted to water vapor pressure at $<300^\circ\text{C}$ (K/H consists of $[KCl + K^+]/[HCl + H^+]$). The kaolin group and white-mica fields are divided into dickite and kaolinite, and muscovite and illite, respectively, based on the temperature stabilities from direct observation in active geothermal systems (Reyes, 1990; Reyes et al., 1993). Fluid compositions and pathways for four hydrolytic alteration environments at $\sim 350^\circ\text{C}$ to 100°C are color coded. Cooling path of white mica to pyrophyllite (Fig. 1) noted with red arrow. Left of $\log m (K/H) = 0$, the diagram is schematic, showing the relative position of the field of residual quartz, where Al hydroxide solubility increases sharply at $\text{pH} < 2$ (Stoffregen, 1987). The composition of acidic springs at White Island and Satsuma Iwojima, with evidence for isochemical dissolution of rock (at $\text{pH} 0.3\text{--}1.7$; Hedenquist et al., 1994a; Giggenbach et al., 2003), is shown by orange bar (with reactivity due to both sulfuric and hydrochloric acids). The residual quartz field and the slope of the cooling magmatic vapor condensates (orange arrow) come from modeling of Satsuma Iwojima condensates at high water/rock ratio and high $\text{SO}_2/\text{H}_2\text{S}$ (Hedenquist and Taran, 2013, fig. 3b); slope of the orange arrow will be lower if solution is closer to $\text{SO}_2 = \text{H}_2\text{S}$. Alunite + pyrite are stable at $<300^\circ\text{C}$ at high sulfate/sulfide (Giggenbach, 1992a), whereas diaspore is the aluminous mineral at more reduced conditions and low sulfate concentrations. The composition of steam-heated acid-sulfate springs at Waioatapu ($\text{pH} 2.0\text{--}2.8$; Hedenquist, 1991) and Yellowstone ($\text{pH} 1.4\text{--}4$; Nordstrom et al., 2009) noted by green bar (with reactivity due to sulfuric acid), locally sufficient to mobilize aluminum (see text). The composition of CO_2 -rich steam-heated fluid sampled at 350- to 850-m depth from wells on the margin of the Ohaaki-Broadlands geothermal system (Hedenquist, 1990, table 5), plotted at measured temperatures ($\sim 120^\circ\text{--}170^\circ\text{C}$; yellow field); reactivity is due to carbonic acid, and alteration products are clays and kaolinite.

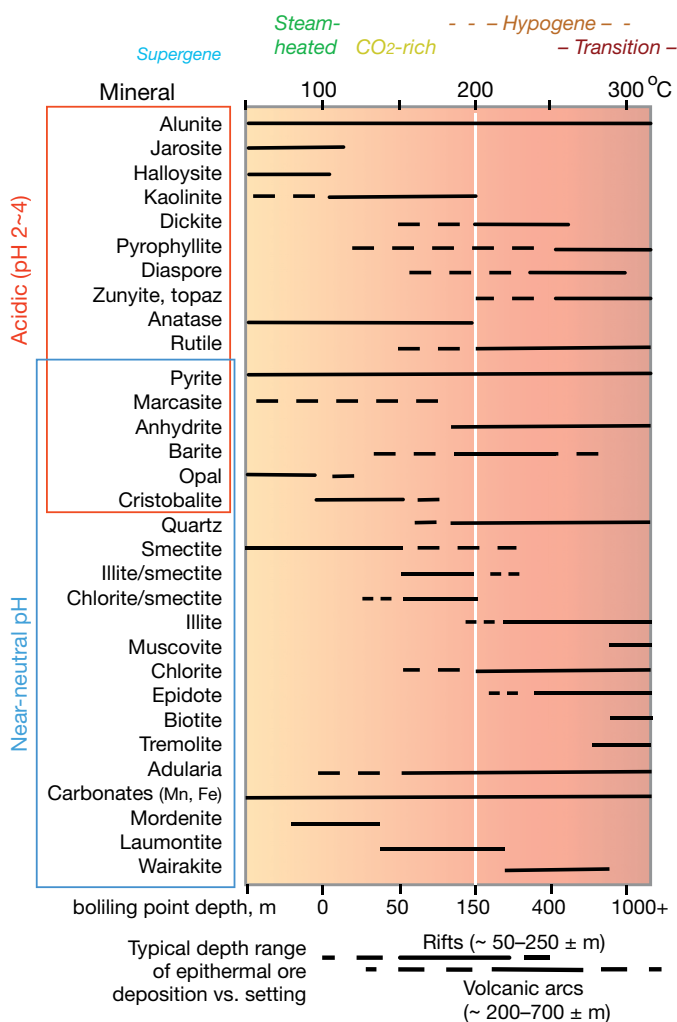


Fig. 3. Temperature stability of minerals typical of epithermal deposits, based largely on observations in active geothermal systems, where present temperatures are measured (Browne, 1978; Henley and Ellis, 1983; Reyes, 1990). The dashed lines refer to observations of minerals present at a wider range of temperature, typically lower, due to either (1) cooling of system but preservation of higher-temperature assemblage or (2) aluminosilicates stable at lower temperature where silica solubility is controlled by a phase that is less ordered than quartz (see Hemley et al., 1980). Although alunite forms over a wide temperature range (from supergene to ~300°C), its composition is temperature dependent, e.g., K rich versus Na rich at lower and higher temperature, respectively (Stoffregen and Cygan, 1990; Chang et al., 2011). The boiling point depth refers to hydrostatic conditions of saturated water-vapor pressure for a low-CO₂ system. Systems with higher CO₂ concentrations will boil at greater depths for the same temperature (e.g., ~1,350-m depth for a 300°C liquid with ~0.6 wt % dissolved CO₂, such as at Ohaaki, NZ, 300+ m deeper than the boiling point for pure H₂O; Hedenquist, 1990). The typical formation depth of epithermal ore zones in rifts is less than that in volcanic arcs, and the vertical range of ore grade also tends to be less (Hedenquist et al., 2000; Sillitoe and Hedenquist, 2003).

crystallinity, with progressive conversion of illite to muscovite up to about 280°–300°C (Reyes et al., 1993; Merriman and Frey, 1999; A. Reyes, pers. commun., 2019), based on observations from active geothermal systems and burial diagenesis.

Cooling of a high-temperature hydrothermal fluid, initially in equilibrium with K-feldspar, results in it eventually becoming stable with respect to white mica (red path; Fig. 2). If the K⁺/H⁺ value is sufficiently low, the composition may trace the

white-mica-andalusite curve, consistent with mineral assemblages observed in some porphyry deposits (e.g., El Salvador and Batu Hijau, Indonesia; Gustafson and Hunt, 1975; Garwin, 2002). Further cooling results in pyrophyllite becoming stable at ~350°C at hydrostatic pressure (i.e., P_{H₂O}, on the vapor-liquid curve; Hemley et al., 1980), and at <300°C kaolin-group minerals become stable, initially dickite (Fig. 2).

Hemley et al. (1980) examined minerals in the aluminosilicate system, including kaolinite (and dickite), pyrophyllite, diaspore, andalusite, and corundum, as a function of temperature and the concentration of silica in solution. A cooling (retrograde) pathway at quartz saturation shifts from andalusite to pyrophyllite and eventually to kaolin-group stability (the latter transition occurs at about 260°C, where dickite is the stable polymorph; Fig. 4). Where quartz solubility is exceeded, cristobalite (Fournier and Rowe, 1962) or even amorphous silica (Gunnarsson and Arnórsson, 2000) solubility may be attained; under such conditions, pyrophyllite can coexist with kaolin-group minerals at lower temperature (Fig. 4). In addition, Hemley et al. (1980) observed that by adding fluoride as well as chloride to the system, zunyite or topaz (Seedorff et al., 2005) may be produced, and with boron added, dumortierite or tourmaline become stable. With sulfate in the system (and a supply of cations from feldspar hydrolysis), alunite or anhydrite are typically stable—anhydrite at a lower pH than alunite (Hedenquist and Taran, 2013).

The stability of alunite was studied by Hemley et al. (1969) and required an examination of the aqueous sulfate as well as the K⁺ and H⁺ concentrations. As they noted, “The experimentally determined phase relations ... constitute a useful frame of reference with regard to the character and compositional limits of natural hydrothermal fluids” (Hemley et al., 1969, p. 610). The results of their experiments agreed with observations made on natural systems, where an increase in the activity products of H⁺ and SO₄²⁻ results in mineral stability shifting from K-feldspar to white mica (muscovite or illite) to kaolin group (dickite or kaolinite) and finally to alunite (Fig. 5); after complete cation leaching of the rock-forming minerals, only a siliceous residue remains. At a higher K⁺ activity (and likely higher temperature; Hemley et al., 1969), white mica can coexist with alunite.

Aluminum solubility, as Al(OH)₃, progressively increases as pH decreases (Stoffregen, 1987); at 250°C and a pH ~2, the predicted aluminum concentration in solution exceeds 1,000 ppm, whereas the dissolved aluminum will be a maximum of a few tens of parts per million at pH ~3. These values can be compared to those of magmatic vapor condensates, such as at White Island, New Zealand, and Satsuma Iwojima, Japan, where hyperacidic springs (pH <1.5) discharge from the flanks of these andesitic and rhyolitic volcanoes, respectively (Fig. 6). White Island hot springs discharge at 80°–99°C with a pH of 0.8–1.3 and contain up to 1,600 ppm Al and 5,000 ppm Fe; the Al and K contents in solution are somewhat depleted from those expected for isochemical rock dissolution, possibly due to fixation by alunite at depth (Giggenbach et al., 2003). Giggenbach and Glasby (1977) noted that precipitates of metal hydroxide from acidic streams entering the ocean from White Island have an overall composition approximating isochemical dissolution of andesite (except for silica). Satsuma Iwojima fumaroles discharge at a temperature of

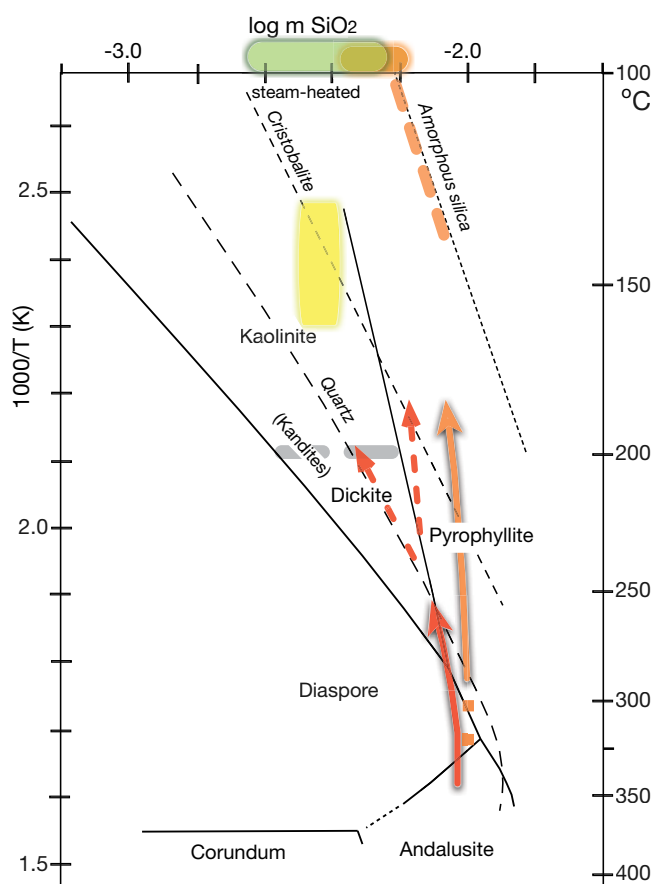


Fig. 4. Stability relationships in the system $\text{Al}_2\text{O}_3\text{-SiO}_2\text{-H}_2\text{O}$ at saturated liquid-vapor pressure, from Hemley et al. (1980); cristobalite and amorphous silica curves from Fournier and Rowe (1962) and Gunnarsson and Arnórsson (2000), respectively. Dickite-kaolinite transition based on stability of kaolinite-group minerals in active geothermal systems (Reyes, 1990). The red path is that of a high-temperature fluid cooling from muscovite (\pm andalusite) stability (Fig. 2), i.e., postpotassic alteration (e.g., El Salvador and Batu Hijau porphyry Cu deposits; Gustafson and Hunt, 1975; Garwin, 2002) to either pyrophyllite or dickite stability below $\sim 320^\circ$ and $\sim 260^\circ\text{C}$, respectively, following quartz solubility. Cooling of this potentially mineralizing fluid (Hedenquist et al., 1998) may continue to follow the path of quartz solubility, whereas a sharp decrease in temperature will result in silica solubility exceeding that of quartz, as evidenced by the presence of chalcedony and amorphous silica gel (see below) associated with overlying epithermal ore (two possible paths noted with red dashed lines). Orange path marks cooling on the margin of a zone of residual quartz, formed by an acidic condensate of hypogene (volcanic) vapors (Fig. 2; Hedenquist et al., 1994a; Giggenbach et al., 2003) during the initial stage of porphyry formation (synpotassic at depth; Hedenquist et al., 1998). On sharp cooling, the silica composition can increase to that of amorphous silica (orange dashed line), as evidenced by the composition of acidic discharges at the surface and the laminated colloidal silica gel in associated acidic crater lakes (Fig. 6d). The composition of CO_2 -rich steam-heated fluid sampled at 350- to 850-m depth from the Ohaaki-Broadlands geothermal system (Hedenquist, 1990) is plotted at the measured temperatures ($130^\circ\text{--}170^\circ\text{C}$; yellow field). The green line at $\leq 100^\circ\text{C}$ reflects the composition of steam-heated acid-sulfate solutions with nil Cl formed above the water table (Hedenquist, 1991; Nordstrom et al., 2009; color code similar to Fig. 1).

$\leq 880^\circ\text{C}$ with ~ 1 mol % total S species ($\text{SO}_2/\text{H}_2\text{S} \sim 5:1$) and 0.5 mol % each HCl and H_2 (Shinohara et al., 1993, 2002). After part of these vapors condenses into meteoric water near the summit, the reactive solution thus formed discharges from the lower flanks of the volcano at $42^\circ\text{--}71^\circ\text{C}$ with a pH 1.1–1.8. These hot springs contain up to 1,440 ppm Al and 370 ppm

Fe, with average values indicating isochemical dissolution of the rhyolitic host rock (Hedenquist et al., 1994a), again except for silica, as observed at White Island.

These results are consistent with the predictions by Stoffregen (1987) of appreciable $\text{Al}(\text{OH})^{2+}$ concentrations in solution at $\text{pH} \leq 2$ due to the dissolution of aluminosilicates and alunite, leaving a siliceous residue. Similar results were indicated by modeling the Satsuma Iwojima fumarolic condensates; alunite is calculated to be stable at $250^\circ\text{--}300^\circ\text{C}$, whereas only siliceous residue, plus anhydrite and pyrite, is stable at $<250^\circ\text{C}$ (Hedenquist and Taran, 2013). The dissolution of the rock is caused by the progressive dissociation of sulfuric and hydrochloric acids upon cooling, which results in more reactive solutions at lower temperature (Hemley et al., 1980; Brimhall and Ghiorso, 1983; Giggenbach, 1987, 1997; Hedenquist and Taran, 2013). This accounts for the upward flare of zones of siliceous residue, referred to as residual quartz, as first noted at Summitville, Colorado (Steven and Ratté, 1960; Stoffregen, 1987).

Silica minerals

Polymorphs of silica include quartz, tridymite, and cristobalite, in order of solubility increase at a given temperature (Fig. 4; Fournier, 1985); chalcedony is cryptocrystalline (microcrystalline) quartz. Opal-CT is a hydrous silica polymorph that is now thought to be a paracrystalline mixture of noncrystalline amorphous silica (opal-A) along with variable amounts of crystalline tridymite \pm cristobalite; diagenesis can result in a transformation of opal-A to opal-CT to quartz (Wilson, 2014).

Meyer and Hemley (1967, p. 172) noted that advanced argillic alteration “represents extreme hydrolytic base-leaching from all aluminous phases, including the K-Al micas. But it is present only where alumina is not appreciably mobilized, grading into silicification (or simply hydrothermal leaching) where the alumina itself is extracted by vein solutions.” These authors included residual quartz (recrystallized from amorphous siliceous residue in the rock) in their silicification category, i.e., residual quartz is not part of their definition of advanced argillic. However, we prefer to reserve use of the term “silicification” for silica deposition from solution, either as replacement or in a fracture, distinct from silica residue that is left behind after leaching.

After most components have been leached from the host rhyolite by acid-sulfate-chloride fumarole condensates at Satsuma Iwojima (Hedenquist and Taran, 2013), the silica residue is present as tridymite and cristobalite (with variable but minor quartz) within the fumarolic crater, whereas the altered flanks of the volcano report mainly cristobalite (Hamasaki, 2002). Similarly, the local silica residue associated with steam-heated acid-sulfate springs at Yellowstone is tridymite and cristobalite (Fournier, 1985). Well-crystallized tridymite has a lower silica solubility than cristobalite, near that of chalcedony, with both between that of quartz and cristobalite; the hydrated and less ordered opal-CT has a higher solubility, between that of cristobalite and amorphous silica (Fig. 6; Fournier, 1985). As these polymorphs order and are dehydrated, they recrystallize to either chalcedony or quartz.

By contrast to residual material, silica precipitation from solution—as replacement (silicification) or deposition in open spaces—typically forms quartz at temperature above $\sim 180^\circ\text{C}$,

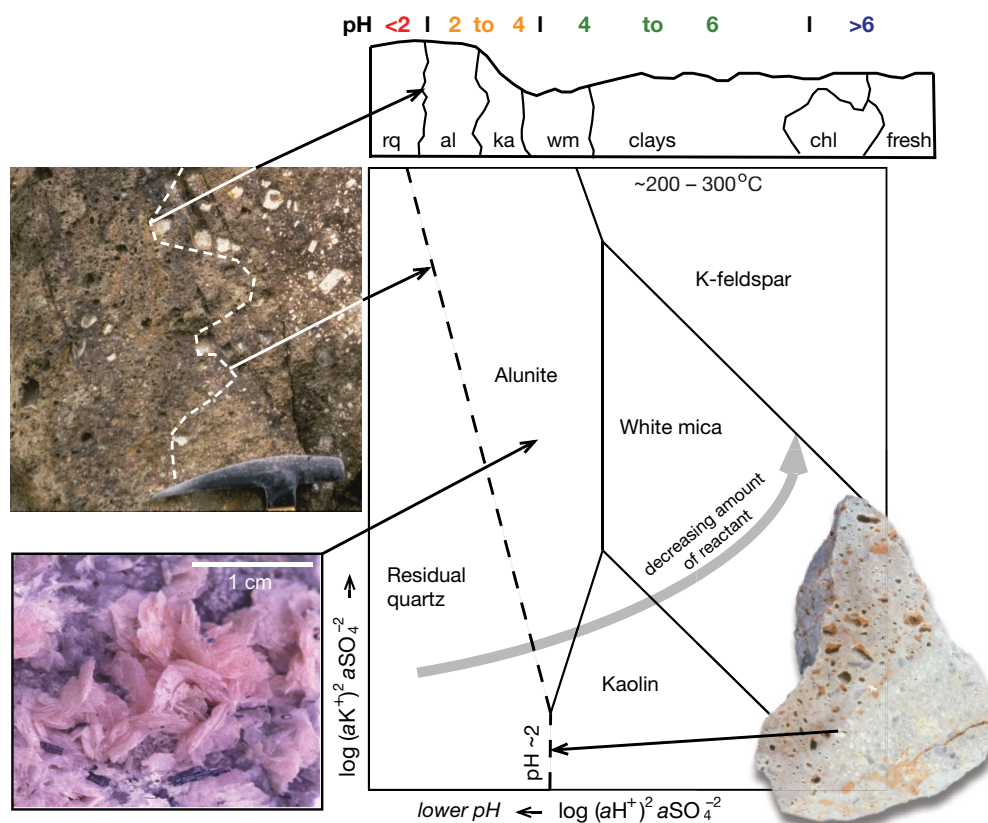


Fig. 5. Stability of alunite and related minerals as a function of H_2SO_4 and K_2SO_4 activities, at $\sim 200\text{--}300^\circ\text{C}$; kaolin minerals (kaolinite or dickite) replaced by pyrophyllite at higher temperature (modified from Hemley et al., 1969). Field of residual quartz (strongest hydrolytic leaching) from Stoffregen (1987); size of field depends on Al^{+3} concentration in solution. Inset photographs: Upper left: contact between vuggy-textured (after feldspar phenocrysts) residual quartz (left) with quartz-alunite (right); photograph by C.G. Cunningham. Lower left: coarse pink hypogene alunite, Tambo mine, Chile. Lower right: contact between residual vuggy quartz and quartz-kaolinite, Rodalquilar. Top: alteration zonation from core of residual quartz (rq), outward to alunite (al), kaolinite-group mineral (ka; kaolinite or dickite), white mica (wm; illite) to clays (illite-smectite), to chlorite (chl) and fresh rock (from Steven and Ratté, 1960). The pH values are based on relative stability of alteration minerals; formation of residual quartz requires $\text{pH} < 2$ at 250°C , based on solubility of aluminum species (Stoffregen, 1987).

whereas chalcedony forms below $\sim 140\text{--}180^\circ\text{C}$ (Fournier, 1985). At the surface, amorphous silica forms sinters around near-neutral pH hot springs, and with time this material crystallizes to quartz or chalcedony, with opal-CT or cristobalite as an intermediate phase (Fournier, 1985). However, at pH less than ~ 4 , hydrogen ions inhibit silica polymerization (Fournier, 1985), leading to dissolved silica remaining in solution during cooling until amorphous silica saturation is attained, at which point amorphous silica colloids form. Such colloids may then form a gel and deposit (see below).

Sulfides

Following the oxidation state concept as applied to ore deposits by Dick Holland (1959), Paul Barton and Pete Toulmin discussed a similar framework for sulfide minerals involving f_{S_2} (P.B. Barton, pers. commun., 2009), to allow quantification of the sulfide mineral paragenesis and zonation observed at Butte (Sales and Meyer, 1949). The sulfidation state of a sulfide mineral assemblage is a function of both f_{S_2} and temperature (Fig. 7; Barton and Skinner, 1979). Barton (1970) suggested a main line evolution toward higher sulfidation state with decreasing temperature, regardless of hydrothermal ore environments. Following on, Einaudi et al. (2003) added the

compositions of fluids sampled from active hydrothermal systems to this framework, including high-temperature volcanic vapors and their acidic condensates as well as neutral-pH geothermal solutions, and integrated these observations with those made in the porphyry and epithermal ore-forming environments. They noted that, in contrast to the suggested main line evolution of sulfidation state increase at lower temperature, sulfide assemblages typically shift back toward lower sulfidation state at lower temperature (below $\sim 250\text{--}300^\circ\text{C}$), as first noted by Meyer and Hemley (1967).

This shift toward lower sulfidation states is likely caused by the influence of the rock (Fe silicate) buffer (Giggenbach, 1987; Einaudi et al., 2003) at lower temperature. By contrast, there is no rock buffer associated with residual quartz, since all Fe silicates have been dissolved, which allows high to very high sulfidation-state sulfides (i.e., enargite and covellite, respectively) to form simply because of cooling of the sulfide-precipitating liquid during ascent (Einaudi et al., 2003, fig. 7). This explains the observation at Summitville of the transition from tennantite to enargite stability at shallower depths (Steven and Ratté, 1960). For this reason, the main hosts to high-sulfidation-state sulfides at epithermal depths are residual quartz lithocaps and related alteration (Sillitoe,



Fig. 6. a) View over Satsuma Iwojima rhyolite dome in 1996, Japan (photograph, Y. Kawanabe), with high-temperature hypogene vapors passively degassing from a shallow magma (Shinohara et al., 2008); alteration near summit includes cristobalite and alunite, with Au anomalies of <2 ppb Au (20 of 21 samples, with one containing 29 ppb Au; Hamasaki, 2002). Vapor condensates discharge as acidic springs, pH 1.1–1.7, along shoreline (Hedenquist et al., 1994a), with metal hydroxide flocculants forming in the ocean. b) W.F. Giggenbach examines residual quartz products of leaching at the summit. c) White Island andesitic stratovolcano in 2009, New Zealand (photograph, S.F. Simmons); acidic crater lake (pH ~0.2) overflows (pH 0.6 stream) to the ocean, forming similar metal hydroxide plumes as seen at Satsuma Iwojima. The color of the acidic lake is due to suspended silica colloids, which settle out of suspension to form d) finely laminated colloidal silica deposits, mud-cracked where exposed. e) White Island crater in 1984 during a period of hypogene vapor discharge in the inner crater, up to 760 °C, including SO₂, HCl, CO₂, and H₂S. View to the northwest (white arrow in c) over from the margin toward the inner crater. Foreground is the Blue Pool, a steam-heated feature at 99 °C, and on far slope, fumarole at 106 °C (designated WA by Giggenbach, 1987, and designated 1 by Giggenbach et al., 2003), with CO₂ and reduced sulfur species (H₂S) in the aqueous vapor. f) Alteration of the Summitville deposit, Colorado; residual quartz, vuggy textured (top), and quartz-alunite (bottom), formed in the environment illustrated by Satsuma Iwojima and White Island.

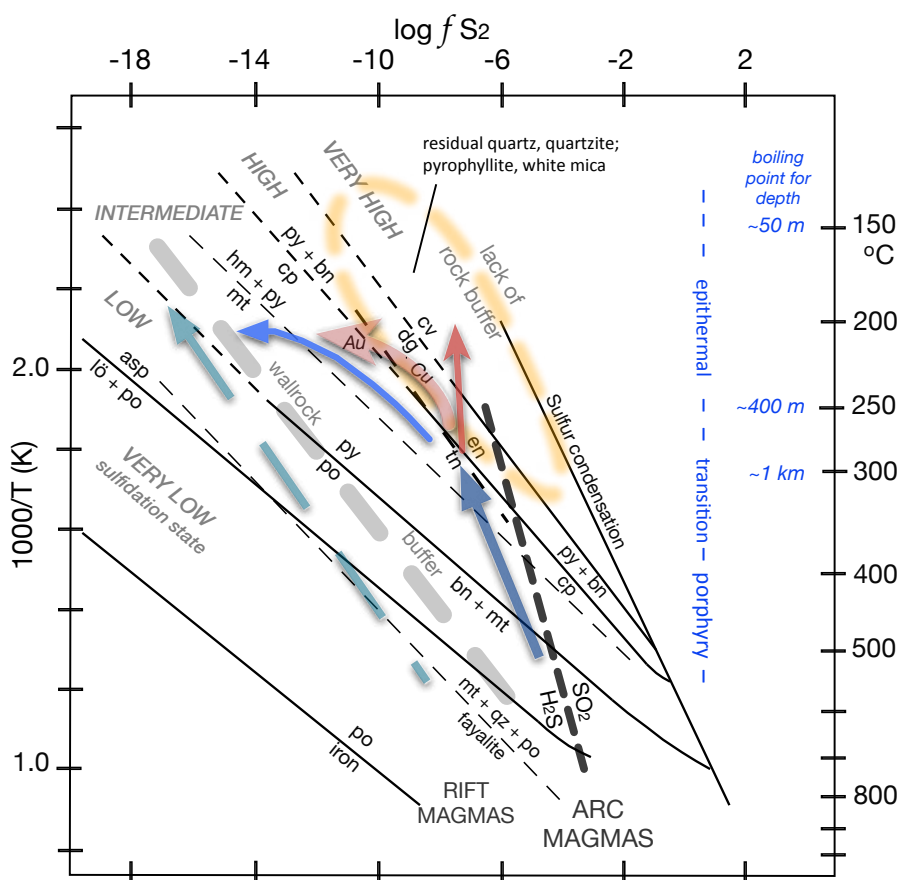


Fig. 7. Temperature versus $\log f_{S_2}$, with relative sulfidation states of various sulfide (and sulfide + oxide) assemblages (based on calculations by Barton and Skinner, 1979; modified by Einaudi et al., 2003). The Fe silicate rock buffer (gray dashed line) and the S gas buffer, at SO_2/H_2S equivalence (dark dashed line), are from Giggenbach, 1987; both coincide at the temperature and composition of typical arc magmas and act as envelopes of most hydrothermal fluids and their minerals (Einaudi et al., 2003); rift magmas are more reduced and have lower sulfidation state. Where rock is strongly leached to residual quartz (hypogene acid fluids, orange dashed field; Fig. 2), there is no rock buffer capacity remaining; cooling of a muscovite-stable magmatic-hydrothermal fluid results in evolution to higher sulfidation states, to enargite and eventually covellite and potentially S^0 (red arrow); where fluid reacts with the rock buffer, assemblage returns to intermediate-sulfidation state, and is observed to shift from Cu to largely Au deposition (light-red arrow; Hedenquist et al., 1998). By contrast, the mineralogy of many hydrothermal systems remains within the field of intermediate-sulfidation state because of interaction with the rock buffer at epithermal temperatures (dark-blue arrow; Einaudi et al., 2003). Low-sulfidation-state fluids approximate the wall-rock buffer trend (light-blue trend), with reactive fluids at depth having undergone primary neutralization (Giggenbach, 1992a, 1997). Depth scale to ~1 km based on temperature at water vapor pressure for hydrostatic conditions. Abbreviations: asp = arsenopyrite, bn = bornite, cp = chalcopyrite, cv = covellite, dg = digenite, en = enargite, hm = hematite, lö = loellinite, mt = magnetite, po = pyrrhotite, py = pyrite, qz = quartz, tn = tennantite.

1999), referred to as “secondary quartzite” in the Russian literature (Nakovnik, 1934, 1968), as well as the true sedimentary equivalent, quartzite (e.g., Bingham Canyon, Utah, Inan and Einaudi, 2002; Lagunas Norte, Peru, Cerpa et al., 2013). Similarly, cooling in the absence of the rock buffer in the upper parts of porphyry-type deposits causes the upward change from chalcopyrite + pyrite to dominantly enargite or other high-sulfidation-state sulfides in zones of white-mica and/or pyrophyllite alteration or where hosted by large quartz veins that lack a rock-buffer mineralogy (Gustafson and Hunt, 1975; Brimhall and Ghiorso, 1983).

Formation Environments of Hydrolytic Alteration

Over a century ago, Ransome (1907, 1909) discussed multiple genetic environments for the alunite-kaolinite-gold association that he observed at the Goldfield, Nevada, epithermal

deposit, including “emanations from crystallizing magma” (i.e., a magmatic hypogene origin; Ransome, 1907, p. 691), “simultaneous solfatarism and oxidation” (steam-heated acid-sulfate origin; Ransome, 1909, p. 196), and “product of the weathering or oxidation of pyrite” (supergene origin; Ransome, 1909, p. 125). The stable isotopic signatures of these three environments of acid generation were eventually studied by Rye et al. (1992), with ore deposit examples of each. Based on their experimental insight, Hemley and Jones (1964, p. 564) observed that “solutions of low cation/ H^+ ratios are generated in meteoric waters by the oxidation of pyrite and H_2S , and by the influx of juvenile gases”—i.e., supergene, steam-heated acid-sulfate, and magmatic hypogene environments, respectively. Where juvenile volatiles “of potential acid reaction” are fractionated at shallow levels, their incorporation into “ground waters could produce with time a solution of

very low cation/H⁺ ratio" (p. 565), a topic that had been previously discussed by Burbank (1950) and White (1957). Subsequently, Hemley et al. (1980) stressed the effect of cooling on the generation of pyrophyllite and other aluminosilicate minerals.

Here we examine five genetic environments of hydrolytic alteration, each directly relevant to the understanding of and exploration for porphyry copper, epithermal precious-metal and related deposits (Fig. 1):

1. Cooling of white-mica-stable fluid: As noted above (Fig. 2), the typical intrusion-related hydrothermal fluid in intermediate-composition calc-alkaline magmatic arcs traverses the K-feldspar and muscovite fields; below ~350°C, cooling leads to increased reactivity and a shift to pyrophyllite (\pm diaspore) stability (Hemley et al., 1980; Watanabe and Hedenquist, 2001). This environment of alteration is common in the upper parts and above porphyry copper deposits (Hedenquist et al., 1998; Sillitoe, 1999, 2010), with pyrophyllite \pm diaspore being increasingly recognized with the wider application of SWIR measurements.
2. Hypogene acid-sulfate-chloride condensate: Hyperacidic solutions form from condensation of high-temperature (~300°–800+°C) aqueous vapor, rich in SO₂ and HCl, of hypogene origin (Ransome, 1907; Steven and Ratté, 1960; Giggenbach, 1987). The resultant solution may attain a pH \leq 1 at temperatures <250°–300°C (Hedenquist and Taran, 2013). Under these conditions the condensate leaches most rock-forming components except for silica (and Zr, Ti), leaving behind a siliceous residue that is largely barren of metals on formation. This residue typically has a halo of quartz-alunite and aluminosilicate minerals (Fig. 5), all part of the lithocap environment (Sillitoe, 1995a, 1999).
3. Steam-heated acid-sulfate condensate: Fumarolic discharges of CO₂- and H₂S-bearing aqueous vapor from hydrothermal systems are generated by boiling of ascending liquid, since volatile species fractionate to the vapor phase (Giggenbach, 1980). If this vapor condenses within the vadose (unsaturated) zone above the water table, much of the H₂S is oxidized at temperatures below ~100°C by atmospheric O₂ to form steam-heated acid-sulfate liquid (Steiner, 1953; Steiner and Rafter, 1966; Schoen et al., 1974), commonly involving microbial mediation (Schoen, 1969). This solution has sulfate concentrations of 500–1,000 ppm, with pH 2–3 (Ellis and Mahon, 1977; Hedenquist, 1991; Nordstrom et al., 2009), which alters the horizon above the paleowater table to kaolinite, alunite, etc., and causes low-temperature silicification of opal at its base (Steiner, 1953; Sillitoe, 1993). This environment occurs above all boiling hydrothermal liquids (both neutral-pH geothermal and acidic magmatic-hydrothermal), meaning that such alteration blankets occur over all styles of epithermal deposit, with no obvious distinction (Sillitoe, 1993).
4. Steam-heated CO₂-rich condensate: Similarly, where CO₂- and H₂S-rich vapor condenses but the environment is below the vadose zone, the CO₂ forms a weakly acidic (pH ~4–5) H₂CO₃ solution, typically as a carapace that includes the deeper margins of hydrothermal systems, i.e., a steam-heated CO₂-rich liquid, with temperature of up to about 170°C (Hedenquist and Stewart, 1985; Hedenquist,

1990). Mineralogy includes clays and kaolinite, as well as Fe-Mn carbonates (e.g., siderite) plus pyrite, characteristic of argillic (intermediate argillic) alteration (Hemley and Jones, 1964; Meyer and Hemley, 1967). This condensate is common on the margins of hydrothermal systems, including the margins of epithermal deposits.

5. Supergene oxidation of sulfide minerals: Posthydrothermal supergene oxidation of sulfide minerals, primarily fine-grained pyrite, a bacterially mediated process, occurs within the vadose zone, again because of the abundance of atmospheric O₂. This creates an acidic (to hyperacidic, pH <1) solution above the paleowater table (Penrose, 1894; Sillitoe, 2005), locally leaching metals such as copper (potentially to be enriched at depth) and leaving behind Fe oxyhydroxides.

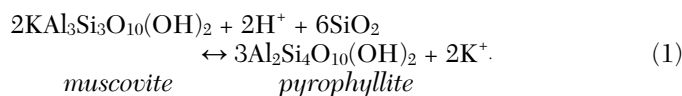
Many of the minerals formed in these five distinct geologic environments of hydrolytic alteration are characteristic of those referred to as advanced argillic (or intermediate argillic for kaolin in an assemblage of other clays plus carbonate minerals; Meyer and Hemley, 1967). We illustrate below the formation of each environment, with examples from active hydrothermal systems (both geothermal and magmatic-hydrothermal) and their equivalent ore deposits. The significance of each environment and alteration style with respect to mineral exploration is also examined, from highest to lowest temperature.

Cooling of White-Mica-Stable Fluid

Formation conditions

In the past, the occurrence of pyrophyllite was regarded as an indicator of acidic conditions near the surface (e.g., suggestion of late hot-spring activity at the El Salvador porphyry Cu deposit; Gustafson and Hunt, 1975). However, as noted by Hemley et al. (1980), pyrophyllite can also form by cooling of a white-mica-stable fluid (Fig. 2). This feature of hydrolytic alteration (Hemley and Jones, 1964), combined with the wide temperature range of pyrophyllite stability, results in pyrophyllite forming in several environments. The wide temperature range is a function of aqueous concentration of silica (Fig. 4), controlled by the solubility of quartz, cristobalite, or amorphous silica (Hemley et al., 1980).

Over the past two decades, evidence for the replacement of white mica by pyrophyllite has increasingly been recognized near the upper parts of porphyry deposits, owing in large part to SWIR measurements. During the formation of pyrophyllite from muscovite, which occurs at ~350°C (Hemley et al., 1980; Watanabe and Hedenquist, 2001), reaction (1) requires a source of silica to proceed, because the molecular Si/Al ratio of pyrophyllite is twice that of muscovite. Where quartz is present, this can lead to dissolution (see "patchy silica," below):



Alteration mineralogy, characteristics, and relationship to ore zones

In the El Salvador porphyry deposit, pyrophyllite is commonly associated with diaspore, with the two minerals replacing muscovite and andalusite, respectively; alunite occurs

locally, but kaolinite is absent. The pyrophyllite is present mainly above 3,000-m elevation, forming as a cupola over the bornite-chalcocite ore zone that has an upper limit of about 2,800-m elevation (Fig. 8; Gustafson and Hunt, 1975). The general inverse correlation between the abundance of muscovite and pyrophyllite, which Watanabe and Hedenquist (2001) attributed to cooling and replacement of the muscovite by the pyrophyllite, is supported by similar isotopic compositions of the causative fluid of both minerals.

This alteration relationship is common at the Far Southeast, Philippines (Garcia, 1991; Hedenquist et al., 1998; Calder et al., in press) and Batu Hijau (Garwin, 2002) porphyry Cu-Au deposits in the southwest Pacific, where assemblages of pyrophyllite \pm diaspore (\pm dickite, zuniite) have been mapped along structures and replace white mica (plus andalusite at the latter deposit). At Far Southeast, the pyrophyllite \pm diaspore assemblage is present as deep as ~1,200 m below the present surface, within the upper portion of the chalcocite zone of the porphyry deposit, and extends up to the base of the lithocap at ~700-m depth (which consists of residual quartz along an unconformity and a halo of alunite-dickite-kaolinite and local pyrophyllite or diaspore; Garcia, 1991; Calder et al., in press). In addition to pyrophyllite \pm diaspore that replace

white mica at depth, kaolin-group minerals and rare alunite are present along with pyrite-bornite and chalcocite in veins in this transition from white mica to the base of the lithocap (Calder et al., in press). The pyrophyllite and white mica have similar stable isotopic compositions, indicating formation by the same fluid; by contrast, alunite in the lithocap halo has a distinctly different isotopic signature, indicating formation from volcanic vapor condensed by meteoric water (Fig. 9; Hedenquist et al., 1998, fig. 14b).

Pyrophyllite (with other aluminosilicate minerals) overlies other porphyry Cu-Au orebodies in a proximal position, closely associated with white-mica alteration that accompanies ore, e.g., Oyu Tolgoi, Mongolia (Khashgerel et al., 2006) and the Pebble, Alaska (Gregory et al., 2013; Gregory, 2017) porphyry deposits and the recently discovered Onto deposit, Indonesia (Burrows et al., 2020). The first two have stable isotopic evidence linking the white mica and pyrophyllite formation, like at Far Southeast and El Salvador.

Above the top of the porphyry Cu \pm Au environment, a distinctive and diagnostic replacement texture is common: a texture long referred to as "patchy silica" was first described by geologists in the Yanacocha district, Peru, particularly in the transitional zone between the San José high-sulfidation

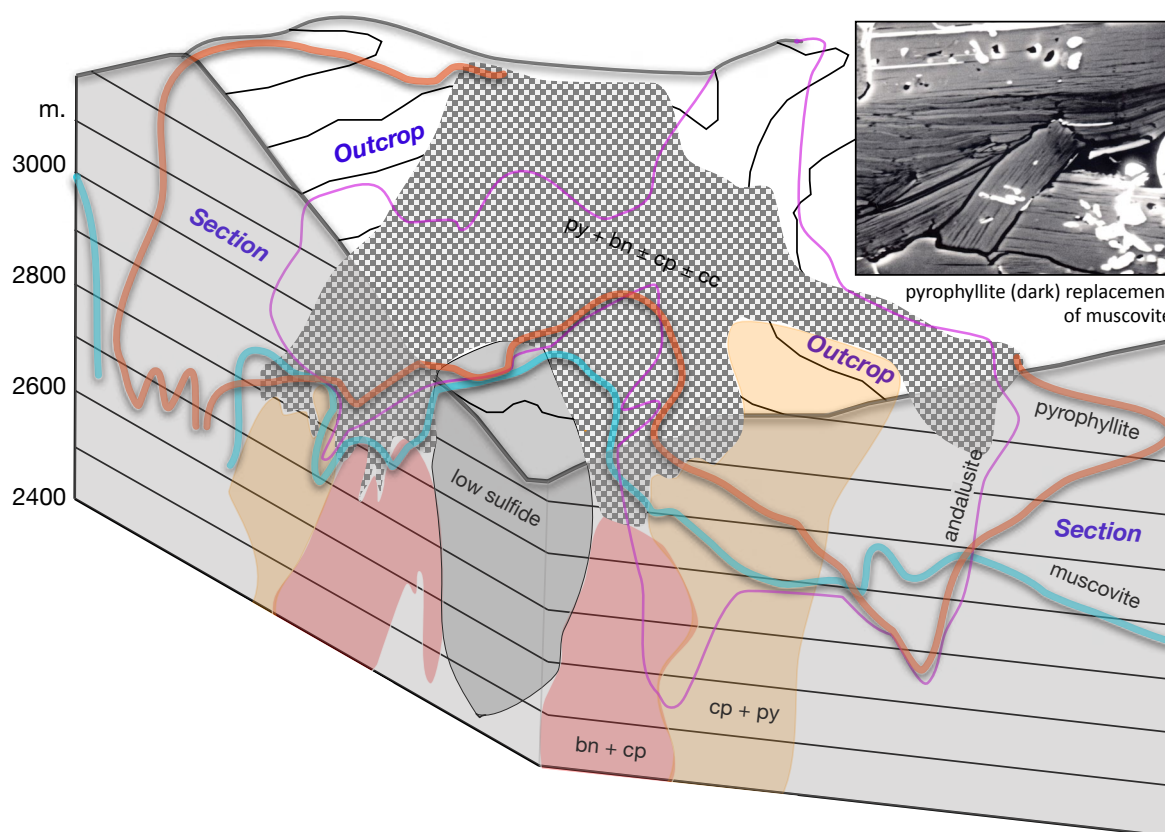


Fig. 8. Outcrop in the depression over, and oblique cutaway through, the El Salvador porphyry Cu deposit, Chile, showing the distribution of sulfide minerals (modified from Gustafson and Hunt, 1975); sulfides in outcrop have been supergene oxidized (only preserved encapsulated in quartz veins). Alteration mineralogy includes the lower extent of muscovite (blue) and andalusite (purple), with an overprint by pyrophyllite (orange); the least altered, sulfide-deficient body (gray) is similar to the position of the late L porphyry intrusion; no vertical exaggeration. Extent of pyrophyllite reflects that of muscovite in the area proximal to the Cu orebody (bn + cp, and at a shallower depth, cp + py) and is largely restricted to a shallower elevation. The inset highlights the relationship of muscovite (light gray) being replaced along cleavage planes by pyrophyllite (dark gray; width is 50 μ m); image from Watanabe and Hedenquist (2001), who discuss the surface extent of muscovite and andalusite and the pyrophyllite replacement of the former. Abbreviations: bn = bornite, cc = chalcocite, cp = chalcocite, py = pyrite.

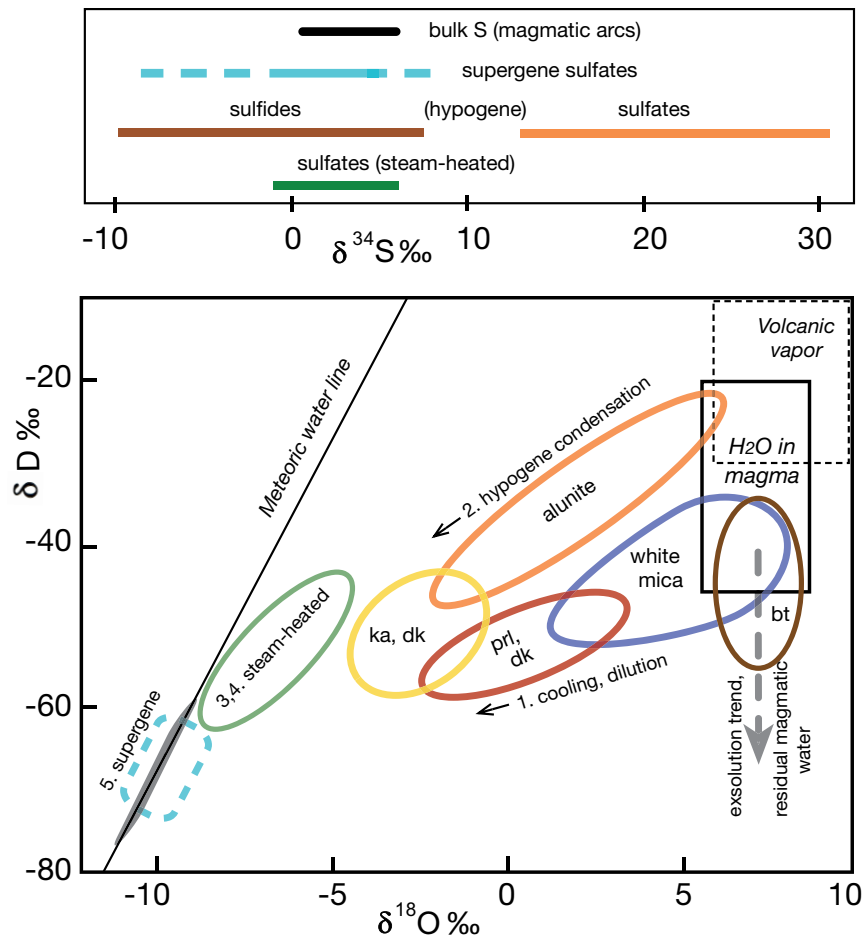
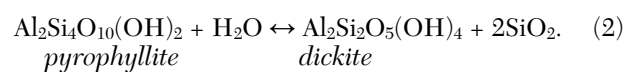


Fig. 9. General trends in δD - $\delta^{18}O$ composition of hydrothermal fluids that form alteration assemblages in the five environments examined here. The average data and trends from the Far Southeast-Lepanto porphyry-epithermal (Hedenquist et al., 1998) and El Salvador porphyry (Watanabe and Hedenquist, 2001) deposits are used, including local meteoric water values (wide gray area); other deposits at different paleolatitudes and elevations will have different meteoric water compositions and thus dilution trends. Composition of H_2O dissolved in felsic magmas (Taylor, 1992) shown, as well as that of high-temperature volcanic vapors (Giggenbach, 1992b) separated from hypersaline liquids at depth, plus the trend of residual H_2O remaining in magmas with progressive crystallization and exsolution (Hedenquist and Richards, 1998). Supergene refers to kaolinite and alunite formed from local meteoric water during weathering. Abbreviations: bt = biotite, dk = dickite, ka = kaolinite associated with alunite formed in lithocaps, prl = pyrophyllite, white mica = muscovite and illite. Steam-heated acid-sulfate solutions formed within the vadose zone define a slope of 3 to 5 (Henley and Stewart, 1983). Top inset: range of $\delta^{34}S$ values of sulfates (and sulfides) in the various environments discussed (Rye et al., 1992; Arribas, 1995). Color code similar to the five environments noted in Figure 1.

epithermal gold deposit and the topographically lower Kupfertal porphyry Cu-Au deposit (Fig. 10a; Klein et al., 1997; Pinto, 2002). This texture consists of nodular replacement of siliceous rock by pyrophyllite \pm alunite, diaspore, dickite, and/or kaolinite, here and in other locations in the district, such as beneath the Maqui Maqui deposit (Longo et al., 2010). At the Milagros porphyry Cu prospect, Peru, adjacent to the Lagunas Norte high-sulfidation Au deposit, Garcia (2009) characterized the nodules of pyrophyllite \pm diaspore \pm dickite, typically with pyrite (Fig. 10f) and identified lobate features that indicate pyrophyllite replacement of siliceous rock (reaction 1; Fig. 10g).

There are similar lobate features indicating nodular pyrophyllite, etc., replacement of quartz at Oyu Tolgoi (Khashgerel et al., 2009), as well as at Escondida (Padilla-Garza et al., 2001, 2004) and Caspiche (Sillitoe et al., 2013), both in

Chile, Öksüt, Turkey (Yildiz et al., 2017), and in other districts of Chile, Turkey, Mexico, Russia, and elsewhere (pers. observations) (Fig. 10a-e). The presence of alunite has yet to be explained, but where the nodules ("patches") consist of dickite, this may be due to its conversion from earlier formed pyrophyllite on continued cooling (Fig. 4). If true, silica will be released to solution (reaction 2), which may account for some of the extensive silicification observed at shallower depths (Henley et al., 1980; Chang et al., 2011):



Another environment of aluminosilicate formation associated with white mica is present in the volcanogenic massive sulfide (VMS) environment. Such alteration, simply referred to as advanced argillic in the literature, occurs in

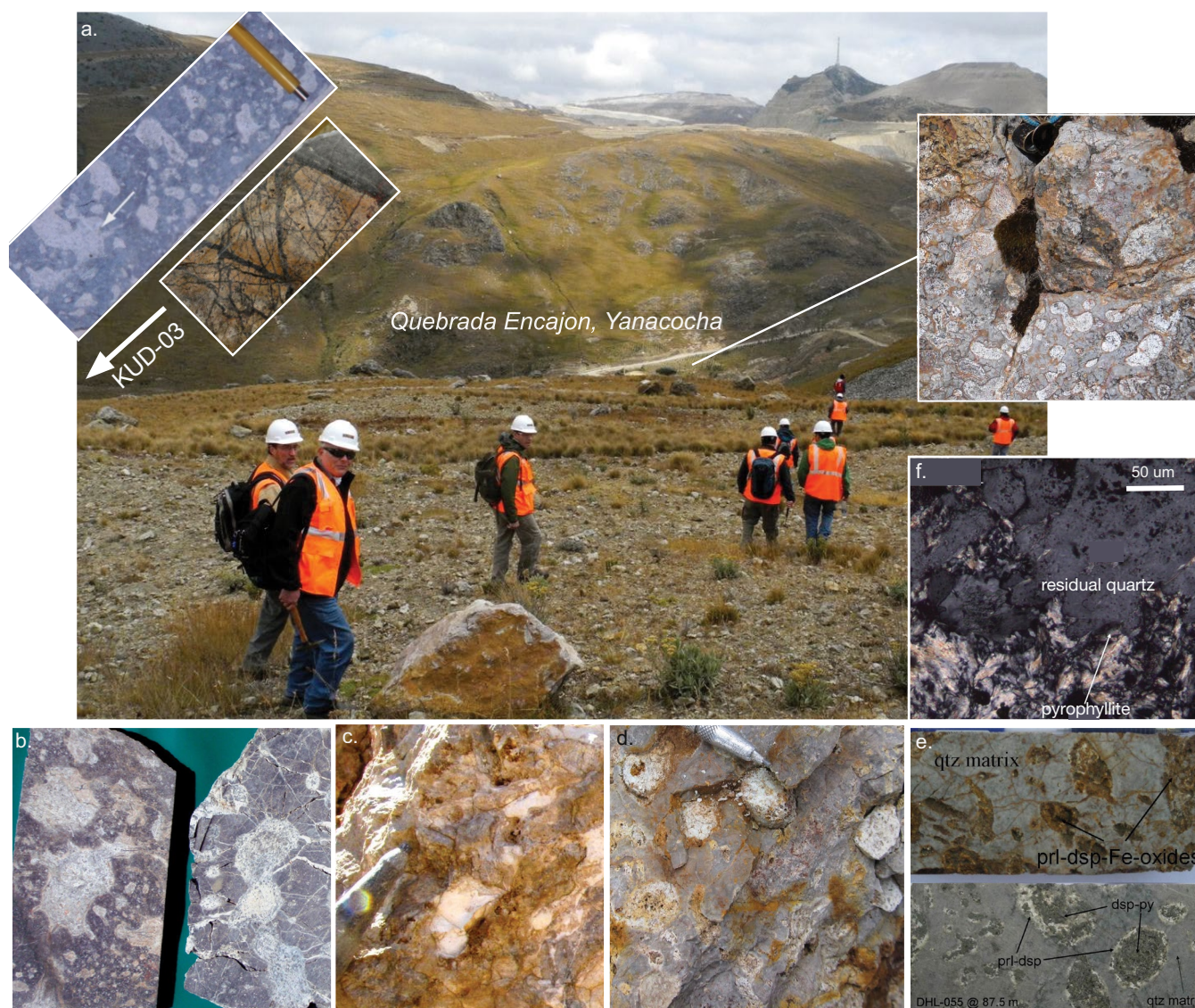


Fig. 10. Patchy pyrophyllite replacement textures. a) Looking north from the margin of the San Jose Au deposit, Yanacocha district, Peru, ~300 m down into the Quebrada Encajon; Cerro Yanacocha on skyline. Foreground consists of quartz-alunite alteration, located on the margin of residual quartz that hosts the San Jose deposit (Longo et al., 2010). Halfway into the valley (inset, upper right), nodular alunite \pm pyrophyllite replaced residual quartz (photograph 15 cm wide), known as patchy replacement (Pinto, 2002). Drilling in the valley penetrated patchy pyrophyllite replacement above stockwork quartz veins with muscovite alteration and chalcopyrite (Klein et al., 1997); drill core from KUD-03 (upper left); drill core 6 cm wide. This texture and mineralogy (pyrophyllite \pm diaspora, dickite, alunite, and pyrite) is now recognized to be common at transition of lithocap to white-mica alteration at greater depth, over the causative porphyry intrusion. Examples include the following (drill core 6 cm wide): b) Oyu Tolgoi, Mongolia (Hugo Dummett porphyry Cu-Au deposit; Khashgerel et al., 2009), c) central Chile and d) northwest Turkey porphyry districts, base of residual quartz lithocaps, and e) Milagros porphyry prospect, south of the Lagunas Norte Au deposit, Peru (Garcia, 2009). f) At Milagros (thin section, cross polars; bar scale 50 μ m), pyrophyllite (+ diaspora and pyrite) clearly replace quartz in an embayed texture (Garcia, 2009), as also described by Khashgerel et al. (2009, fig. 7). Abbreviations: dsp = diaspora, prl = pyrophyllite, py = pyrite, qtz = quartz.

VMS deposits rich in precious metals (Mercier-Langevin et al., 2011, 2015). Aluminous minerals have been invoked as evidence for a reactive magmatic input, e.g., at the metamorphosed Archean deposits of Bousquet 2-Dumagami and LaRonde Penna, Canada (Dubé et al., 2007, 2014). Although there likely was a magmatic component, simple cooling from muscovite \pm andalusite to pyrophyllite and dickite stability can explain the aluminosilicate occurrence, including Archean metamorphosed equivalents of kyanite,

sillimanite, and andalusite in Fennoscandia (Hallberg, 1994; Eilu et al., 2003).

Relevance to exploration

Where pyrophyllite (with diaspora \pm dickite or zunyite) occurs with white mica (usually muscovite \pm andalusite) as a replacement, the top of the porphyry environment is indicated (e.g., Far Southeast, El Salvador, Oyu Tolgoi; also Agua Rica, Argentina, Franchini et al., 2011). This relationship was first

observed at Kounrad, Kazakhstan (Nakovnik, 1934, 1968). Such alteration is not expected below typical low-sulfidation deposits, since they do not share the tectonic environment of porphyry ore deposits (Sillitoe and Hedenquist, 2003) except where there is an overprint of earlier alteration. The nodular replacement of siliceous rock (residual quartz, quartz-alunite, etc.) by pyrophyllite, etc., is commonly observed in this transitional porphyry to epithermal environment, consistent with proximity to the base of a lithocap. Porphyry-style quartz veins may also be present, as well as evidence of muscovite alteration of the postpotassic stage of porphyry deposit formation. Such a deep pyrophyllite-muscovite \pm quartz assemblage has been identified recently (Al Furqan et al., 2021) within the giant Grasberg porphyry copper system in Indonesia (Leys et al., 2019), where it is associated with the Gajah Tidur porphyry intrusion at a depth below that of the potassic (K-feldspar-biotite-magnetite) alteration zone of the Grasberg Cu-Au deposit.

The relatively deep pyrophyllite replacement of white mica that is caused by cooling contrasts with the local occurrence of pyrophyllite with alunite in parts of lithocaps at shallower depths, with abundant alunite (and its O/H isotope composition) indicating formation from a sulfate-rich condensate of volcanic vapor. These two distinctly different environments of formation of pyrophyllite were confirmed by stable isotopic studies at El Salvador (Watanabe and Hedenquist, 2001, fig. 8b).

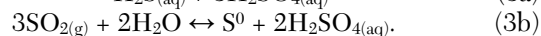
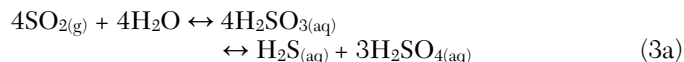
Hypogene Acid-Sulfate-Chloride Condensate

Formation conditions

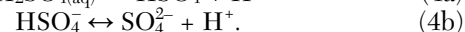
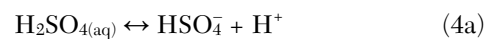
Hypogene advanced argillic alteration, typically quartz-alunite with halos of kaolinite \pm dickite and roots of pyrophyllite \pm dickite, forms in the epithermal environment (Fig. 1) from condensates of magmatic vapor (Steven and Ratté, 1960; Rye et al., 1992; Arribas, 1995). The vapor contains SO_2 , HCl, and HF (Giggenbach, 1987), which separates from a mixture of vapor and hypersaline liquid at depth; this mixture forms where a critical-behavior fluid, exsolved from a shallow intrusive source, intersects its solvus (Henley and McNabb, 1978;

Hedenquist et al., 1998). The term “acid sulfate” (e.g., Heald et al., 1987) has been used for this style of alteration but is potentially confusing, because both steam-heated and supergene alteration also involve acid-sulfate solutions.

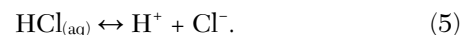
The principal reactions that generate hyperacidic (pH <1.5) solutions were summarized by Hedenquist and Taran (2013). The dominant chemical process in condensed magmatic vapors is aqueous redox-disproportionation of the absorbed SO_2 according to the following reactions (Iwasaki and Ozawa, 1960; Kusakabe and Komoda, 1992), which were confirmed by sulfur isotope measurements (Oana and Ishikawa, 1966):



This is followed by dissociation of H_2SO_4 on cooling, which yields H^+ ion and ionized aqueous-sulfate species:



$\text{H}_2\text{SO}_{4(aq)}$ becomes a strong acid as temperature decreases, with the dissociation constant K_{4a} at 100°C close to 10^2 , versus ~ 0.01 at 350°C (Hnedkovsky et al., 2005). Similarly, HCl in volcanic vapors dissociates after absorption by the condensate, according to the equilibrium:



The most aggressive, nearly isochemical hydrolytic leaching of cations from the host rock by the hyperacidic condensate, commonly at a pH ~ 1 (Table 1), leaves a siliceous residue, locally with a vuggy texture (Fig. 5) that reflects the original lithology and rock texture. At the Summitville mine, a quartz latite with large sanidine crystals was either replaced by alunite-dickite or completely dissolved (Fig. 6; Steven and Ratté, 1960). This zone of leaching occurs within the upward flow channel at a high condensate/rock ratio (Hedenquist and Taran, 2013). The siliceous residue, initially cristobalite or tridymite (Hamasaki, 2002) but recrystallizing to quartz or chalcedony with time, forms the core of alteration,

Table 1. Summary of Chemical Reactions in Each of Five Environments that Generate Reactivity

Environment	Representative reactions	Concentrations	Temperature (°C, pH ₂₅)
Cooling of white mica-stable fluid	$2\text{KAl}_3\text{Si}_3\text{O}_{10}(\text{OH})_2$ (white mica) + 2H^+ + 6SiO_2 $\rightarrow 3\text{Al}_2\text{Si}_4\text{O}_{10}(\text{OH})_2$ (pyrophyllite) + 2K^+		$\sim 350^\circ$ – 250°C $\log (\text{mK}^+/\text{mH}^+) \text{ pH} < 2$
Hypogene acid-sulfate-chloride	$4\text{SO}_2 + 4\text{H}_2\text{O} \rightarrow 3\text{H}_2\text{SO}_4 + \text{H}_2\text{S}$ $\text{H}_2\text{SO}_4 \rightarrow \text{H}^+ + \text{HSO}_4^-$ $\text{HCl} \rightarrow \text{H}^+ + \text{Cl}^-$	$\leq 7,000$ ppm H_2SO_4 , $\leq 3,000$ ppm HCl, 500–1,500 ppm Al, <1,000–5,000 ppm Fe	$\sim 300^\circ$ to $\leq 100^\circ\text{C}$, pH ~ 1 –1.7 (pH <0.5 in crater lakes due to evaporation; Giggenbach et al., 2003)
Steam-heated acid-sulfate	$\text{H}_2\text{S} + 2\text{O}_2 \rightarrow \text{H}_2\text{SO}_4 \rightarrow \text{H}^+ + \text{HSO}_4^-$	$\leq 1,000$ ppm (locally up to 6,000 ppm) H_2SO_4 , <5–20 (40–150) ppm Al, 1–10 (≤ 50) ppm Fe	$\sim 100^\circ$ – $<70^\circ\text{C}$, pH ~ 2 –3+ (pH 1.5–2 due to evaporation; Nordstrom et al., 2009)
Steam-heated CO_2 -rich	$\text{CO}_2 + \text{H}_2\text{O} \rightarrow \text{H}_2\text{CO}_3 \rightarrow \text{H}^+ + \text{HCO}_3^-$ ($\text{H}_2\text{S} + \text{minor } 2\text{O}_2 \rightarrow \text{H}_2\text{SO}_4$)	≤ 1 –3 wt % H_2CO_3 (<100 ppm H_2SO_4)	$\sim 120^\circ$ – 170°C , pH ~ 4 –5
Supergene oxidation of sulfide minerals	$2\text{FeS}_2 + 7.5\text{O}_2 + 5\text{H}_2\text{O}$ (+ bacterial catalyst) $\rightarrow 2\text{FeO}(\text{OH}) + 4\text{H}_2\text{SO}_4$ (intermediate step to S^0 , further oxidized by bacteria?)	Up to >1 wt % H_2SO_4	$<10^\circ$ – 40°C , pH to <1 (acid mine drainage)

with zoning outward to halos of quartz-alunite and quartz-aluminosilicate minerals. This characteristic zonation pattern was first documented by Nakovnik (1934, 1968) in Eurasia and by Steven and Ratté (1960) at Summitville (Fig. 5, inset); the latter authors correctly deduced the environment of formation as being “characterized by acid sulfate solutions” (p. 51) due to volcanic emanations. Such alteration typically flares upward along feeder structures (Steven and Ratté, 1960; Stoffregen, 1987) because of the increase in reactivity caused by dissociation of H_2SO_4 and HCl as the temperature decreases (Giggenbach, 1987; Hedenquist and Taran, 2013).

Despite suggestions to the contrary (Scher et al., 2013; King et al., 2014), formation of residual quartz does not involve significant metal enrichment at the time of leaching and pyrite deposition (Hedenquist and Taran, 2013), owing to the low metal concentrations in the high-temperature but near-atmospheric pressure fumarolic vapors. For example, such residual rock contains <2 ppb Au at the Satsuma Iwojima rhyolitic volcano, accompanying altered rhyolite with 84–97% SiO_2 (avg 92.5%, $n = 10$; one of 21 analyses contained 29 ppb Au) (Fig. 6b; Hamasaki, 2002). Here, condensates of the high-temperature but low-pressure vapor have low metal concentrations (avg 29 ppb Cu [6–64 ppb, $n = 5$] and 3.0 ppt Au [0.8–6.5 ppt, $n = 5$]; Hedenquist et al., 1994a). Fumarolic condensates from the Kudryavy basaltic andesite volcano (535°–940°C) have metal contents that average 251 ppb Cu [32–910 ppb, $n = 6$], with up to 2.7 ppb Au (Taran et al., 1995; Y. Taran, pers. commun., 2020), typical of more mafic volcanoes. Where carefully sampled, passively discharging vapors (500°–800°C) that generate acidic condensates have a low metal content (<1–20 ppm Cu and <0.01–5 ppb Au) (Symonds, 1992; Hedenquist et al., 1994a; Hedenquist, 1995; Taran et al., 1995; Y. Taran, pers. commun., 2020), with some of the highest values (20 ppm Cu and 5 ppb Au) likely caused by local remobilization, in the case of Tobalchik (Zelenski et al., 2016), or entrainment of rock particles or previously deposited sublimates in vapor during sampling (Zelenski et al., 2014; Taran et al., 2018, and references therein).

Alteration and sulfide mineralogy, characteristics, and relationship to ore zones

The first comprehensive documentation of numerous examples of hypogene advanced argillic mineralogy and zonation was made by Nakovnik (1934, 1968), initially with regards to porphyry Cu deposits in Kazakhstan. Steven and Ratté (1960) constructed a schematic alteration zonation section for Summitville (Fig. 5, inset) that is characteristic of similar epithermal deposits around the world (Arribas, 1995). Aluminum-phosphate-sulfate (APS) minerals of the alunite group form as the result of apatite dissolution that provides phosphate to the sulfate-rich solution (Stoffregen and Alpers, 1987). The quartz-alunite and quartz-kaolinite/dickite halos can be a few meters (Nansatsu, Japan; Fig. 11) to hundreds of meters in width (e.g., Yanacocha; Harvey et al., 1999; Pilco and McCann, 2020). The proximal alteration of porphyritic quartz latite at Summitville is controlled by fractures and their intersections, resulting in pipe-like bodies (Stoffregen, 1987). The strong fracture control on alteration at Summitville was caused by limited primary permeability in the quartz latite, interpreted to be a volcanic dome (Gray and Coolbaugh,

1994). Steven and Ratté (1960, p. 61) described alteration as “leached vuggy quartz rock within the large silicified mass.” “In cross section the knob ... somewhat resembles a tooth, with a solid compact mass on top and a series of roots projecting downward.” Such a “molar tooth-like” morphology, caused by the upward coalescing of zones of residual quartz, is common in many epithermal deposits where the roots have been drill-defined in detail (Harvey et al., 1999).

In contrast to the near-vertical feeder zone at Summitville, in the Nansatsu district of southern Kyushu, the tuff breccia above the feeder zones in the Nansatsu Group andesite flows provided a permeable host that was leached to residual quartz, because of mushrooming of acidic solutions from multiple feeder zones (Fig. 11a, lower inset; Urashima et al., 1981); however, the alteration zonation at Iwato is the same as at Summitville (Fig. 11a, upper inset). After initial leaching, residual quartz is commonly silicified, with original vuggy texture partly maintained, through to a massive chalcedony appearance, such as at Akeshi, also in the Nansatsu district (Fig. 11b) and in Turkey (Fig. 11c, bottom). This massive silicification (also illustrated at Lepanto, Philippines; Hedenquist et al., 2017, fig. 3b) can be gray to light brown in color or even white after supergene oxidation of fine pyrite. Where open spaces are filled, laminations with geopetal structures demonstrate that the infill was a colloidal silica gel (e.g., Rodalquilar; Arribas et al., 1995b), indicating sharp cooling to attain amorphous silica saturation (Fig. 11b, d). The appreciable gold grades associated with this creamy colored silica-colloid cement (Fig. 11b-d) prove that this silicification was related to a metal-rich stage, subsequent to the initial leaching event.

Mushrooming of residual quartz and related alteration also occurred but on a much larger scale in the Yanacocha district (Harvey et al., 1999; Pilco and McCann, 2020, and references therein), forming extensive stratabound bodies of residual quartz, each several kilometers in size; these residual quartz lithocaps are the principal host of (now oxidized) gold mineralization, although much of the residual quartz is barren. A survey of mainly residual quartz alteration (207 samples) across the district determined that 53% reported <50 ppb Au, and 26% returned <10 ppb Au (Turner, 1997), despite some being within hundreds of meters or less of orebodies. As noted above, residual quartz and quartz-alunite do not acquire strong metal anomalies on formation (Steven and Ratté, 1960; Stoffregen, 1987; Hedenquist et al., 1998; Turner, 1997), with initially low gold and copper contents, typically <10–50 ppb and <50 ppm, respectively, in the Lepanto district (Chang et al., 2011).

In other examples, numerous lithocaps around the world are apparently unmineralized (see below), arguably because of the lack of a subsequent metal-rich liquid ascending to the level of the residual quartz. In cases where the residual quartz is mineralized after its formation, Hedenquist et al. (1998) provided evidence that the metal-bearing fluid is associated with white-mica alteration of the deeper porphyry deposit. Consistent with this interpretation, the bonanza-grade gold veins at the El Indio deposit, Chile, have halos of white-mica alteration where they cut the propylitic halo beyond the aluminosilicate-hosted enargite lodes (Jannas et al., 1999). A similar relationship is present at the Victoria intermediate-sulfidation veins in the Philippines, with halos

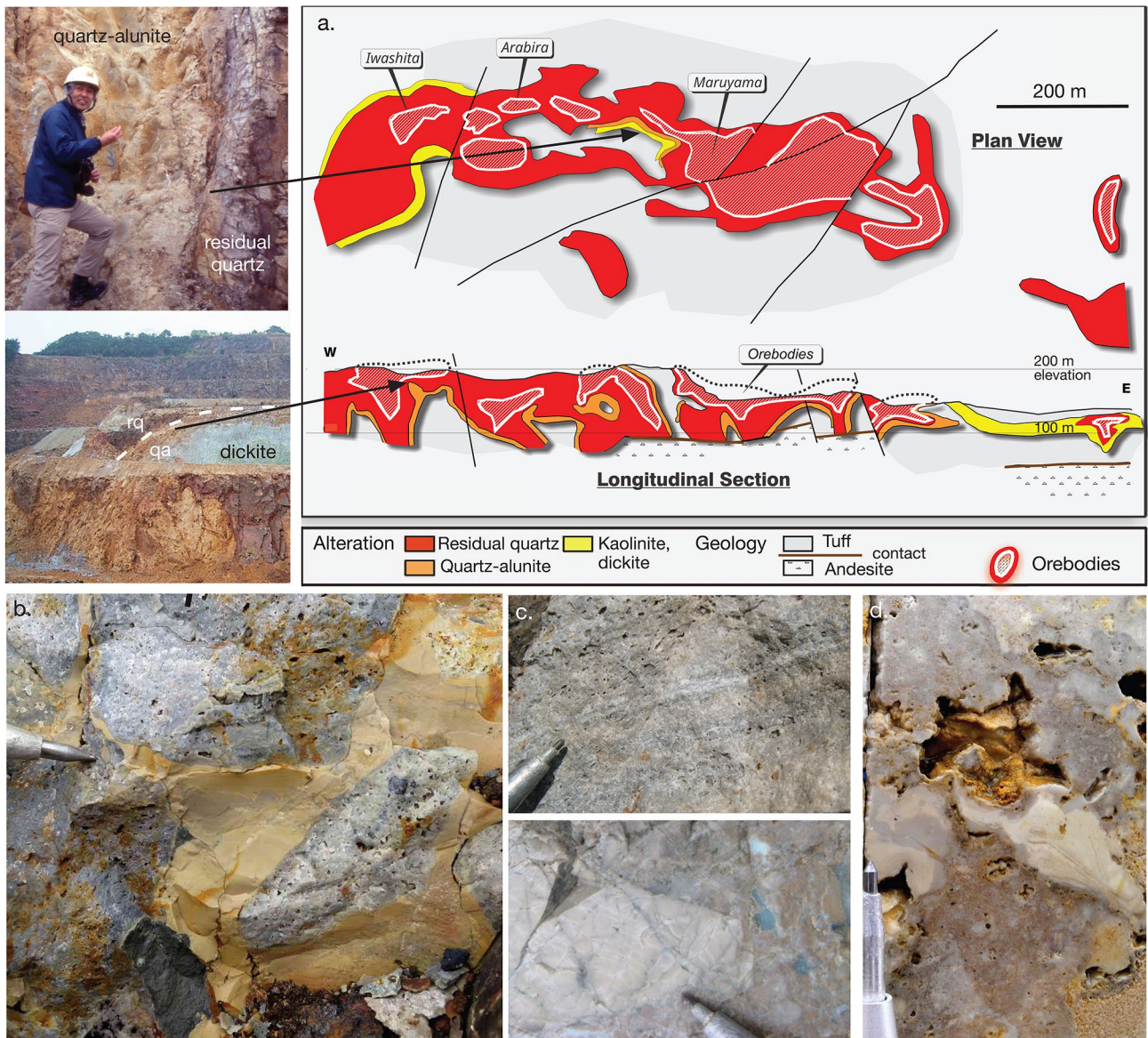


Fig. 11. a) Plan and long section, Iwato lithocap-hosted high-sulfidation deposit, Nansatsu, Japan (Urashima et al., 1981). Plan shows an elongate body of residual quartz (red) that hosts several orebodies (outlined in white, >1 g/t Au). The long section reveals several structurally controlled feeder zones that cut the basal andesite flows, with alteration mushrooming outward where reactive fluid ascended into the more permeable tuffaceous and sedimentary units and flowed laterally. The subsequent ore deposition was focused above the feeder zones. The leached, residual quartz (rq) cores have sharp contacts with narrow (1–2 m wide) halos of quartz-alunite (qa; inset, upper left), which pass outward to kaolinite and smectite on alteration margins, distant from feeder zones. By contrast, close to feeder zones (inset, lower left), the quartz-alunite has a sharp contact outward to dickite \pm pyrophyllite (Hedenquist et al., 1994b). b) Residual quartz in the ore zone of Akeshi, 5 km east of Iwato, with residual quartz and vuggy texture, locally massively silicified, then brecciated and cemented by creamy colored colloidal silica gel (now recrystallized to chalcedony), locally preserving geopetal structures (photograph, W. Pratt). c) Lithocap-hosted high-sulfidation Au deposit, Turkey. Outcrop (top) of residual quartz, local vuggy texture preserved, and band of subsequent massive silicification in sample middle; <100 ppb Au; drill core (bottom), ~100-m depth, with residual quartz, massive light gray silicification, brecciated and cement of massive dark-gray silicification plus dickite (blue green), with bonanza Au grade. d) Drill core from a high-sulfidation deposit, Chile; brecciated residual quartz, infill by colloidal silica gel, creamy color with laminated geopetal texture, bonanza Au grade; coated by supergene jarosite.

of white mica where they intersect the slightly older enargite bodies hosted by residual quartz, the latter with barite gangue and halos of quartz-alunite and kaolin \pm pyrophyllite (Chang et al., 2011).

The white-mica-stage liquid, subsequent to formation of deep potassic and shallow residual quartz lithocap alteration,

is stable with respect to tennantite and chalcopyrite at the top of the porphyry environment (Einaudi et al., 2003) and at the base of the residual quartz (Steven and Ratté, 1960). As the liquid ascends into the residual quartz and cools, it evolves to a higher sulfidation state because of the lack of the Fe silicate rock buffer (Fig. 7; Einaudi et al., 2003). For this reason, most

occurrences of enargite are caused by cooling of a fluid within residual quartz-altered rock or within quartzite units or large quartz veins. In addition, high-sulfidation-state sulfides may also form in other alteration zones of hydrolytic alteration that lack the Fe-rock buffer, including pervasive white mica and/or pyrophyllite (e.g., Butte, Montana, Brimhall and Ghiorso, 1983; Chuquicamata, Chile, Ossandón et al., 2001; Onto, Burrows et al., 2020). Where residual quartz bodies contain only intermediate-sulfidation-state sulfides such as tennantite-tetrahedrite and chalcopyrite plus sphalerite, e.g., at Svetloy, Russia, this may be an indication that the shallower enargite level of the orebody has been eroded (Yakich et al., 2021).

Subaqueous environments: The best-known examples of hypogene vapor condensation and formation of advanced argillic minerals are subaerial, related to active volcanic centers as well as to their extinct equivalents, ore deposits. However, such alteration can also occur in subaqueous settings. Sahlström et al. (2018, 2020) recently documented a Permian sublacustrine deposit at Mt. Carlton, Queensland, Australia. The deposit formed during extension and the creation of half grabens that were filled with volcanic and sedimentary strata, the latter including lacustrine beds. High- and intermediate-sulfidation sulfides plus precious metals are hosted by residual quartz with halos of alunite, dickite, and kaolinite, with stable isotopic systematics similar to those of subaerial deposits.

Volcanic crater lakes, such as that at Kawah Ijen, Indonesia, have a pH as low as <0.5, caused by evaporative concentration of the hypogene acidic condensates (Delmelle et al., 2000). In such acidic lakes, finely laminated colloidal silica settles out of suspension from the amorphous silica-saturated lake solution, along with beds of native sulfur (S^0) (Delmelle and Bernard, 1994, 2015). Silica sinters are absent near such acidic discharges, since polymerization of amorphous silica is inhibited at pH <3–4 (Fournier, 1985); thus, laminated deposits of silica colloids are the equivalent of silica sinters, indicating preservation of the paleosurface. Evidence for acidic crater lakes spatially associated with volcanic domes is common near high-sulfidation deposits during their formation, as demonstrated by the preservation of laminated siliceous sediments at Yanacocha (Longo et al., 2010; Pilco and McCann, 2020).

Submarine volcanic arcs, typically calc-alkaline, total about 22,000 km (roughly equal to the length of subaerial arcs and about one-third the length of oceanic spreading ridges); 90% are located in the Pacific, both as island arcs and intraoceanic arcs (de Ronde et al., 2003). Hydrothermal systems are common on the submarine flanks of these arc volcanoes, typically discharging at 500- to 2,000-m water depth (Embley et al., 2008). In addition, back-arc spreading centers, ~10,000 km in length, form submarine back-arc basins in both intraoceanic and rifted island arcs, again with calc-alkaline magmatism accompanied by abundant felsic volcanic products. Hydrothermal activity is also common in these settings, explaining the observation that ~80% of known VMS deposits formed in submarine rifts (Hannington et al., 2005).

Early evidence of alteration by acidic solutions came from observations of pyrophyllite, kaolinite, and alunite associated with seafloor hydrothermal systems in the Lau back-arc basin (Fouquet et al., 1993; Herzig et al., 1993). A direct magmatic contribution was not favored initially, with the pH ~2 solutions erroneously thought to be caused by sulfide formation,

or even by H_2S oxidation (Fouquet et al., 1993; Herzig et al., 1993). However, the presence of a magmatic component was assured (de Ronde, 1995), given the volatile-rich nature of the crystallizing calc-alkaline magmas.

Mineralogic and sulfur isotope data from the Hine Hina site on the Southern Valu Fa ridge in the Lau basin (Herzig et al., 1998) and at Conical Seamount in the New Ireland fore arc near Lihir Island (Petersen et al., 2002) were interpreted as the result of direct contributions of magmatic volatiles to these submarine hydrothermal systems. Gamo et al. (1997) sampled thermal fluids ($\leq 120^\circ\text{C}$) in the Manus back-arc basin, Papua New Guinea, discharging at a pH ~2 with stable isotopic signatures indicating up to ~25% magmatic component. At the Susu Knolls, also in the Manus basin, acidic (pH 1.3–2) fluid discharges at $\leq 240^\circ\text{C}$ with evidence of a magmatic fluid component (Seewald et al., 2019), whereas higher-temperature discharges at pH 2–3 are argued to have become acidic through interaction with earlier formed alteration that consists of quartz-illite-pyrophyllite-anhydrite \pm alunite. At the Brothers dacitic volcano in the Kermadec intraoceanic arc, acidic fluid with a pH ≥ 1.8 discharges at $\leq 120^\circ\text{C}$; drilling revealed alteration that includes diaspore, pyrophyllite, rutile, zunyite, natroalunite, and quartz (de Ronde et al., 2019). The presence of enargite and other high-sulfidation-state sulfides on the seafloor, as documented by Dekov et al. (2016) and others, may simply be a function of sharp cooling (Einaudi et al., 2003) at the seafloor interface, rather than these occurrences necessarily indicating a direct analogy to high-sulfidation deposits. However, the eventual recognition of the nature of acidic fluids at the seafloor was presaged by the observation of Sillitoe et al. (1996) of an acidic component to the alteration of some precious metal-rich VMS deposits, followed by deposition in these cases of high-sulfidation-state minerals within leached rock.

Relevance to exploration

Where mineralized, the residual quartz of the feeder zone(s) is the prime target for initial mineral exploration, because it typically has higher metal grades but smaller tonnages than residual quartz in any stratabound portion of a potential lithocap, where a lithology or contact was laterally permeable (Hedenquist et al., 1994b). For example, the feeder zone at Quimsacocha (Loma Larga), Ecuador, hosts high-grade ore, and the halo of pyrophyllite contributed to its discovery (Jones et al., 2005). Although the quartz-alunite alteration halo is typically barren to slightly anomalous (<10–50 ppb Au; e.g., Turner, 1997; Chang et al., 2011), it may attain low grade adjacent to residual quartz-hosted orebodies (Harvey et al., 1999) and locally constitute ore if supergene oxidized (Pilco and McCann, 2020). The characteristic zonation of lithocaps provides a useful mineralogic vector and proximity indicator to a potential residual quartz-hosted ore zone.

The best-developed zone of residual quartz in a lithocap forms at a temperature of $\leq 250^\circ\text{C}$, where the sulfuric and hydrochloric acids increasingly dissociate and become more reactive (Hedenquist and Taran, 2013). Thus, the strongest lithocap alteration occurs in the shallowest parts and/or on the shoulder(s) of the causative intrusion because of cooling along shallow hydraulic gradients, away from the highest-temperature portion of the volcanic-hydrothermal system

(250°–200°C corresponds to ~400- to ~150-m depth at saturated water vapor pressure, i.e., at depths where surface topography causes hydraulic gradients). As a result, most large high-sulfidation deposits formed immediately beneath paleowater tables, as demonstrated by partial preservation of the overlying steam-heated alteration (Sillitoe, 1999).

Even where residual quartz is largely barren, either in a lithocap and/or its feeder structure (e.g., Valeriano, Chile; Sillitoe et al., 2016), this extensive hydrolytic alteration indicates a magmatic source of volatiles from a shallow intrusion. The spatial association between lithocap-hosted mineralization and deeper porphyry copper deposits was predicted by Sillitoe (1983), with the temporal and genetic affiliation subsequently identified, based on study of the linked Lepanto epithermal enargite-gold and Far Southeast porphyry copper-gold deposits (Arribas et al., 1995a; Hedenquist et al., 1998). Thus, lithocaps (barren or mineralized), now accepted to be associated with deeper porphyry deposits (Sillitoe, 1999, 2010), indicate deeper intrusive centers, with a broad distribution in volcanic arcs as old as Paleoproterozoic (Hallberg, 1994; Eilu et al., 2003). Alteration mineralogy of these shallow-formed lithocaps, even where barren, can assist exploration for deeper porphyry deposits, with paleotemperature zonation recorded by alunite compositions (Chang et al., 2011), and whole-rock Rb/Sr values (Arribas et al., 1995b, fig. 15), potentially indicating intrusion-proximal portions of lithocaps. Again, this type of alteration is not associated with typical low-sulfidation deposits, since they do not share the tectonic environment of lithocap and porphyry ore formation (Sillitoe and Hedenquist, 2003).

The lithocap of residual quartz and quartz-alunite \pm aluminosilicate minerals at Shuteen, Mongolia (Batkhisig et al., 2014) is 7 km long but is barren: <10 ppb Au in nearly 2,000 samples (Z. Chang, pers. commun., 2009). The lithocap, possibly the product of more than one thermal center, has been tested with four shallow (~500 m) holes in the so-far-unsuccessful search for porphyry Cu mineralization. However, other barren to low-grade lithocaps are spatially and temporally related to known porphyry deposits, such as beneath the Valeriano lithocap (Sillitoe et al., 2016). Adjacent to the Cerro Cocañez lithocap (mostly <100 ppb Au), Peru, east of the Yanacocha district, the Perol porphyry Cu-Au deposit has the same age as the lithocap (Gustafson et al., 2004). In other districts with multiple intrusions emplaced over several million years, the relationships between intrusive bodies, alteration, and mineralization of different types can be more complex. At Escondida, hypogene quartz-alunite alteration overprints the eroded and shallow Escondida porphyry Cu deposit. However, rather than being caused by a telescoping of alteration, the alunite is ~1.5 m.y. younger than the shallow porphyry deposit and is associated with the younger, and deeper, Escondida Este deposit, discovered 25 years after identification of the shallower Escondida deposit (Hervé et al., 2012).

Quartz-alunite-pyrite alteration forms an elongate (~1.5 km) zone at Alunite Hill in the Buckskin Range, Nevada, ~15 km west-northwest of the Jurassic-age Yerington porphyry Cu deposit. Lipske (2002) defined three principal advanced argillic associations, all with pyrite where not oxidized (the $\delta^{34}\text{S}$ of alunite and pyrite are consistent with a hypogene origin): quartz-alunite-pyrophyllite plus variable dickite or

diaspore (dickite replaces the margins of the pyrophyllite), quartz-pyrophyllite-muscovite (muscovite appears to replace pyrophyllite), and quartz-alunite-muscovite. Based on mapping by Lipske (2002), quartz-muscovite occurs northeast at lower elevations (below the advanced argillic alteration when the postmineral W-directed tilt is removed), with propylitic alteration to the southwest. Subsequent to this alteration, up to 500 m of more weakly altered dacitic volcanic rocks were deposited. Such a synhydrothermal aggradation may explain the apparent prograde alteration of pyrophyllite by higher-temperature muscovite, consistent with the late although minor Au- and Cu-bearing veins of quartz, pyrite, chlorite, hematite, and magnetite that cut most alteration.

Alunite \pm pyrophyllite, diaspore, dickite, and kaolinite form halos to some intermediate-sulfidation epithermal veins, such as in the Comstock district of Nevada, with the advanced argillic alteration caused by acidic condensates of hypogene magmatic origin. The structures were reopened ~1 m.y. later by a subsequent hydrothermal event involving neutral-pH fluids, leading to the formation of quartz-adularia and precious metal veins. Their apparently enigmatic alteration halos are an artefact of the younger vein overprint on earlier acidic alteration along the same structures (Hudson, 2003; Hudson et al., 2009).

Sillitoe et al. (1996) reviewed the occurrences of advanced argillic alteration associated with VMS deposits, of Cenozoic to Proterozoic and Archean age, with most of the older deposits having been regionally metamorphosed. The occurrence of pyrophyllite, dickite, and/or kaolinite in some deposits can be due to cooling from white-mica stability, as noted above, or in Kuroko deposits may be associated with seafloor carbonic acid-rich condensates (see below). However, the occurrence of residual quartz, alunite, and F-bearing minerals, accompanied by the subsequent deposition of high-sulfidation-state sulfides due to the lack of the rock buffer, indicates a magmatic source of acidity, which Hannington et al. (1999) argued was the cause of high gold contents in some VMS deposits. Sillitoe et al. (1996) noted the similarity of these deposits to the different styles of subaerial epithermal deposits and stressed the exploration implications of a seafloor setting for submarine-formed high-sulfidation deposits, including assessment at and below favorable stratigraphic horizons. An additional feature is the common presence of an overlying horizon of barite in such VMS deposits (Scotney et al., 2005).

Steam-Heated Acid-Sulfate Condensate

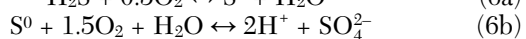
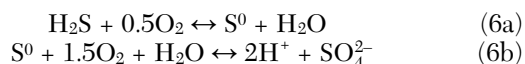
Formation conditions

Allen and Day (1935) studied the thermal features of Yellowstone National Park and grouped hot springs into various types based on their compositions, including acid-sulfate and alkaline carbonate as well as chloride. They believed that the sulfate of the acid springs was derived by atmospheric oxidation of H_2S and referred to observations by C.B. van Niel, who in 1929 had suggested that the oxidation was aided by bacteria. These acidic springs are commonly associated with mud pools that include kaolin-group minerals, opal, and/or cristobalite, and Allen and Day concluded that this style of alteration was limited to 10-m depth, but they suggested, also correctly, that the acid-sulfate liquid could penetrate deeper.

Similar hot springs are common in the Taupo Volcanic Zone of New Zealand, where Steiner (1953) first characterized the occurrence of kaolinite, alunite, pyrite, and opal to 25-m depth at Wairakei, underlain by a montmorillonite-like clay, pyrite, and siderite. He attributed the kaolinite and alunite to formation by acid-sulfate solutions. This was confirmed by Steiner and Rafter (1966), who conducted the first S isotope study of steam-heated alunite and pyrite. There was little difference in the sulfur isotope composition of H₂S in vapor ($3 \pm 2\text{‰}$ $\delta^{34}\text{S}$), of alunite ($5\text{--}6\text{‰}$ $\delta^{34}\text{S}$), and pyrite ($4\text{--}6\text{‰}$ $\delta^{34}\text{S}$), leading them to conclude that there was a lack of isotopic fractionation in the formation of the low-temperature ($\sim 100^\circ\text{C}$) alunite, but they were unsure if the sulfate was derived from atmospheric oxidation of H₂S or pyrite. These and other early authors used the term “supergene” for the steam-heated kaolinite and alunite, whereas this paper and many before it restrict usage of the supergene term (below) to sulfate formed from the atmospheric oxidation of sulfide minerals, typically after hydrothermal activity has ceased. Several epithermal deposits and prospects in the Coromandel peninsula, also in New Zealand, have paleowater table horizons of silicification, which Hamilton et al. (2019) note deposited as amorphous silica, and during diagenesis converted to opal-CT and chalcedony.

White (1957) recognized an end-member style of geothermal discharge that he referred to as acid sulfate, which tended to form on “relatively high ground” (p. 1651) in contrast to near-neutral-pH sodium-chloride springs. Like Steiner (1953), he concluded (p. 1652) that “steam that has boiled from chloride water at depth and has condensed again near the surface” is acidified where the H₂S is converted to sulfate in the zone of “extensive oxidation.”

Schoen (1969) studied the flux of sulfate from hot springs in various areas of Yellowstone and determined that the areal extent of thermal activity is a major factor in the production of sulfate by the oxidation of H₂S, which he determined had a rate of 7.5–15 g/m²/day, independent of location. He concluded (p. 643) that this is “consistent with a biological origin for the acid by aerobic sulfur-oxidizing bacteria.” Similarly, Takano et al. (1997) conducted a study of acidic groundwater (pH ~ 2.6) draining into Yugama crater lake, Kusatsu-Shirane volcano, Japan. They found that bacteria, *T. thiooxidans* and *T. ferrooxidans*, are involved in the oxidation of S⁰ and H₂S, as well as some pyrite, resulting in high sulfate and iron concentrations in solution, respectively. The sulfate has $\delta^{34}\text{S}$ of 0–2‰ versus –3 to –1‰ of S⁰ in the soils (Kusakabe et al., 2000). The sulfate production in the Yugama lake catchment is ~ 10 g/m²/day, similar to that determined by Schoen (1969) and Hurwitz et al. (2007) in Yellowstone thermal areas. The constancy of sulfate production per unit area indicates an intermediate step in the oxidation of H₂S to sulfate, supporting the conclusion by Nordstrom et al. (2009) that, although oxidation of H₂S in condensed vapor is the origin of the aqueous sulfate, there is a microbially mediated intermediary step of S⁰ production. This was also suggested by Pope et al. (2004), based on diurnal variations in sulfate production in the Waiotapu geothermal system, New Zealand (Fig. 12), and from S isotope studies of acidic crater lakes in Japan (Kusakabe et al., 1986, 2000):



Steam-heated condensates typically have sulfate concentrations up to $\sim 1,000$ ppm, with a corresponding pH of $\sim 2\text{--}3$ (Nordstrom et al., 2009; Power et al., 2018). Surface discharges, typically in the hanging wall of faults, occur as bubbling mud pools containing kaolinite and other clays (Fig. 12, inset). Nordstrom et al. (2009) demonstrated that steam-heated solutions with pH of ~ 2.2 to as low as 1.5 in Yellowstone are caused by enriched sulfate concentrations (1,000–6,000 ppm), with stable isotopic compositions indicating that this is due to evaporative concentration, likely where the groundwater is stagnant, i.e., a low hydraulic gradient. Of the 709 thermal features sampled in Yellowstone, about one quarter have a pH < 4 due to their steam-heated sulfate content; a further quarter of these have a pH < 2 caused by evaporation (Nordstrom et al., 2009). In the Taupo Volcanic Zone (aside from White Island volcano; Power et al., 2018), 8% of steam-heated waters have a pH < 2 to as low as 1.4. Most of the latter have $\sim 1,000\text{--}4,000$ ppm SO₄ but < 10 ppm Cl (close to the Cl concentration of rainwater at ~ 3 ppm), indicating a nil component of deep thermal liquid and no HCl input. As at Yellowstone, the high sulfate and corresponding low pH, < 2 (sufficient to dissolve some Al from the host rocks and leave a friable siliceous residue; Table 1), is likely due to low hydraulic gradients and hence stagnant groundwater recharge.

Vapor boiled from a deep liquid and containing H₂S (and CO₂) that condenses in the vadose zone, regardless of the nature of the boiling hydrothermal system at depth, results in the formation of similar steam-heated acid-sulfate condensates. Such $< 70^\circ$ to $\sim 100^\circ\text{C}$ condensates at the water table form the same bubbling mud pools of kaolinite, whether associated with neutral-pH hot springs depositing silica sinter (Fig. 12), or nearby high-temperature volcanic fumaroles, such as on White Island volcano (Fig. 6e; where the two distinctly different vapor discharges are < 500 m of each other). The resulting alteration is also indistinguishable, regardless of setting.

Alteration mineralogy, characteristics, and relationship to ore zones

In spite of its shallow depth of formation, above the paleowater table, preservation of at least parts of the steam-heated alteration zone is common in younger (Cenozoic age) volcanic rock-hosted epithermal districts, irrespective of the type of epithermal mineralization (high-, intermediate-, or low-sulfidation; Fig. 1) (Sillitoe, 1993, 2015). The preservation may be due to a young age of the deposit (e.g., < 0.5 Ma for Ladolam Au-Ag deposit in Papua New Guinea; Carman, 2003) or to burial under younger rocks (e.g., La Coipa district, Chile), with burial facilitated by high-angle, extensional faults (e.g., Sleeper Au-Ag deposit, Nevada; Nash et al., 1995). Thus, the lack of a steam-heated alteration zone in any epithermal deposit or district may simply reflect erosion, accentuated in nonarid regions, or areas that had a very shallow groundwater table. Where preserved, the steam-heated altered rocks are typically barren of base and precious metals plus the epithermal suite of indicator elements (As, Sb, etc.), as these are not transported by low-pressure vapor, instead being fractionated into the liquid at deeper levels where boiling of the hydrothermal fluid released H₂S and other volatiles. Exceptions are elements with high vapor pressure, such as mercury and sulfur.



Fig. 12. Oblique aerial view to the south-southeast over the Champagne Pool area of the Waiotapu geothermal system, New Zealand (Google Earth image, August 22, 2010). Champagne Pool discharges at $\sim 72^{\circ}$ – 75°C from a 900- to 700-yr-old hydrothermal eruption crater; surface discharge cools from $\sim 160^{\circ}\text{C}$ at 62+-m depth (saturated liquid-vapor pressure) due to evaporative heat loss at surface and rapid convection within the crater (K.L. Brown and J.W. Hedenquist, unpub. data, 1983). Polymictic unsorted eruption deposits occur north and southwest of the crater; an arcuate silica sinter < 1 m thick has formed southeast of the hot spring (Hedenquist and Henley, 1985). Other hydrothermal eruption craters occur farther south, mainly hosting acid-sulfate hot springs. Steam-heated acid-sulfate features are located mainly west of a W-dipping fault, in the hanging wall (areas outlined by light-green dashed lines), with alunite (natroalunite), kaolinite, montmorillonite, amorphous silica, cristobalite, and S^0 ; craters formed because of dissolution and collapse. Alunite and kaolinite alteration extends to ~ 50 -m depth, locally 135 m (Simmons et al., 2004). Bubbling mud pools similar to Fountain Paint Pots, Yellowstone (inset, right) are present at the base of collapse craters, with kaolinite, opal-CT, quartz, and finely disseminated pyrite. The steam-heated condensates have a subsurface outflow north along the water table, discharging to the Waiotapu stream at 98°C and pH 2.2, with 1,500 L/min flow (stream indicated by blue line; Hedenquist, 1983). This subsurface outflow silicified tuffaceous beds up to ~ 4 m above stream level (inset, lower right), because of a previously higher stand of stream and water table.

The La Coipa district (combined production plus reserves of ~ 220 t Au equivalent, Ag + Au) provides a good example of the relationships between epithermal Ag-Au mineralization and both hypogene and steam-heated acid-sulfate alteration environments (Fig. 1). The district is characterized by a large ($80+$ km 2) area of alteration that gave rise to a prominent color anomaly in this arid region. Six supergene-oxidized high-sulfidation deposits discovered to date (Sillitoe, 1995b; Illanes et al., 2005; Kinross Gold Corporation, 2020) were partially to completely covered by a district-wide subhorizontal zone of barren steam-heated alteration that forms a plateau at average 4,300-m elevation. At the Coipa Norte Ag-Au high-sulfidation deposit, the upper benches of the open pit are characterized by bright-white, friable, sponge-like rock composed of kaolinite and opal that extends downward and overprints the disseminated (now supergene oxidized) Ag-Au mineralization within bodies of vuggy residual quartz. Using this observation,

exploration was conducted in the early 2000s below barren steam-heated alteration in the northeast part of the district (Illanes et al., 2005). At the South Purén target, a complete steam-heated profile, including intense kaolinite, opal, and S^0 and an underlying horizon of massive opal (Fig. 13a), was tested without success. Three kilometers to the north, drilling through 50–80 m of similar steam-heated alteration of tuffs intersected hypogene intermediate-sulfidation Ag-Au-Zn-Cu-Pb ore associated with silicification within an envelope of illite alteration, leading to the discovery of the ~ 60 t Au equivalent Purén Norte deposit (Arribas et al., 2005; Illanes et al., 2005).

Essentially the same geologic model was applied successfully for the discovery in 2011 of the Salares Norte deposit, 75 km northeast of Purén. A 96 t Au and $\sim 1,200$ t Ag deposit was discovered at a depth of ~ 200 m beneath a ≤ 120 -m-thick horizon of steam-heated alteration of kaolinite, cristobalite, S^0 , and chalcedony (Azevedo et al., 2015). Similar to Purén

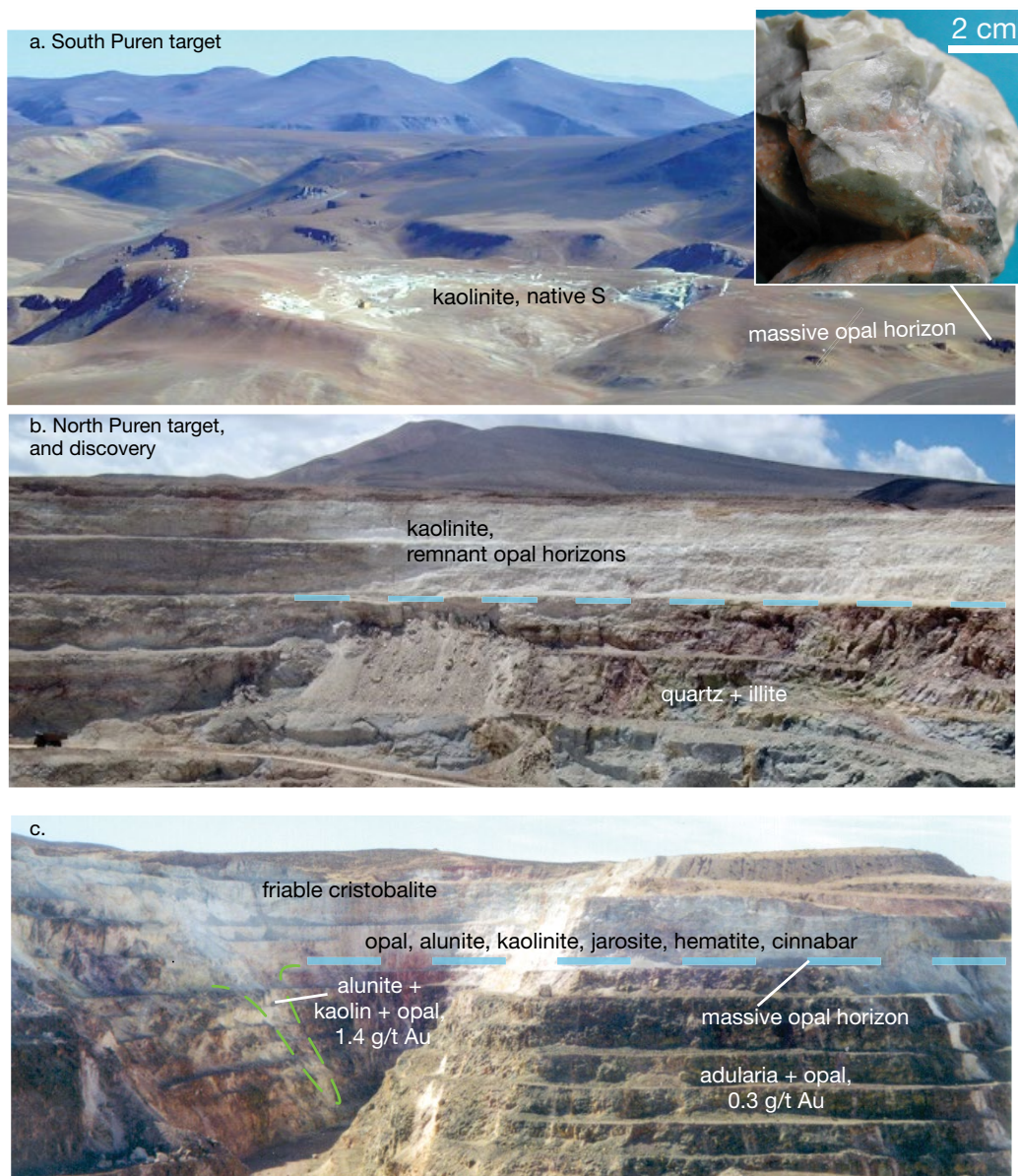


Fig. 13. Horizons of steam-heated alteration over the a, b) Puren, Chile, and c) Crofoot-Lewis, Nevada, epithermal deposits, intermediate and low sulfidation, respectively. a) Steam-heated kaolinite at South Puren, underlain by horizon of massive opal replacement of a crystal lithic tuff (inset, latter with conchoidal fractures). b) The North Puren deposit underlies a 30+-m-thick horizon of steam-heated kaolinite, including remnant horizons of conchoidal-fractured opal, overlying deposit; Ag-Au is hosted by quartz-illite alteration (haul truck, lower left, for scale). The deeper part of the steam-heated horizon returned up to 3 ppm Ag anomalies where overlying the deposit, in contrast to <0.3 ppm Ag background values (Arribas et al., 2005). c) South pit, Crofoot-Lewis deposit, looking south, with tens-of-meters-thick horizon of steam-heated alteration, overlain by historically mined S⁰ deposits, leading to the original name of Sulphur. A falling water table (Ebert and Rye, 1997) caused an overprint of low-grade (0.3 g/t Au) adularia-opal alteration, resulting in remobilization of Au and Ag with alunite and kaolinite in fracture zones below the horizon of steam-heated alteration. Silica sinters and silicified lacustrine sedimentary horizons occur a few kilometers north of and at lower elevation than the original area of steam-heated alteration, which lies over the ore deposits; evidence has been cited for at least 50 m of fluctuations in the paleowater table, both falling and rising (Ebert and Rye, 1997).

and elsewhere, the friable, steam-heated altered rocks at Salares Norte are low density and host at least two irregular chalcedony horizons related to multiple levels of the paleowater table (Azevedo et al., 2015). Although jarosite is a common supergene mineral, as at Salares Norte (Azevedo et al., 2015), there is stable isotopic evidence that the mineral may form in steam-heated conditions, at Crofoot-Lewis and elsewhere

(e.g., Pascua-Lama; Deyell et al., 2005), as well as in other acidic environments (Rye and Alpers, 1997), consistent with a wide range of formation temperatures (Stoffregen, 1993).

Ebert and Rye (1997) conducted a detailed study of the extensive steam-heated alteration zone at the Crofoot-Lewis (Hycroft) mine, a low-sulfidation Au-Ag deposit in northern Nevada. Gold was discovered through drilling in the early

1970s in the historical Sulphur district, where native sulfur production in the late 1800s was followed by production of silver, cinnabar, and alunite during the first half of the 20th century, all within a district-scale steam-heated zone. Between the surface outcrops, exploration drill holes, and recent mining exposure, it is evident that the Crofoot-Lewis deposit represents a well-preserved epithermal system (Wallace, 1987), formed at ~4 Ma. This includes (1) vertically zoned steam-heated acid-sulfate alteration, consisting of an upper skeletal residue of powdery quartz plus cristobalite with lesser amounts of opal-A (amorphous silica), alunite, kaolinite, gypsum, cinnabar, S⁰, hematite, and jarosite, and a lower, 1- to 12-m-thick horizon of massive opal ± alunite, kaolinite, and hematite; (2) a distal (~2 km north of the South Pit) 7-m-thick outcrop of silica sinter and silicified lacustrine sediments that define the paleosurface; and (3) the deeper alteration zone of quartz-adularia-pyrite with subvertical Au-Ag-quartz veins (Fig. 13c; Ebert and Rye, 1997). The thick steam-heated horizon at Crofoot-Lewis (up to 80 m in the Brimstone pit) was attributed to a falling water table, which may have caused remobilization of gold and silver and subsequent enrichment in fractures below the water table (Fig. 13c; Ebert and Rye, 1997).

About 170 km east of Crofoot-Lewis, also in Nevada, the low-sulfidation vein and disseminated Au-Ag deposits of the Ivanhoe/Hollister district occur below a horizon of opal and chalcedony several tens of meters thick, with the conchoidal-fracturing material quarried for tools and arrowheads by ancient Native Americans. This horizon extends for up to 2+ km away from the deposits toward the northwest quadrant (apparently the hydraulic gradient of the paleowater table), with local concentrations of cinnabar mined during the early 20th century, prior to the discovery of economic Au-Ag mineralization in the 1980s (Wallace, 2003). A similar 2-km-long chalcedony horizon is associated with the Furtei epithermal deposit in Sardinia, albeit of high-sulfidation affiliation, hosted by a layered volcano-sedimentary unit, which is anomalous in Hg and As and associated with kaolinite and nacrite (Ruggieri et al., 1997).

As noted above, in low-relief settings with small hydraulic gradients, stagnant groundwater in areas of steam-heated acid-sulfate condensates can evaporate and generate acidities with pH 1.5–2 (Nordstrom et al., 2009), such that aluminum can be leached. This situation explains the formation of friable powdery silica-altered tuff in the midst of steam-heated alteration that has been mined for silica at Silicon, Nevada (Coolbaugh et al., 2020), and elsewhere.

Larson et al. (2009) document over 200 m of water-table descent in the Grand Canyon of Yellowstone, due to erosion by the Yellowstone River since the end of the Pinedale glaciation at ~14 ka. This extreme example of synhydrothermal erosion has resulted in silica sinters, as well as chalcedony horizons related to steam-heated alteration, occurring far above the present water table, with an overprint of the underlying quartz-illite-pyrite ± adularia alteration; discharge of hot springs depositing silica sinter now occurs in the valley bottom. Buchanan (1979) and Simmons (1991, 2017) each noted evidence of steam-heated blankets in large epithermal mining districts of Mexico, where ore grades in quartz veins typically occur 200–300 m below the paleowater table (Simmons,

1991; Megaw, 2010). However, epithermal ores can also form near the paleowater table, close to the base of silica sinters (e.g., McLaughlin, California, and Fruta del Norte, Ecuador, deposits; Sherlock et al., 1995; Leary et al., 2016).

In all respects, the mineralogy (kaolinite ± alunite, with pyrite/marcasite and S⁰ plus Hg anomalies) and morphology (flat-lying blankets of alteration underlain by opal/chalcedony silicification at the paleowater table) of this alteration type is similar, regardless of style of hydrothermal system and potential ore deposit (Sillitoe, 1993).

Relevance to exploration

Regardless of the type of epithermal deposit, the presence of a horizon of steam-heated alteration indicates a shallow level of erosion and thus preservation of the deeper hydrothermal system. Perhaps nowhere is this relationship as clearly illustrated as in the giant Pascua-Lama high-sulfidation Au-Ag-Cu deposit in Chile-Argentina, where 675 t Au and 24.3 kt Ag are contained within breccia bodies in an ~200-m subhorizontal mineralized horizon of residual quartz and hypogene acid-altered rock, which is covered by a 150- to 300-m-thick steam-heated zone of low-grade to barren opal, chalcedony (now recrystallized to quartz), kaolinite, and S⁰ (Fig. 14; Chouinard et al., 2005; Deyell et al., 2005). Adjacent to this extensive steam-heated alteration in an area originally known as Nevada, shallow mineralization is present in altered outcrop (Sillitoe, 1995b).

Steam-heated alteration is typically friable and easily eroded; even where present, identification of its origin may not be straightforward, in part because of potential overprinting by surficial oxidation. Its recognition is aided by an understanding of the genetic processes and of the main structural features of a magmatic-hydrothermal system (Fig. 1) and by the development of a working hypothesis that needs to be tested through collection of a broad range of evidence. Features to look for include a broadly tabular shape subparallel to the surface; a white, friable, sponge-like, low-density rock with a mineralogical association that includes low-temperature forms of silica minerals, such as opal-CT and chalcedony; and commonly abundant kaolinite as well as S⁰ and/or finely crystalline alunite, plus local cinnabar and/or metacinnabar (Table 2). A basal layer of massive silicification is common (opal or chalcedony, albeit recrystallized to cryptocrystalline and conchoidal-fracturing quartz), potentially extending 2+ km from source; since it is a resistant unit, there is commonly topographic inversion.

An excellent description of alteration mineralogy, texture, and morphology of such a zone was provided by Davies and Ballantyne (1987) in an early paper on the giant alkaline epithermal gold discovery on Lihir Island, Papua New Guinea (Carman, 2003). They wrote (p. 282), “Advanced argillic: White to light gray rocks consisting entirely of kaolinite-alunite-opal-pyrite + native sulphur are common in an horizon immediately below the base of oxidation in the Coastal, Lienetz and Minifie areas.... Advanced argillic material contains ore grade mineralisation more commonly than argillic material.... White rock is a distinctive, white porous material which appears to be the oxidized equivalent of the advanced argillic ore type.” Although they used the term “advanced argillic” to classify this alteration, they concluded a steam-heated origin and

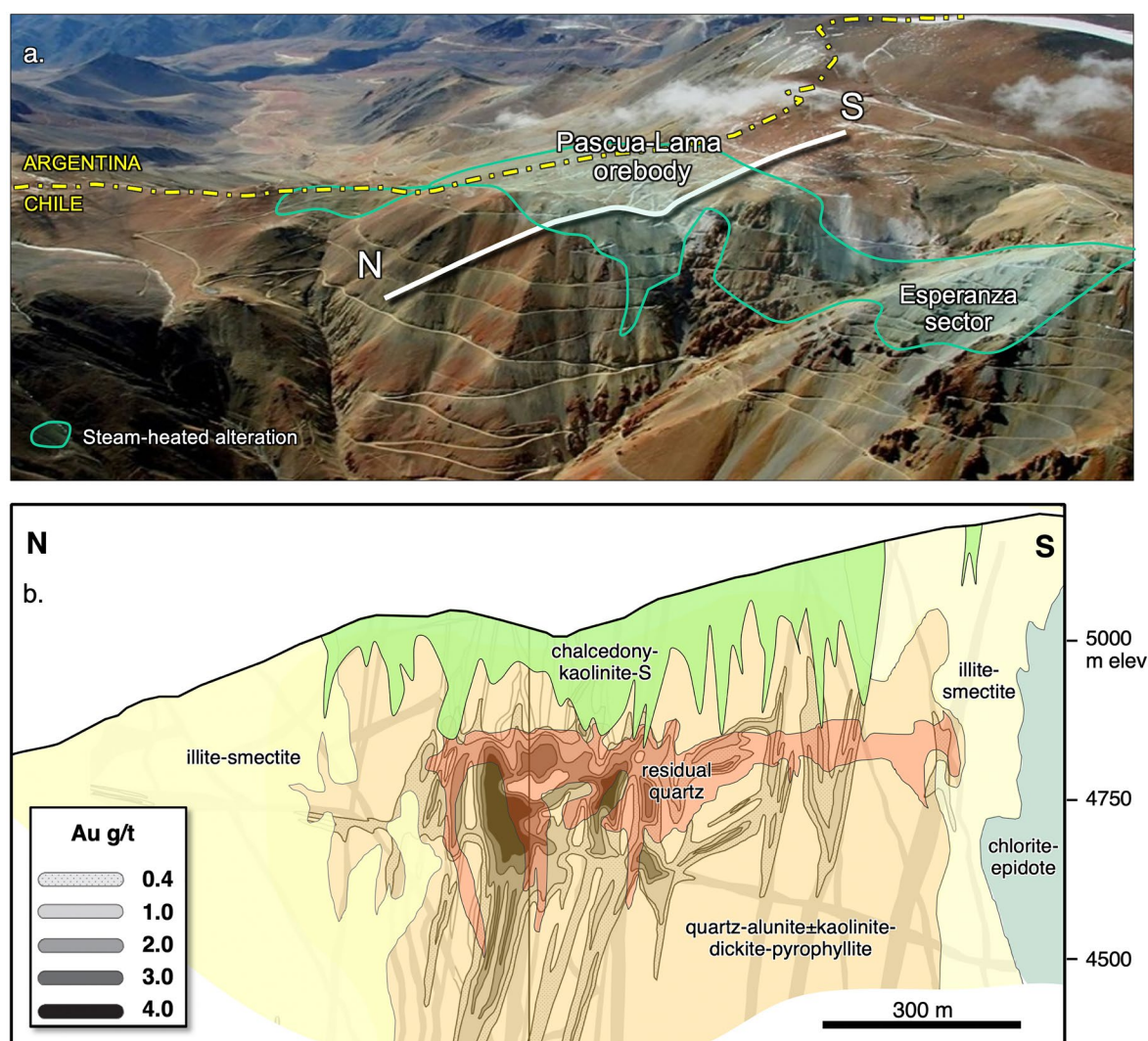


Fig. 14. a) Oblique air view looking southeast over Pascua-Lama Au-Ag-Cu deposit, straddling border between Chile and Argentina in the Central Andes at elevation ~5,000 m (image: Barrick Gold). The approximate extent of steam-heated acid-sulfate alteration (from Chouinard et al., 2005) shown in green. b) North-south cross section through Pascua-Lama notes wall-rock alteration minerals and gold concentrations (modified from Chouinard et al., 2005). The deposit is centered on the Brecha Central orebody, which forms the steep core of high-grade mineralization in this section.

suggested it was mineralized because of a lowering of the water table, which resulted in an overprint of earlier ore.

Minerals such as pyrophyllite and dickite rarely form in the steam-heated environment, because of their typical higher-temperature stability (Fig. 3), and diaspore and zunyite plus topaz never do. However, these minerals, like resistant outcrops of hypogene residual quartz, may be inherited if a downward-migrating water table results in an overprint by steam-heated alteration. Similarly, white mica (illite or muscovite, formed at >200°C; Fig. 3), should not be present within the steam-heated zone unless the deeper, neutral-pH fluid environment was subject to overprint by a falling water table (e.g., at Yellowstone; Larson et al., 2009). Conversely, a rise in the paleowater table (e.g., due to synhydrothermal deposition of volcanic products) may lead to aggradation and higher-temperature overprint of steam-heated alteration (Sillitoe, 2015). Identification and documentation of any structure, such as faults, fractures, breccia bodies, high-angle altered zones, or

veins, as well as permeable lithologies (e.g., tuffs) that indicate the paleopermeability of the hydrothermal system may provide guides to mineralization present beneath steam-heated zones. A key genetic consideration to keep in mind during exploration is that the formation of steam-heated alteration in all environments requires H₂S-containing vapor derived from boiling of a hydrothermal liquid (Buchanan, 1981); this boiling at depth represents a common mechanism for mineral deposition in many epithermal deposits (e.g., Hedenquist et al., 2000).

Steam-Heated CO₂-Rich Condensates

Formation conditions

White (1957, p. 1650) noted that “sodium bicarbonate waters” occur where vapor that contains CO₂ and H₂S condenses “below the zone of easy access of air,” i.e., implying a lack of O₂ to oxidize H₂S to sulfate, as in the vadose zone. Such

Table 2. Comparative Features of Different Formation Environments of Hydrolytic Alteration

Feature	Cooling of white-mica-stable fluid	Hypogene acid-sulfate-chloride	Steam-heated acid-sulfate	Steam-heated CO ₂ -rich	Supergene oxidation
Alteration type	Advanced argillic	Advanced argillic	Advanced argillic	Intermediate argillic	Advanced argillic
Alteration mineralogy	wm ± anh ± and → prl, dsp, dk	rq core, halo of qz-al, qz-ka ± dk ± prl, outer halo of wm or I/S	al, ja, ka, sm, underlain by opal, chalcedony, deeper clays, (jarosite?)	wm (illite) ± ka, I/S, sm, chl, sid, Mg-Mn carb, cal	ka, al, FeOOH (jarosite)
Associated sulfides	py ± cp, tn-td, en, bn-dg-cc-cv	py, S disseminated; where subsequently mineralized, en, lz, cv, bn-py, Au, te, tn-td, S ⁰	S ⁰ ; py at base	py, marcasite	py oxidized, Cu enrichment blanket (cc) possible at base
Silica mineralogy	Pervasive qz with wm, prl	Widespread rq, common dense silicif (chal) after leaching; laminated in open space (originally black due to py, Ox to gray, cream, or white color)	Local friable rq; opal-CT (chal) horizon (replacement) at water table, latter resistant to erosion	Variable silicif	Minor silica remobilization, porous
Textures	prl after wm, pervasive; nodular prl (dsp, dk, py) replacement of rq, qz-al at lithocap base	rq reflects original rock texture, ± vuggy; rq, and qz-al-py resistant (qz-al-py friable if py ox and al leached, qz saccaroidal)	ka, al friable	Replacement	Overprint
Form, morphology of alteration zone	Locally pervasive, commonly related to structures; halo over wm	Structural control to feeder; lithocap where permeable horizon is intersected; rq, qz-al resistant, cliff former	Blanket, replacement of aquifer horizon (e.g., air fall tuff), typically friable; opal horizon at base	Pervasive, in hanging wall of veins; 100s m below paleowater table	Blanket, formed above paleowater table
Geochemical anomalies	Cu (Au, As, Sb)	Initial barren lithocap: Au <10–50 ppb, As-Sb <100, Cu <100, Mo <20, Zn <20, Pb (al) <200 ppm (where subsequently mineralized, high Au, Ag, Cu, As, Sb, Te, Bi ± Mo)	Hg (overprint of deeper anomalies if falling paleowater table)	Marginal expression of deposit, may be late; commonly as overprint	Reflects primary mineralization, except where elements supergene mobilized; leached capping
Geophysical anomalies	Early mt destroyed, negative magnetic anomaly	rq-py: >>1,000 Ω-m, chargeable high (if rq oxidized: chargeable low); qz-al, <1,000 Ω-m	Shallow horizons of resistivity high due to opal	Low resistivity anomaly due to clay	py oxidized, chargeable high destroyed
Relationship to potential ore	Over potential porphyry center	Over or adjacent potential Au-(en, etc.) in rq; above, and lateral (distal) from intrusion center	Over boiling zone and up to >1–2+ km lateral (mainly opal horizon) from potential ore	Supra-adjacent boiling zone, on margins, in hanging walls	Broad extent, strongest after abundant pyrite (which may not be proximal)
Alunite texture, crystal habit, color	Minor al, fine xstals	Coarse (≤1 cm) to finer grained (~100 μm) xstal aggregates, tabular or bladed; colorless, pink, white, cream, yellow, tan, brown	Most fine (<20 μm) friable, powdery aggregates; rhombohedral xstals, cubic angles; generally white	NA	Massive, chalky porcelaneous veinlets, masses; fine (<20–50 μm) rhombohedral xstals, cubic angles; white, cream, yellow-brown (staining)

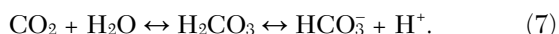
Abbreviations: al = alunite, and = andalusite, anh = anhydrite, ba = barite, cal = calcite, chal = chalcedony, chl = chlorite, dk = dickite, dsp = diasporite, I/S = interstratified illite/smectite, ja = jarosite, ka = kaolinite, Mg-Mn carb = Mg-Mn carbonate, qz = quartz, rq = residual quartz, sid = siderite, silicif = silicification, sm = smectite, prl = pyrophyllite, to = topaz, wm = white mica, zu = zunyite
Sulfides, etc.: Au = gold or electrum, bn-py = bornite + pyrite, cc = chalcocite, cp = chalcopyrite, cv = covellite, di = digenite, en = enargite, Hg = cinnabar, lz = luzonite, mt = magnetite, Ox = supergene oxidized, S⁰ = native sulfur, Te = tellurides, tn-td = tennantite-tetrahedrite, xstals = crystals

hot springs have been observed in many locations around the world, and where sampled at the surface, they have an alkaline pH and are rich in bicarbonate (HCO₃). Early compositions were reported from the Taupo Volcanic Zone, including samples from deep (>500 m) wells (but with collection

at atmospheric pressure), which Ellis and Mahon (1977) referred to as bicarbonate-rich waters, with pH ≥ 8. Similar thermal discharges were recorded from Yellowstone National Park and Steamboat hot springs in the western United States, including from shallow wells (<200-m depth at Yellowstone;

White, 1957). These springs are distinctly different from those that form large travertine terraces, caused by deep circulation of groundwater and dissolution of limestone (e.g., Mammoth Hot Springs, Yellowstone National Park).

The discovery of CO₂-rich steam-heated solutions on the margins of the Broadlands-Ohaaki system, New Zealand, was made during an investigation of external corrosion of stainless-steel well casing at 450-m depth (Fig. 15; Hedenquist and Stewart, 1985; Hedenquist, 1990). These solutions are related to CO₂- and H₂S-bearing vapors that originate from boiling liquid in the deep upflow. Such vapors condense into meteoric water on the margin of the system, below the water table, based on an assessment of their enthalpy-Cl, δ¹⁸O-δD, and Cl-δ¹⁸O compositions (Hedenquist, 1990, figs. 8, 9), generating CO₂-rich (carbonic acid) solutions:



The condensate typically forms an end-member solution at several hundreds of meters depth at a temperature of ~120°–170°C, with nil NaCl content. The formation of this condensate on the margin of the system subsequently acts as a diluent of the ascending boiling liquids (NaCl-bearing), as at Broadlands-Ohaaki (Hedenquist, 1990), Waiotapu (Hedenquist, 1991), and many other geothermal systems in the Taupo Volcanic Zone (Hedenquist, 1986) and elsewhere. Sulfate

formation in end-member CO₂-rich steam-heated condensate is minor (~20–100 ppm; Hedenquist, 1990) because of the low dissolved O₂ content in meteoric water below the water table (theoretical minimum being ~15 ppm sulfate, given the limit of 10 ppm O₂ solubility in cold groundwater). As these H₂CO₃ (carbonic acid)-rich solutions ascend, cool, and depressurize, CO₂ (and H₂S) is lost because of effervescence of the subboiling liquid, causing a pH increase and bicarbonate dominance in surface hot springs (reaction 7). Where such effervescing solutions discharge as hot springs (typically ≤70°–80°C) on the margins of geothermal systems (e.g., vigorously bubbling Artesia geyser next to Firehole Lake, Lower Geyser basin, Yellowstone National Park), Ca carbonate precipitates (personal observation, 2019).

Smectite and interstratified clays form on the subboiling margins at Broadlands-Ohaaki (Browne, 1971; Simmons and Browne, 2000), accompanied by kaolinite (plus siderite and other carbonates) at 100- to 800+-m depth (Fig. 15; Browne, 1971; Wood, 1983; Simpson and Rae, 2018). The clays and kaolinite are stable at the in situ pH of ~4.2–5.4 and 120°–170+°C, with pH value determined from the measured concentrations of 1–2 wt % H₂CO₃ (Hedenquist, 1990).

CO₂-rich solutions have been encountered in other settings, particularly associated with seafloor hydrothermal systems. Sakai et al. (1990) reported liquid CO₂ at the Jade

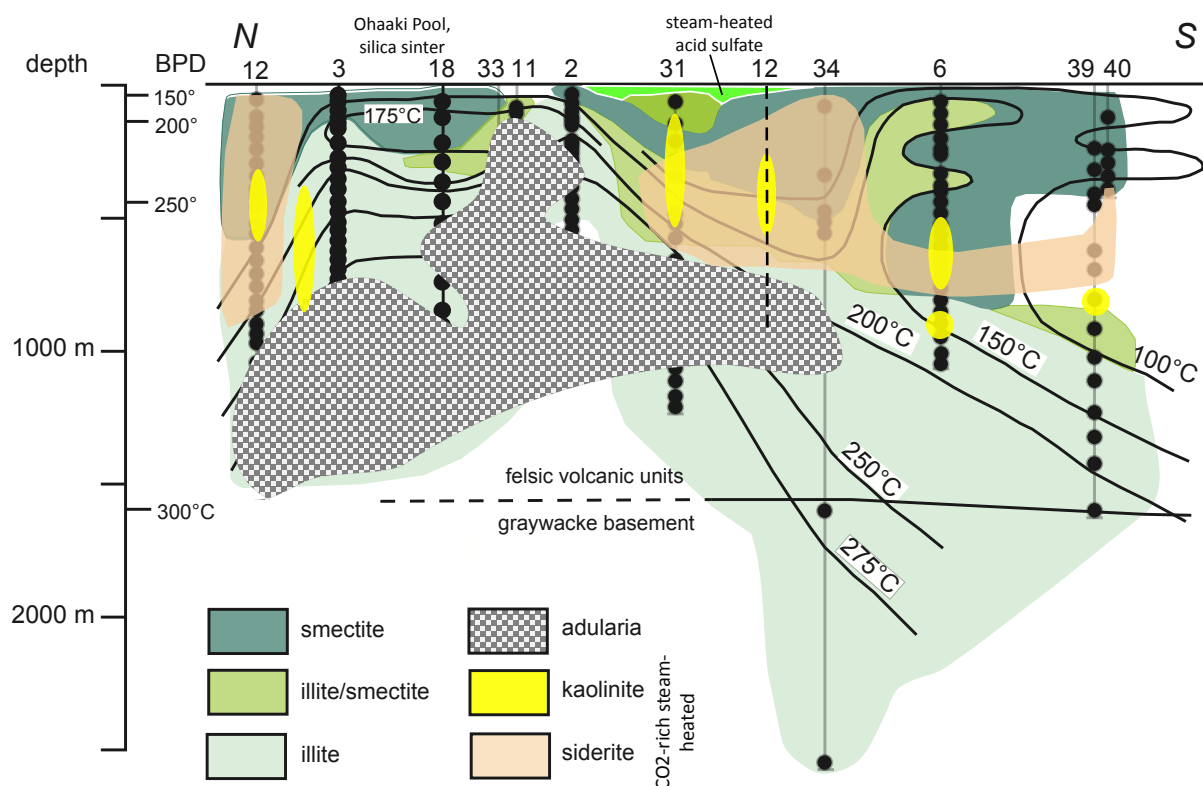


Fig. 15. North-northeast to south-southwest cross section through the Broadlands-Ohaaki geothermal system, showing the measured isotherms (Hedenquist, 1990) and distribution of temperature-dependent clay minerals and adularia (sample depths noted with closed circle on well; Simmons and Browne, 2000), as well as kaolinite and siderite on the margins of the geothermal system (Browne, 1971; Wood, 1983). The latter minerals reflect the presence of CO₂-rich condensates (~120°–170°C with pH ~4–5, stable with respect to these minerals; Hedenquist, 1990), which form a carapace (umbrella) on the margins of the upflow. The location of Ohaaki Pool, with silica sinter, steam-heated acid-sulfate alteration, and BR-12 (with casing corroded at 450-m depth) all projected onto the section from the east. The hydrostatic boiling point temperature for depth (BPD) is shown for the CO₂-bearing fluid (Hedenquist, 1990).

site, Okinawa trough, at 1,400-m ocean depth, concentrated from CO₂-rich vapor that condensed near the cool seawater interface; associated alteration includes kaolin and clay minerals (Marumo and Hattori, 1999). Such high concentrations of CO₂ in solution are likely responsible for the occurrences of kaolin-group minerals (kaolinite, nacrite, and dickite) plus interstratified clays and local pyrophyllite (at high SiO₂ concentrations) in both hanging-wall and footwall locations of VMS deposits, such as those in the Kuroko district of northern Honshu, Japan (Marumo, 1989). In a somewhat analogous situation, Fowler et al. (2019) reported the discovery of CO₂-rich thermal discharges (with nil chloride and sulfate) on the floor of Yellowstone Lake at 120-m water depth and 150°C; the alteration is dominated by kaolinite, with boehmite, mixed-layer clays, and pyrite.

Alteration mineralogy, characteristics, and relationship to ore zones

The alteration assemblage of clays and kaolinite is typical of intermediate argillic alteration (Meyer and Hemley, 1967). We include discussion of this alteration style here because, in our experience, the presence of kaolinite on the deep margins of epithermal veins may be misinterpreted as steam-heated acid-sulfate solutions that descended from the paleowater table into the mineral system (e.g., illite-kaolinite ± smectite halos to quartz veins at the Cerro Bayo intermediate-sulfidation deposit, Chile; Poblete et al., 2014). In some interpretations, both styles of steam-heated alteration, acid sulfate and carbonic acid, are combined, e.g., “referred to as the low pH assemblage. This assemblage may contain any or all of the following minerals: alunite, sericite, illite, kaolinite, montmorillonite, or any of the kaolin-clay minerals” (Buchanan, 1981, p. 252). Rather, the common presence of CO₂-rich condensates on the margins of geothermal systems, and by analogy in similar locations during the formation of epithermal (and VMS) deposits, is consistent with the occurrence of illite plus other clays, kaolinite, and pyrite, distinct from shallow-formed blankets of kaolinite and alunite in the steam-heated vadose zone, or deeper dickite-kaolinite-alunite-pyrophyllite in the hypogene acid-sulfate-chloride environment.

Evidence for a CO₂-rich steam-heated solution on the margin of a deposit was documented at Creede, Colorado, an intermediate-sulfidation epithermal vein system that displays a simple dilution trend in composition of fluid inclusion assemblages of ore samples, from about 260°C and 11 wt % NaCl equiv to ~160°C at nil salinity (Roedder, 1977; Hayba et al., 1986). Barton et al. (1977, p. 16, 17) noted that “the solutions boiled as they approached the level of the orebody, preferentially distilling the acid forming components, especially CO₂ but also H₂S,” and “the acid-forming gases recondensed at or near the top of the orebody, reacting with the wall rock to form the highly altered cappings.” The CO₂-rich condensate that formed over the orebody, in addition to acting as the diluent of the ore fluid, was also responsible for formation of the “intense, mixed-layers illite/smectite alteration cap ... interpreted to have been generated by condensation along the top of the system of acid volatiles distilled off the deeply circulating ore fluids” (Hayba et al., 1986, p. 151). Horton (1985) recognized a change in the illite/smectite alteration in the hanging wall to the Amethyst vein, with a progressive increase

in the illite component of the interstratified clay as the vein was approached. Rhodochrosite and siderite are observed in the deposit, but kaolinite has not been reported.

Relevance to exploration

The occurrence of CO₂-rich steam-heated alteration on the margins of shallow-formed epithermal (and VMS) deposits may be expected in any system with CO₂- (and H₂S-) rich vapor that is derived from boiling at depth. However, its presence appears to be most common on the margins (and in late stages) of low- and intermediate-sulfidation vein deposits, with dilution trends of fluid inclusion data to nil salinity at ~150°–180°C being additional evidence.

The Kupol deposit in Chukotka, Russia, is a low-sulfidation epithermal vein system of Jurassic age that has a low sulfide content and high gold grades, discovered in outcrop. Exploration of the vein where its surface expression terminated to the north revealed that the clay alteration halo changed from illite to smectite in the vicinity of a crosscutting fault. Drilling indicated that the lithologic units had been downfaulted to the north, with a thick sequence of low-paleotemperature smectite in the hanging wall to the vein. At 200-m depth the clay changes from smectite to illite, then illite-kaolinite, followed 100 m deeper by an ore zone with chlorite-illite alteration halo (Fischl et al., 2013; B. Thomson, unpub. data, 2021), the chlorite reflecting the andesitic nature of the host rock. This clay (illite)-kaolinite intermediate argillic alteration assemblage, with pyrite, is interpreted as being due to a steam-heated CO₂-rich solution in the hanging wall of the vein. Determination of the clay zonation assisted the assessment of vein potential (i.e., as a paleodepth indicator) in the district, contributed to the discovery of a satellite orebody at Moroshka (Fischl et al., 2013), and helps to guide further exploration in the district (B. Thomson, unpub. data, 2021).

The Rosebud deposit, located ~9 km south-southeast of the Hycroft mine, contains ~1 Moz Au with local bonanza grades. Hecla mined 0.4 Moz of gold from underground in the late 1990s, over a vertical interval of ~150 m, at an average grade of ~12 g/t Au. Cuffney (2008) describes early white-mica alteration with minor pyrite and marcasite, followed by the gold stage of quartz-pyrite-bladed marcasite stockwork veinlets with electrum and chalcopyrite and a subsequent silver-rich stockwork with Mn- or Fe-rich calcite, followed by late barite and stibnite veins. Cuffney (2008, p. 20) notes “a distinct correlation between fracture fillings of white clay (illite and dickite/nacrite with lesser kaolinite and smectite) and higher gold grades.”

The Kelian intermediate-sulfidation deposit in Kalimantan (van Leeuwen et al., 1990) produced 179 t Au (from 241 t contained Au) at an average grade of 2.65 g/t. Mineralization is associated with multiple phreatomagmatic and hydrothermal breccia bodies (Davies et al., 2008). During the waning of activity, the orebody was overprinted by an association including kaolinite (locally intergrown with white mica)-Fe/Mn carbonate-pyrite/marcasite ± hematite ± cinnabar, which van Leeuwen et al. (1990) interpreted was caused by the ingress of CO₂-rich liquid from the margins. The kaolinite and/or dickite is associated with carbonates (siderite and rhodochrosite plus Mg/Mn kutnahorite and calcite), mostly at <300-m depth, locally present at 600 m. Davies et al. (2008) suggested

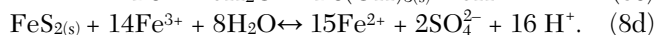
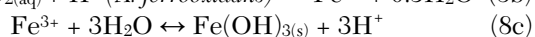
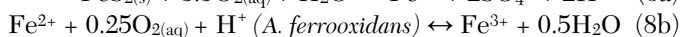
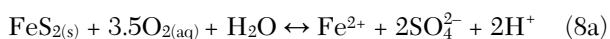
that the late kaolinite cement may have been supergene, but its association demonstrates a clear hypogene origin (van Leeuwen et al., 1990).

Supergene Oxidation of Sulfide Minerals

Formation conditions

Supergene oxidation of sulfide minerals (mainly pyrite) requires atmospheric O_2 in order to proceed; therefore, the process is restricted to the vadose zone, like steam-heated acid-sulfate generation, and for this reason there are similar features shared by the two environments. For example, the water-table limit results in alteration zones that form blankets. In addition, bacterial activity is also recognized as a critical catalyst in the process of pyrite oxidation (Singer and Stumm, 1970; Nordstrom and Southam, 1997; Mielke et al., 2003; Enders et al., 2006), the principal source of sulfuric acid solutions in the posthydrothermal supergene (or weathering) environment.

During supergene oxidation of pyrite, the ferrous to ferric reaction—mediated by bacteria—is essential to the decomposition of pyrite, deposition of Fe oxyhydroxide, and formation of aqueous sulfate that leads to hydrolytic alteration (Singer and Stumm, 1970):



Alteration mineralogy, characteristics, and relationship to ore zones

Historically, the supergene oxidized part of a primary deposit is often the first sign of metallic mineralization because of its conspicuous outcrops (i.e., the presence of a surficial gossan of Fe hydroxides or secondary metallic mineralization). In addition to hematite, goethite, and other Fe oxyhydroxides, the surficial oxidation of sulfide-bearing deposits, typically fine-grained pyrite, results in acidic (as low as pH <1) H_2SO_4 -rich waters within the vadose zone that may form alunite, jarosite, kaolinite, and halloysite, all minerals that fall under the advanced argillic umbrella. These downward-migrating supergene solutions form topography-influenced horizons within the weathering profile, above the paleowater table and commonly underlying leached cappings or gossans. Where protore mineralization is vein controlled, the alteration may occur as curtains along structures over vertical distances up to a hundred meters or more (Fig. 16a; Rye et al., 1992).

Kaolinite, halloysite, and/or alunite of supergene origin have been documented in a wide variety of mineral deposit types, including porphyry copper (Emmons, 1917; Sillitoe and McKee, 1996; Sillitoe, 2005), epithermal (Sillitoe and Lorson, 1994; Arribas et al., 1995b; Nash et al., 1995; Deyell et al., 2005; Warren et al., 2008), VMS (Matos et al., 2003; Tornos et al., 2017), and Carlin-type (Arehart et al., 1992) deposits, among other sulfide-bearing deposit types (e.g., Bird et al., 1989). In addition, supergene alunite and/or kaolinite (or halloysite) may form in environments other than those associated with hydrothermal ore deposits, including (1) inland lakes in Australia, where marine sulfate aerosols

from the ocean that accumulated over long time periods mix with groundwater in basins (Bird et al., 1989), (2) weathering oxidation of fine-grained pyrite in black shales or metamorphic rocks (e.g., Silurian black shales in Central Spain; Cañada Guerrero, 1974), or (3) alunite found in caves, together with hydrated halloysite, as sediments within carbonate bedrock pockets caused by acid generated from the oxidation of H_2S -bearing basinal solutions (e.g., at Carlsbad Cavern, New Mexico; Polyak et al., 1998).

The timing of supergene alteration in most cases is substantially younger than the hypogene sulfide mineralization—a reflection of the time needed for it to be exposed by erosion. Sillitoe (2005) noted at least 10 m.y. from hypogene porphyry copper formation to first exposure to supergene alteration in the central Andes, although timing is dependent on local geologic histories. In the Rodalquilar high-sulfidation Au-Ag deposit, the age of supergene alunite (4–3 Ma) coincides with the removal of a coral reef cover sequence and exposure of the primary ores (avg age ~10.8 Ma) to surficial weathering, in response to accelerated erosion in the region during the Mediterranean Messinian Salinity Crisis of aridity at ~6–5 Ma (Fig. 16; Arribas et al., 1995b). However, some supergene oxidation of shallow-formed epithermal deposits may begin during the waning stages of hydrothermal activity. This was suggested to have occurred at deposits such as Pierina, Peru (Fifarek and Rye, 2005; Rainbow et al., 2005) and Pascual-Lama (Chouinard et al., 2005; Deyell et al., 2005).

In addition to erosion and exposure to atmospheric oxidation, tectonically induced uplift and climatic conditions also have a crucial role. The arid and semiarid climates resulting from uplift of the central Andes during much of the Tertiary favored supergene alteration and the development of chalcocite enrichment blankets in many copper deposits of the region (Quang et al., 2003; Sillitoe, 2005). By contrast, onset of hyperarid conditions in northern Chile in the mid-Miocene ended the formation of supergene alunite-kaolinite there (Alpers and Brimhall, 1988; Sillitoe and McKee, 1996; Arancibia et al., 2006).

Relevance to exploration and mining

Supergene oxidation of sulfides leads to metals such as copper, and to a much lesser extent gold and silver, being mobilized; the latter two typically remain in place (Sillitoe, 2009). A factor of economic significance in gold deposits is the breakdown of refractory sulfides, allowing metal recoveries at much lower cutoff grade by cyanide heap leaching; where gold is present in arsenian pyrite, after release, arsenic may be absorbed onto Fe oxyhydroxides or incorporated into scorodite.

The oxidation of copper-bearing sulfides, particularly in porphyry deposits, and the formation of zones of supergene enrichment or transported, exotic deposits, have been discussed extensively, particularly their importance to the economics of copper resources (e.g., Sillitoe, 2005). In addition, weathering can also influence our understanding of the primary deposit. For example, attempts to date the supergene alunite at El Salvador met with poor results (Gustafson et al., 2001), due to the supergene alunite partially altering hypogene alunite, resulting in mineral mixtures. This can be identified by sulfur isotope analysis of the alunite (Watanabe and Hedenquist, 2001), which led to successfully identifying and dating hypogene alunite (Hedenquist et al., 2020). In turn,

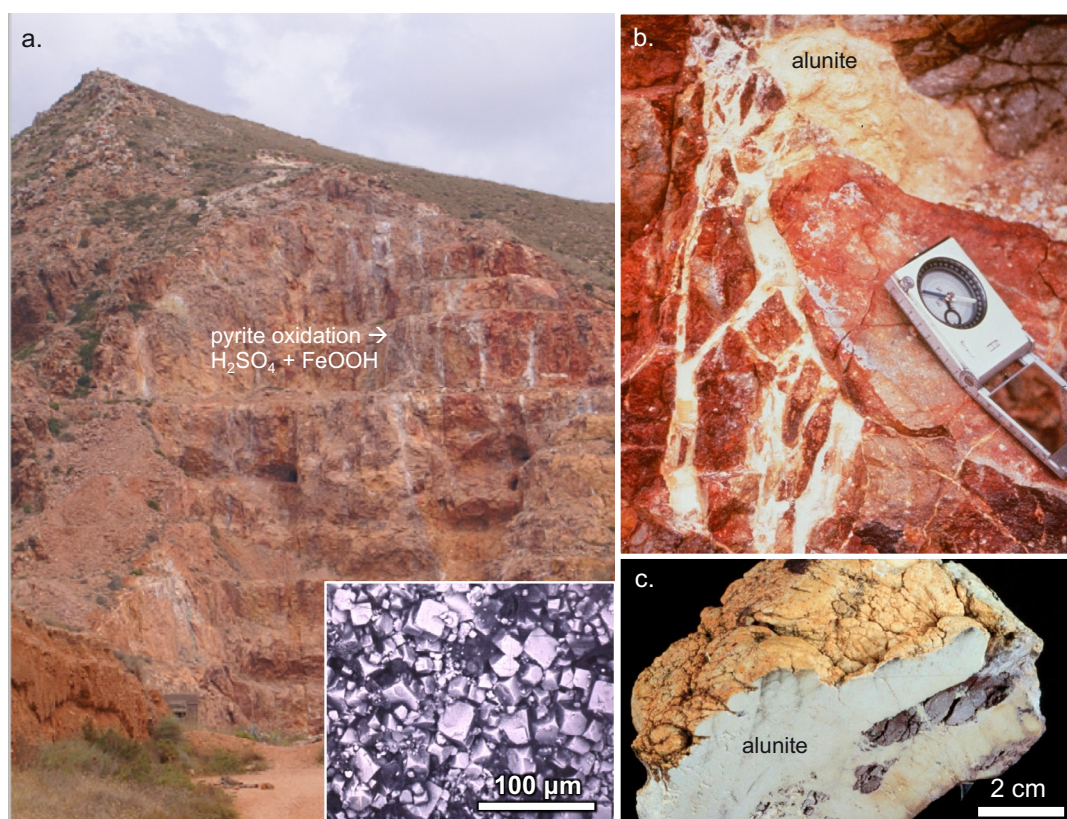


Fig. 16. a) Supergene alteration overprint of high-sulfidation Au deposit, Rodalquilar, Spain (Arribas et al., 1995b). Pyrite in hypogene residual quartz and marginal quartz-alunite-kaolinite (avg age: 10.8 Ma) was supergene oxidized to ~100 m below the present surface at 4–3 Ma. b, c) Supergene alunite forms thin to locally blocky cryptocrystalline veins that cut all previous alteration and can be associated with supergene kaolinite, jarosite, and hematite. Inset: Scanning electron image of supergene alunite, which is fine grained (<1–50 μm) with typical pseudocubic morphology.

the recognition of hypogene alunite with a younger age than that of the El Salvador porphyry copper deposit (~38 vs. ~41.5 Ma; Hedenquist et al., 2020) highlighted the potential for an undiscovered, blind porphyry copper deposit in the district.

Supergene oxidation of hypogene quartz-alunite-pyrite has been recognized over several high-sulfidation ore deposits, most notably Yanacocha (Longo et al., 2010). Oxidation of pyrite produces sufficiently acidic solutions to leach the alunite, leaving only the quartz component, which is informally called “granular silica,” given the saccharoidal appearance of the typically friable remnant quartz. This portion of the lithocap may be barren or contain low grades of gold (whatever was originally in the quartz-alunite-pyrite but upgraded because of the decrease in density). This supergene alteration can lie above or below residual quartz that may be ore and commonly occurs adjacent to quartz-alunite, where the amount of oxidized pyrite was insufficient to result in alunite dissolution. Huge expanses of granular silica, e.g., in the Yanacocha district (Pilco and McCann, 2020), cannot form from steam-heated acid-sulfate condensates, since most of these solutions do not develop sufficient acidity to mobilize aluminum.

Webster and Mann (1984) reviewed the redistribution of secondary gold and silver through the weathering profile, noting that this is dependent on the nature and stability of anionic complexes present in fluid of the oxidized zone, which is influenced in large part by the hypogene mineralogy of the deposit,

as well as by topography and climate. For example, sulfide oxidation in Western Australia occurs in acidic, chloride-rich groundwater, formed by seawater aerosol chloride concentration by evaporation in the desert environment. This solution causes electrum dissolution and secondary gold reprecipitation by reduction at the site of iron oxidation. In contrast, in the jungles of Papua New Guinea, heavy rainfall in a region of high relief causes dilution of groundwater, preventing the development of acidic conditions. Where carbonate-rich veins are oxidized, the pH remains neutral and electrum dissolution causes gold and silver to be transported as thiosulfate complexes and reprecipitation with a similar composition. However, Stoffregen (1986) demonstrated that during oxidation of sulfides hosted by residual quartz of Summitville, i.e., lacking the Fe-rock buffer, the supergene chloride-poor acid-sulfate solutions dissolved primary electrum, with minor gold and limited silver transport. A similar conclusion for limited supergene remobilization of gold and silver was reached by Sillitoe and Lorson (1994) for the Paradise Peak high-sulfidation deposit in Nevada. Unlike copper, secondary enrichment concentrations of silver as Ag sulfides, although locally occurring, are not considered to be of major economic significance (Sillitoe, 2009).

Discussion

Several different genetic environments form minerals that can be classified as advanced argillic, as documented above.

In addition, kaolinite of intermediate argillic alteration may potentially be misinterpreted as having formed in an advanced argillic environment. Where in contact, alteration formed in these different environments reflects either evolving (gradational) physicochemical processes or a different timing of formation. As shown schematically in Figure 1 for magmatic-hydrothermal systems developed in volcanic arcs, the locations of these different acidic environments correspond to distinct spatial domains with respect to associated ore deposits. Five environments have been examined here, although others may be possible in different magmatic settings (e.g., Kreiner and Barton, 2017).

The potential for overprinting among these alteration environments is particularly high within specific parts of the system, such as the shallowest region of hypogene acid-sulfate-chloride alteration, which may be overprinted by both steam-heated acid-sulfate as well as supergene alteration due to syn- and posthydrothermal erosion, respectively. Thus, the end result may be particularly complex and difficult to decipher. In this context, the correct identification of the formation environment of alteration is one of the most effective tools to guide exploration for precious and base metal mineralization. Because of the reasons explained here, with few exceptions, we recommend the use of mineralogy on maps and sections, as well as mineralogic diagrams, versus lumping of numerous alteration minerals into the singular terms “advanced argillic” or “argillic” (“intermediate argillic”), etc., during early stages of prospect assessment.

The main features to focus on in order to be able to distinguish these different alteration environments are based on mineralogy, rock and/or mineral textures, and morphology of the alteration zone. Through careful documentation (e.g., field mapping and core logging) of the mineralogy and associated alteration textures, including paragenetic evolution and evidence for overprinting, the morphology of different alteration zones and stages can be determined and the resulting hypotheses tested during more advanced stages of exploration. Combined with data collected from other exploration methods, such as geologic/structural mapping, geochemistry, geophysics, spectroscopic techniques, this information can then be used to interpret alteration genesis and relationship to potential ore zones.

Criteria for distinction

Alunite is of particular interest among the minerals discussed here (Bethke, 1984; Rye et al., 1992; Sillitoe, 1993), as it forms in several of the environments in Figure 1, and its field characteristics are typically easy to distinguish. Alunite of the hypogene acid-sulfate-chloride environment commonly forms clast or phenocryst pseudomorphs and can line cavities with tabular or bladed crystals large enough to identify with a 20× hand lens (Figs. 5, 6c; Table 2; Sillitoe, 1993; Hedenquist et al., 2000). These textures and crystal habits contrast with those of alunite in the steam-heated acid-sulfate and supergene environments, where alunite is typically fine grained (i.e., too fine to distinguish crystals with a hand lens) and powdery or chalky, with a rhombohedral (often pseudocubic) crystal habit (Table 2). Many geologic and mineralogic features of the steam-heated acid-sulfate and supergene environments are similar, including, in the case of alunite, a potentially comparable age of

formation and similar chemical composition and fine-grained crystallinity. However, supergene alunite can be distinguished from the steam-heated variety by distinctive textures: commonly massive, porcellaneous veinlets and patches and local replacement of wall rock (Fig. 16c) versus friable, powdery, and low density, respectively (Table 2). In addition, Fe oxyhydroxide minerals are typical products of supergene alteration.

Techniques to help constrain the environment of formation, such as O/H and S isotope systematics (Field, 1966; Rye et al., 1992; Rye, 2005), require careful mineral separation (e.g., Wasserman et al., 1992; Arribas et al., 1995b) but increasingly straightforward analytical procedures. Although not necessarily a tool to use during most exploration programs, published research (e.g., Rye et al., 1992; Arribas, 1995) demonstrates that stable isotopic systematics can provide constraints on geologic and genetic environments (Fig. 9; Table 2). For instance, the $\delta^{34}\text{S}$ value of alunite formed in the hypogene acid-sulfate-chloride setting is typically heavy, whereas alunite formed in the two low-temperature vadose zone environments will be lighter and similar in composition (Fig. 9; Field, 1966; Bethke, 1984), since they reflect the isotopic ratio of H_2S in the steam-heated condensate ($<100^\circ\text{C}$) or in the sulfides undergoing supergene oxidation ($<40^\circ\text{C}$), with low temperatures precluding fractionation (Rye et al., 1992). A good example is provided by John et al. (2019, table 2, fig. 9), where alteration mineralogy, morphology of the zones, and stable isotopic compositions were all used effectively to reconstruct the complex hydrothermal history of the Brokeoff volcano, Lassen volcanic center, California (their fig. 13).

Distinguishing mineral assemblages and alteration zone morphologies, in descriptions as well as on maps, has allowed numerous authors to interpret the mineralogy and zonation, both shallow and deep, of different deposits and districts. Recent major discoveries that have detailed mineralogic descriptions include the Apala, Ecuador (Garwin et al., 2017), and Onto, Indonesia (Burrows et al., 2020), porphyry Cu-Au deposits. However, alteration terminology can also be used loosely. Mars et al. (2019) compiled a variety of information from the Southwest United States in the region of Laramide copper porphyry deposits, including remote sensing data used to provide “regional, yet detailed, hydrothermal alteration maps” in order to identify “potential copper bearing, structurally deformed, hydrothermal systems” (p. 1096). And yet, “hydrothermal alteration units used in the study include argillic (kaolinite, alunite, pyrophyllite)” (p. 1100). This is incorrect use of the term argillic (only kaolinite is included), with alteration minerals that may potentially have formed in three distinctly different environments, including supergene, hypogene, and the transition from white mica, respectively, all at different depths and periods within the evolution of a system (Sillitoe, 2010). Lumping numerous alteration minerals into the singular term advanced argillic (or argillic) on maps or cross sections and mineralogic diagrams continues to occur in the literature on porphyry Cu and associated deposits, despite the availability of good information on mineralogy, commonly from a 20× hand lens and supported by SWIR spectroscopy.

Conclusions

One of the goals when mapping or logging is to interpret the significance of a given assemblage of alteration minerals by

being specific about the mineralogy and features of an alteration zone, as well as the relationship to sulfide assemblages (cf. Hemley and Hunt, 1992). Minerals referred to by the term advanced argillic, mainly aluminosilicates and sulfates, form in multiple and distinctly different geologic environments, and argillic alteration also includes a mineral, kaolinite, that is part of some advanced argillic assemblages. For this reason, identification of the minerals present and description of the alteration occurrence, both textures and alteration zone morphology, are essential evidence to allow an informed interpretation of formation conditions and implications of alteration for exploration. The blanket use of the term advanced argillic for any occurrence of minerals in this group should be avoided during the early stages of any project, even though use of the generic term may have some use for simplification at later stages. This recommendation can also apply to the widely, and often incorrectly, used terms such as potassic, phyllic, argillic (intermediate argillic), propylitic, and other general groups that were initially introduced during the study of porphyry deposits (cf. Seedorff et al., 2005) but are now used as alteration descriptions in many ore environments. Meyer and Hemley (1967, p. 166) devised this broad alteration terminology to be useful for the "evaluation of processes of ore deposition," rather than necessarily to guide exploration targeting. At a minimum, such terms used on a project must be carefully defined and used consistently.

The principal features of the five alteration environments examined here, and their implications for exploration, include the following:

1. Pyrophyllite (and dickite \pm diasporite) may form at the top of the porphyry environment, in the transitional zone to the base of the lithocap, due to cooling of a white-mica (\pm andalusite)-stable fluid. This is the hottest setting of hydrolytic alteration, and recognition of this environment indicates location within a porphyry system.
2. Formation of residual quartz with a halo of quartz-alunite and associated alteration, accompanied by pyrite (\pm anhydrite, S^0), is caused by condensation of hypogene magmatic vapor into groundwater. The resulting solution pH (as low as ~ 1) causes leaching of all components except for SiO_2 because of the increase in aluminum hydroxide solubility at a pH < 2 . This zoned hypogene alteration is largely barren of metals (typically < 50 ppb Au, even within the residual quartz core of the alteration) because of the low concentration of Au, Cu, As, etc., in high-temperature but low-pressure volcanic vapors. Where some lithocaps are subsequently mineralized, accompanied by silicification, the gold and sulfides are related to input of an originally white-mica-stable fluid. The use of the term high-sulfidation alteration is a misnomer, since sulfidation state only refers to sulfides that may be introduced after leaching and alteration, whereas pyrite is the only significant sulfide (plus S^0) formed during the actual leaching event.
3. A condensate of low-temperature aqueous vapor ($< 70^\circ$ – $\sim 100^\circ C$ and 120° – $\sim 170^\circ C$, respectively) released from boiling of CO_2 - and H_2S -bearing liquids into meteoric water creates two environments of hydrolytic alteration. Blankets of steam-heated acid-sulfate (pH ~ 2 – 3) alteration form by the atmospheric oxidation of H_2S above the

water table in the vadose zone, leading to kaolinite and alunite $\pm S^0$ alteration. This style is not associated with metal anomalies, aside from mercury; metal anomalies spatially associated with such alteration were likely inherited from preexisting mineralization as the result of a steam-heated alteration overprint caused by a descending water table. The kaolinite is friable and easily eroded, whereas chalcedony/opal replacement at the paleowater table can result in resistant horizons and topographic inversion during erosion. Lesser known and distinctly different in distribution, steam-heated CO_2 -rich (carbonic acid) condensates (pH ~ 4 – 5) form below the water table on the margins of hydrothermal systems and commonly act as a diluent of the ascending liquid. Broad halos of clay alteration plus kaolinite and Fe-Mn carbonate minerals form in this environment, typically in the hanging walls of epithermal veins (and VMS deposits). This style of alteration is intermediate argillic, but the kaolinite is commonly misinterpreted as having formed because of an overprint.

4. Erosion and exposure of pyrite to weathering and atmospheric oxidation may generate supergene acidity, even while some hydrothermal systems are active. In most cases, however, supergene alteration is a postmineral event that overprints previous alteration assemblages. A solution with high concentrations of H_2SO_4 (pH < 1) forms within the vadose zone, creating kaolinite, finely crystalline, porcelainous alunite, jarosite, Fe oxyhydroxides, and a variety of other supergene minerals in many geologic environments.

When mapping and logging of drill core, we advocate reporting minerals and mineral assemblages. This allows crucial mineralogical information to be maintained, which is essential for exploration as well as for development (e.g., geometallurgical and engineering) studies. Identification of alteration mineralogy and mineral assemblages, incorporated with textural observations, helps to determine the alteration zone morphology, which can distinguish formation environment. This information then allows an estimation of likely erosion depths (from temperature stabilities of minerals). Assessment of metal anomalies (or their lack) must be interpreted in the context of alteration mineralogy and formation environment. Familiarity with the mineralogy relevant to the style of prospect or deposit being explored contributes to its evaluation, including awareness of the numerous minerals that can indicate formation environment and zonation during exploration-stage mapping, and minerals that are essential to quantify for mining studies, such as clays, anhydrite, and sulfides.

Acknowledgments

We dedicate this paper to J. Julian Hemley, whose landmark studies and prescient interpretations provided an understanding of the conditions leading to hydrolytic alteration and recognition of the different environments of advanced argillic minerals that we examine here. From the exploration perspective, studies by Richard Sillitoe and others provided insight on the importance of distinguishing between various alteration environments and the relevance to prospect assessment. Constructive comments by Sillitoe on an earlier version focused our discussion, and detailed reviews by David John,

Stephen Turner, and Associate Editor Anthony Longo helped to clarify our presentation.

REFERENCES

- Al Furqan, R., Watanabe, Y., Arribas, A., Sulaksono, A., and Leys, C., 2021, White mica discrimination of two overlapping sericitic alteration stages at the deep Grasberg porphyry system, Indonesia: Society of Resource Geology Annual Meeting, Tokyo, June 30–July 2, 2021, Conference Abstract, p. 23.
- Allen, E.T., and Day, A.L., 1935, Hot springs of the Yellowstone National Park: Washington, D.C., Carnegie Institution, Publication 466, 525 p.
- Alpers, C.N., and Brimhall, G.H., 1988, Middle Miocene climatic change in the Atacama Desert, northern Chile: Evidence from supergene mineralization at La Escondida: Geological Society of America Bulletin, v. 100, p. 1640–1656.
- Arancibia, G., Matthews, S.J., and Pérez de Arce, C., 2006, K-Ar and $^{40}\text{Ar}/^{39}\text{Ar}$ geochronology of supergene processes in the Atacama Desert, northern Chile: Tectonic and climatic relations: Journal of the Geological Society, London, v. 163, p. 107–118.
- Arehart, G.B., Kesler, S.E., O'Neil, J.R., and Foland, K.A., 1992, Evidence for the supergene origin of alunite in sediment-hosted micron gold deposits, Nevada: Economic Geology, v. 87, p. 263–270.
- Arribas, A., Jr., 1995, Characteristics of high-sulfidation epithermal deposits, and their relation to magmatic fluid: Mineralogical Association of Canada Short Course Series, v. 23, p. 419–454.
- Arribas, A., Jr., Hedenquist, J.W., Itaya, T., Okada, T., Concepcion, R.A., and Garcia, J.S., Jr., 1995a, Contemporaneous formation of adjacent porphyry and epithermal Cu-Au deposits over 300 ka in northern Luzon, Philippines: Geology, v. 23, p. 337–340.
- Arribas, A., Jr., Cunningham, C.G., Rytuba, J.J., Rye, R.O., Kelly, W.C., Podwysoki, M.H., McKee, E.H., and Tosdal, R.M., 1995b, Geology, geochronology, fluid inclusions, and isotope geochemistry of the Rodalquilar gold-alunite deposit, Spain: Economic Geology, v. 90, p. 795–822.
- Arribas, A., Illanes, J.L., Peralta, C., and Fuentes, M., 2005, Geochemical study of the steam-heated lithocap above the Puren deposit, La Coipa mine, Chile [abs.], in Rhoden, H.N., Steininger, R.C., and Vikre, P.G., eds., Symposium 2005: Window to the World, v. 2: Reno, Nevada, Geological Society of Nevada, p. 1304.
- Azevedo, F., Brewer, N., Santos, A., Huete Verdugo, D., Baumgartner, R., Roncal, L., Trueman, A., and Foley, A., 2015, The discovery and geology of the Salares Norte epithermal gold-silver deposit, northern Chile: NewGen-Gold 2015: Case histories of discovery, Perth, Australia, 2015, Proceedings, p. 145–157.
- Barton, P.B., Jr., 1970, Sulfide petrology: Mineralogical Society of America Special Paper 3, p. 187–198.
- Barton, P.B., Jr., and Skinner, B.J., 1979, Sulfide mineral stabilities, in Barnes, H.L., ed., Geochemistry of hydrothermal ore deposits, 2nd ed.: New York, Wiley Interscience, p. 278–403.
- Barton, P.B., Jr., Bethke, P.M., and Roedder, E., 1977, Environment of ore deposition in the Creede mining district, San Juan Mountains, Colorado: Part III. Progress toward interpretation of the chemistry of the ore-forming fluid for the OH vein: Economic Geology, v. 72, p. 1–24.
- Bathkishig, B., Noriyoshi, T., and Bignall, G., 2014, Magmatic-hydrothermal activity in the Shuteen area, South Mongolia: Economic Geology, v. 109, p. 1929–1942.
- Bethke, P.M., 1984, Controls on base and precious metal mineralization in deeper epithermal environments: U.S. Geological Survey Open-File Report 84-890, 40 p.
- Bird, M.I., Andrew, A.S., Chivas, A.R., and Lock, D.E., 1989, An isotopic study of surficial alunite in Australia: 1. Hydrogen and sulphur isotopes: Geochimica et Cosmochimica Acta, v. 53, p. 3223–3237.
- Brimhall, G.H., Jr., and Ghiorso, M.S., 1983, Origin and ore-forming consequences of the advanced argillic alteration process in hypogene environments by magmatic gas contamination of meteoric fluids: Economic Geology, v. 78, p. 73–90.
- Browne, P.R.L., 1971, Petrological logs of Broadlands drillholes BR1 to BR25: New Zealand Geological Survey Report 52, 86 p.
- 1978, Hydrothermal alteration in active geothermal fields: Annual Review of Earth and Planetary Sciences, v. 6, p. 229–250.
- Buchanan, L.J., 1979, The Las Torres mine, Guanajuato, Mexico: Ore controls of a fossil geothermal system, Unpublished Ph.D. thesis, Golden, Colorado, Colorado School of Mines, 138 p.
- 1981, Precious metal deposits associated with volcanic environments in the southwest: Arizona Geological Society Digest, v. 14, p. 237–261.
- Burbank, W.S., 1950, Problems of wall-rock alteration in shallow volcanic environments: Colorado School of Mines Quarterly, v. 45, p. 287–319.
- Burrows, D.R., Remison, M., Burt, D., and Davies, R., 2020, The Onto Cu-Au discovery, eastern Sumbawa, Indonesia: A large middle Pleistocene lithocap-hosted high-sulfidation covellite-pyrite porphyry deposit: Economic Geology, v. 115, p. 1385–1412.
- Calder, M.F., Chang, Z., Arribas, A., Gaibor, A., Dunkley, P., Pastoral, J., Kouzmanov, K., Spandler, C., and Hedenquist, J.W., in press, High-grade copper and gold deposited during post-potassic chlorite-white mica-albite stage in the Far Southeast porphyry deposit, Philippines: Economic Geology.
- Cañada Guerrero, F., 1974, El yacimiento de alunite de Negredo (Segovia). Consideraciones sobre su genesis: Boletín Geológico y Minero, v. 85-4, p. 430–435.
- Carman, G., 2003, Geology, mineralisation and hydrothermal evolution of the Ladolam gold deposit, Lihir Island, Papua New Guinea: Society of Economic Geologists, Special Publication 10, p. 247–284.
- Cerpa, L.M., Bissig, T., Kyser, K., McEwan, C., Macassi, A., and Rios, H.W., 2013, Lithologic controls on mineralization at the Lagunas Norte high-sulfidation epithermal gold deposit, northern Peru: Mineralium Deposita, v. 48, p. 653–673.
- Chang, Z., Hedenquist, J.W., White, N.C., Cooke, D.R., Roach, M., Deyell, C.L., Garcia, J., Jr., Gemmell, J.B., McKnight, S., and Cuison, A.L., 2011, Exploration tools for linked porphyry and epithermal deposits: Example from the Mankayan intrusion-centered Cu-Au district, Luzon, Philippines: Economic Geology, v. 106, p. 1365–1398.
- Chouinard, A., Williams-Jones, A.E., Leonardson, R.W., Hodgson, C.J., Silva, P., Téllez, C., Vega, J., and Rojas, F., 2005, Geology and genesis of the multistage high-sulfidation epithermal Pascua Au-Ag-Cu deposit, Chile and Argentina: Economic Geology, v. 100, p. 463–490.
- Coolbaugh, M.F., Pace, D., Craig, L.D., Bedell, R.L., and Miller, M.S., 2020, The Silicon gold project, Nye County, Nevada: Prospect generation methods leading to initial recognition, acquisition, and characterization, in Koutz, F.R., and Pennell, W.M., eds., Vision for discovery. Geology and ore deposits of the Great Basin, v. 2: Reno, Nevada, Geological Society of Nevada, p. 1027–1041.
- Cuffney, R.G., 2008, Technical report on the Rosebud property, Pershing County, Nevada, USA: Canadian National Instrument 43-101 Report, September 10, 2008, 52 p., www.sedar.com.
- Davies, A.G.S., Cooke, D.R., Gemmell, J.B., van Leeuwen, T., Cesare, P., and Hartshorn, G., 2008, Hydrothermal breccias and veins at the Kelian gold mine, Kalimantan, Indonesia: Genesis of a large epithermal gold deposit: Economic Geology, v. 103, p. 717–757.
- Davies, R.M., and Ballantyne, G.H., 1987, Geology of the Ladolam gold deposit, Lihir Island, Papua New Guinea: Pacific Rim Congress 87, Australasian Institute of Mining and Metallurgy, Gold Coast, Australia, August 25–29, 1987, Proceedings, p. 943–949.
- Dekov, V.M., Rouxel, O., Kouzmanov, K., Bindi, L., Asael, D., Fouquet, Y., Etoubleau, J., Burgaud, G., and Wälle, M., 2016, Enargite-luzonite hydrothermal vents in Manus back-arc basin: Submarine analogues of high-sulfidation epithermal mineralization: Chemical Geology, v. 438, p. 36–57.
- Delmelle, P., and Bernard, A., 1994, Geochemistry, mineralogy, and chemical modelling of the acid crater lake of Kawah Ijen volcano, Indonesia: Geochimica et Cosmochimica Acta, v. 58, p. 2445–2460.
- 2015, The remarkable chemistry of sulfur in acid crater lakes: A scientific tribute to Bokuichiro Takano and Minoru Kusakabe, in Rouwet, D., Christenson, B., Tassi, F., and Vandemeulebrouck, J., eds., Volcanic lakes: Advances in volcanology: Heidelberg, Springer, p. 239–259.
- Delmelle, P., Bernard, A., Kusakabe, M., Fischer, T.P., and Takano, B., 2000, Geochemistry of the magmatic-hydrothermal system of Kawah Ijen volcano, East Java, Indonesia: Journal of Volcanology and Geothermal Research, v. 97, no. 1–4, p. 31–53.
- de Ronde, C.E.J., 1995, Fluid chemistry and isotopic characteristics of sea-floor hydrothermal systems and associated VMS deposits: Potential for magmatic contributions: Mineralogical Association of Canada Short Course Series, v. 23, p. 479–509.
- de Ronde, C.E.J., Massoth, G.J., Baker, E.T., and Lupton, J.E., 2003, Submarine hydrothermal venting related to volcanic arcs: Society of Economic Geologists Special Publication 10, p. 91–110.
- de Ronde, C.E.J., Humphris, S.E., Höfig, T.W., Reyes, A.G., and the IODP Expedition 376 Scientists, 2019, Critical role of caldera collapse in the


- formation of seafloor mineralization: The case of Brothers volcano: *Geology*, v. 47, p. 762–766.
- Deyell, C.L., Leonardson, R., Rye, R.O., Thompson, J.F.H., Bissig, T., and Cooke, D.R., 2005, Alunite in the Pascua-Lama high-sulfidation deposit: Constraints on alteration and ore deposition using stable isotope geochemistry: *Economic Geology*, v. 100, p. 131–148.
- Dubé, B., Mercier-Langevin, P., Hannington, M.D., Lafrance, B., Gosselin, P., and Gosselin, G., 2007, The LaRonde Penna world-class Au-rich volcanogenic massive sulfide deposit, Abitibi, Québec: Mineralogy and geochemistry of alteration and implications for genesis and exploration: *Economic Geology*, v. 102, p. 633–666.
- Dubé, B., Mercier-Langevin, P., Kjarsgaard, I., Hannington, M., Bécu, V., Côté, J., Moorhead, J., Legault, M., and Bédard, N., 2014, The Bousquet 2-Dumagami world-class Archean Au-rich volcanogenic massive sulfide deposit, Abitibi, Quebec: Metamorphosed submarine advanced argillic alteration footprint and genesis: *Economic Geology*, v. 109, p. 121–166.
- Ebert, S.W., and Rye, R.O., 1997, Secondary precious metal enrichment by steam-heated fluids in the Crofoot-Lewis hot spring gold-silver deposit and relation to paleoclimate: *Economic Geology*, v. 92, p. 578–600.
- Eilu, P., Sorjonen-Ward, P., Nurmi, P., and Niiranen, T., 2003, A review of gold mineralization styles in Finland: *Economic Geology*, v. 98, p. 1329–1353.
- Einaudi, M.T., Hedenquist, J.W., and Inan, E.E., 2003, Sulfidation state of fluids in active and extinct hydrothermal systems: Transitions from porphyry to epithermal environments: *Society of Economic Geologists Special Publication 10*, p. 285–313.
- Ellis, A.J., and Mahon, W.A.J., 1977, *Chemistry and geothermal systems*: New York, Academic Press, 392 p.
- Embley, R.W., de Ronde, C.E.J., and Ishibashi, J., 2008, Introduction to special section on active magmatic, tectonic, and hydrothermal processes at intraoceanic arc submarine volcanoes: *Journal of Geophysical Research*, v. 113, 6 p., doi: 10.1029/2008JB005871.
- Emmons, W.H., 1917, The enrichment of ore deposits: *U.S. Geological Survey Bulletin* 625, 530 p.
- Enders, M.S., Knickerbocker, C., Titley, S.R., and Southam, G., 2006, The role of bacteria in the supergene environment of the Morenci porphyry copper deposit, Greenlee County, Arizona: *Economic Geology*, v. 101, p. 59–70.
- Field, C.W., 1966, Sulfur isotopic method for discriminating between sulfates of hypogene and supergene origin: *Economic Geology*, v. 61, p. 1428–1435.
- Fifarek, R.H., and Rye, R.O., 2005, Stable-isotope geochemistry of the Pinar high-sulfidation Au-Ag deposit, Peru: Influence of hydrodynamics on SO_4^{2-} - H_2S sulfur isotopic exchange in magmatic-steam and steam-heated environments: *Chemical Geology*, v. 215, p. 253–279.
- Fischl, P., Morozov, S., Mamatysupov, V., Halley, S., Tellez, C., and Thomson, B., 2013, Kupol low-sulfidation epithermal vein district, Russian Federation: Integration of exploration datasets to understand post-mineral disruption of the vein-alteration system [abs.]: SEG 2013: Geoscience for Discovery, Society of Economic Geologists, Whistler, British Columbia, September 24–27, 2013, Proceedings.
- Fouquet, Y., von Stackelberg, U., Charlou, J.L., Erzinger, J., Herzig, P.M., Muhe, R., and Wiedicke, M., 1993, Metallogenesis in back-arc environments: The Lau basin example: *Economic Geology*, v. 88, p. 2154–2181.
- Fournier, R.O., 1985, The behavior of silica in hydrothermal solutions: *Reviews in Economic Geology*, v. 2, p. 45–60.
- Fournier, R.O., and Rowe, J.J., 1962, The solubility of cristobalite along the three-phase curve, gas plus liquid plus cristobalite: *American Mineralogist*, v. 47, p. 897–902.
- Fowler, A.P.G., Chunyang Tan, C., Cino, C., Scheuermann, P., Volk, M.W.R., Shanks III, W.C.P., and Seyfried, W.E., Jr., 2019, Vapor-driven sublacustrine vents in Yellowstone Lake, Wyoming, USA: *Geology*, v. 47, p. 223–226.
- Franchini, M., Impiccini, A., Lentz, D., Ríos, F.J., O'Leary, S., Pons, J., and Schalamuk, A.I., 2011, Porphyry to epithermal transition in the Agua Rica polymetallic deposit, Catamarca, Argentina: An integrated petrologic analysis of ore and alteration parageneses: *Ore Geology Reviews*, v. 41, p. 49–74.
- Gamo, T., Okamura, K., Charlou, J.L., Urabe, T., Auzende, J.M., Ishibashi, J., Shitashima, K., and Chiba, H., 1997, Acidic and sulfate-rich hydrothermal fluids from the Manus back-arc basin, Papua New Guinea: *Geology*, v. 25, p. 139–142.
- Garcia, J.S., Jr., 1991, *Geology and mineralization characteristics of the Mankayan mineral district, Philippines*: Geological Survey of Japan, Tsukuba, Report 277, p. 21–30.
- Garcia, W.V., 2009, *Geology of the Milagros project, Alto Chicama district, La Libertad, Peru*: M.Sc. thesis, Golden, Colorado, Colorado School of Mines, 145 p.
- Garwin, S., 2002, Ore geology setting of intrusion-related hydrothermal systems near Batu Hijau porphyry copper-gold deposit, Sumbawa, Indonesia: *Society of Economic Geologists Special Publication 9*, p. 333–366.
- Garwin, S., Whistler, B., Ward, J., Mather, N., Rohrlach, B., Vaca, S., Silva, J., Rosero, B., Cruz, A., Diaz, C., Chafra, A., Mantilla, S., Aguilar, L., and Guachamin, A., 2017, Alpala: The discovery and geology of a world-class porphyry copper-gold deposit in the Cascabel project of northern Ecuador: *NewGenGold 2017: Case Histories of Discovery*, Perth, 2017, Proceedings, p. 235–254.
- Giggenbach, W.F., 1980, Geothermal gas equilibria: *Geochimica et Cosmochimica Acta*, v. 44, p. 2021–2032.
- 1987, Redox processes governing the chemistry of fumarolic gas discharges from White Island, New Zealand: *Applied Geochemistry*, v. 2, p. 143–161.
- 1992a, Magma degassing and mineral deposition in hydrothermal systems along convergent plate boundaries: *Economic Geology*, v. 87, p. 1927–1944.
- 1992b, Isotopic shifts in waters from geothermal and volcanic systems along convergent plate boundaries and their origin: *Earth and Planetary Science Letters*, v. 113, p. 495–510.
- 1997, The origin and evolution of fluids in magmatic-hydrothermal systems, in Barnes, H.L., ed., *Geochemistry of hydrothermal ore deposits*, 3rd ed.: New York, Wiley, p. 737–796.
- Giggenbach, W.F., and Glasby, C.P., 1977, Influence of thermal activity on the trace metal distribution in marine sediments around White Island, New Zealand: *New Zealand DSIR Bulletin*, v. 218, p. 121–126.
- Giggenbach, W.F., Shinohara, H., Kusakabe, M., and Ohba, T., 2003, Formation of acid volcanic brines through interaction of magmatic gases, seawater, and rock within the White Island volcanic-hydrothermal system, New Zealand: *Society of Economic Geologists Special Publication 10*, p. 19–40.
- Gray, J.E., and Coolbaugh, M.F., 1994, *Geology and geochemistry of Summitville, Colorado: An epithermal acid sulfate deposit in a volcanic dome*: *Economic Geology*, v. 89, p. 1906–1923.
- Gregory, M.J., 2017, A fluid inclusion and stable isotope study of the Pebble porphyry copper-gold-molybdenum deposit, Alaska: *Ore Geology Reviews*, v. 80, p. 1279–1303.
- Gregory, M.J., Lang, J.R., Gilbert, S., and Hoal, K.O., 2013, Geometallurgy of the Pebble porphyry copper-gold-molybdenum deposit, Alaska: Implications for gold distribution and paragenesis: *Economic Geology*, v. 108, p. 463–482.
- Gunnarsson, I., and Arnórsson, S., 2000, Amorphous silica solubility and the thermodynamic properties of $\text{H}_4\text{SiO}_4^\circ$ in the range of 0° to 350°C at Psat: *Geochimica et Cosmochimica Acta*, v. 64, p. 2295–2307.
- Gustafson, L.B., and Hunt, J.P., 1975, The porphyry copper deposit at El Salvador, Chile: *Economic Geology*, v. 70, p. 857–912.
- Gustafson, L.B., Orquera, W., McWilliams, M., Castro, M., Olivares, O., Rojas, G., Maluenda, J., and Mendez, M., 2001, Multiple centers of mineralization in the Indio Muerto district, El Salvador, Chile: *Economic Geology*, v. 96, p. 325–350.
- Gustafson, L.B., Vidal, C.E., Pinto, R., and Noble, D.C., 2004, Porphyry-epithermal transition, Cajamarca region, northern Peru: *Society of Economic Geologists Special Publication 11*, p. 279–300.
- Hallberg, A., 1994, The Enåsen gold deposit, central Sweden. 1. A Paleoproterozoic high sulphidation epithermal gold mineralization: *Mineralium Deposita*, v. 29, p. 150–162.
- Hamasaki, S., 2002, Volcanic-related alteration and geochemistry of Iwodake volcano, Satsuma Iwojima, Kyushu, SW Japan, in Shinohara, H., Iguchi, M., Hedenquist, J.W., and Koyaguchi, T., eds., *Satsuma-Iwojima: Continuous degassing of a rhyolitic volcano*, *Earth Planets Space*, v. 54, p. 217–229.
- Hamilton, A.R., Campbell, K.A., Rowland, J.V., Barker, S., and Guido, D.M., 2019, Fossilized geothermal surface features of the Whitianga volcanic centre (Miocene), Coromandel volcanic zone, New Zealand: Controls and characteristics: *Journal of Volcanology and Geothermal Research*, v. 381, p. 209–226.
- Hannington, M.D., Poulsen, K.H., Thompson, J.F.H., and Sillitoe, R.H., 1999, Volcanogenic gold in the massive sulfide environment: *Reviews in Economic Geology*, v. 8, p. 319–350.
- Hannington, M.D., de Ronde, C.E.J., and Petersen, S., 2005, Modern seafloor tectonics and submarine hydrothermal systems: *Economic Geology 100th Anniversary Volume*, p. 111–141.
- Harvey, B.A., Myers, S.A., and Klein, T., 1999, Yanacocha gold district, northern Peru, in Weber, G., ed., *Pacrim '99 Congress*, Bali, Indonesia, 1999, Proceedings: Parkville, Victoria, The Australasian Institute of Mining and Metallurgy, p. 445–459.

- Hayba, D.O., Bethke, P.M., Heald, P., and Foley, N.F., 1986, Geologic, mineralogic, and geochemical characteristics of volcanic-hosted epithermal precious-metal deposits: *Reviews in Economic Geology*, v. 2, p. 129–167.
- Heald, P., Foley, N.K., and Hayba, D.O., 1987, Comparative anatomy of volcanic-hosted epithermal deposits: Acid sulfate and adularia-sericite types: *Economic Geology*, v. 82, p. 1–26.
- Hedenquist, J.W., 1983, Waiotapu, New Zealand: The geochemical evolution and mineralization of an active hydrothermal system: Unpublished Ph.D. dissertation, Auckland, New Zealand, University of Auckland, 242 p.
- 1986, Geothermal systems of the Taupo Volcanic Zone, New Zealand: Their characteristics and relation to volcanism and mineralization: *Royal Society of New Zealand Bulletin*, v. 23, p. 134–168.
- 1990, The thermal and geochemical structure of the Broadlands-Ohaaki geothermal system, New Zealand: *Geothermics*, v. 19, p. 151–185.
- 1991, Boiling and dilution in the shallow portion of the Waiotapu geothermal system, New Zealand: *Geochimica et Cosmochimica Acta*, v. 55, p. 2753–2765.
- 1995, The ascent of magmatic fluid: Discharge versus mineralization: *Mineralogical Association of Canada Short Course Series*, v. 23, p. 263–289.
- Hedenquist, J.W., and Henley, R.W., 1985, Hydrothermal eruptions in the Waiotapu geothermal system, New Zealand: Their origin, associated breccias, and relation to precious metal mineralization: *Economic Geology*, v. 80, p. 1640–1668.
- Hedenquist, J.W., and Richards, J.P., 1998, The influence of geochemical techniques on the development of genetic models for porphyry copper deposits: *Reviews in Economic Geology*, v. 10, p. 235–256.
- Hedenquist, J.W., and Stewart, M.K., 1985, Natural CO₂-rich steam-heated waters at Broadlands, New Zealand: Their chemistry, distribution and corrosive nature, *Transactions—Geothermal Resources Council*, v. 9, p. 245–250.
- Hedenquist, J.W., and Taran, Y.A., 2013, Modeling the formation of advanced argillic lithocaps: Volcanic vapor condensation above porphyry intrusions. *Economic Geology*, v. 108, p. 1523–1540.
- Hedenquist, J.W., Aoki, M., and Shinohara, H., 1994a, Flux of volatiles and ore-forming metals from the magmatic-hydrothermal system of Satsuma Iwojima volcano: *Geology*, v. 22, p. 585–588.
- Hedenquist, J.W., Matsuhisa, Y., Izawa, E., White, N.C., Giggenbach, W.F., and Aoki, M., 1994b, Geology, geochemistry, and origin of high sulfidation Cu-Au mineralization in the Nansatsu district, Japan: *Economic Geology*, v. 89, p. 1–30.
- Hedenquist, J.W., Arribas, A., and Reynolds, T.J., 1998, Evolution of an intrusion-centered hydrothermal system: Far Southeast-Lepanto porphyry and epithermal Cu-Au deposits, Philippines: *Economic Geology*, v. 93, p. 373–404.
- Hedenquist, J.W., Arribas, A., Jr., and Gonzalez-Urien, E., 2000, Exploration for epithermal gold deposits: *Reviews in Economic Geology*, v. 13, p. 245–277.
- Hedenquist, J.W., Arribas, A., and Aoki, M., 2017, Zonation of sulfate and sulfide minerals and isotopic composition in the Far Southeast porphyry and Lepanto epithermal Cu-Au deposits, Philippines: *Resource Geology*, v. 67, p. 174–196.
- Hedenquist, J.W., Taguchi, S., and Shinohara, H., 2018, Features of large magmatic-hydrothermal systems in Japan: Characteristics similar to the tops of porphyry copper deposits: *Resource Geology*, v. 68, p. 164–180.
- Hedenquist, J.W., Watanabe, Y., and Arribas, A., 2020, Hypogene alunite from the El Salvador district, Chile, indicates potential for a blind porphyry copper center: *Economic Geology*, v. 115, p. 231–239.
- Hemley, J.J., 1959, Some mineralogical equilibria in the system K₂O-Al₂O₃-SiO₂-H₂O: *American Journal of Science*, v. 257, p. 241–270.
- Hemley, J.J., and Hunt, J.P., 1992, Hydrothermal ore-forming processes in the light of studies in rock-buffered systems: II. Some general geologic applications: *Economic Geology*, v. 87, p. 23–43.
- Hemley, J.J., and Jones, W.R., 1964, Chemical aspects of hydrothermal alteration with emphasis on hydrogen metasomatism: *Economic Geology*, v. 59, p. 538–569.
- Hemley, J.J., Hostetler, P.B., Gude, A.J., and Mountjoy, W.T., 1969, Some stability relations of alunite: *Economic Geology*, v. 64, p. 599–612.
- Hemley, J.J., Montoya, J.W., Marinenko, J.W., and Luce, R.W., 1980, Equilibria in the system Al₂O₃-SiO₂-H₂O and some general implications for alteration/mineralization processes: *Economic Geology*, v. 75, p. 210–228.
- Henley, R.W., and Ellis, A.J., 1983, Geothermal systems, ancient and modern: A geochemical review: *Earth-Science Reviews*, v. 19, p. 1–50.
- Henley, R.W., and McNabb, A., 1978, Magmatic vapor plumes and ground-water interaction in porphyry copper emplacement: *Economic Geology*, v. 73, p. 1–20.
- Henley, R.W., and Stewart, M.K., 1983, Chemical and isotopic changes in the hydrology of the Tauhara geothermal field due to exploitation at Wairakei: *Journal of Volcanology and Geothermal Research*, v. 15, p. 285–314.
- Hervé, M., Sillitoe, R.H., Wong, C., Fernández, P., Crignola, F., Ipinza, M., and Urzúa, F., 2012, Geologic overview of the Escondida porphyry copper district, northern Chile: *Society of Economic Geologists Special Publication* 16, p. 55–78.
- Herzig, P.M., Hannington, M.D., Fouquet, Y., von Stackelberg, U., and Petersen, S., 1993, Gold-rich polymetallic sulfides from the Lau back arc and implications for the geochemistry of gold in sea-floor hydrothermal systems of the southwest Pacific: *Economic Geology*, v. 88, p. 2182–2209.
- Herzig, P.M., Hannington, M., and Arribas, A., 1998, Sulfur isotopic composition of hydrothermal precipitates from the Lau back-arc: Magmatic contributions to seafloor systems: *Mineralium Deposita*, v. 33, p. 226–237.
- Hnedkovsky, L., Wood, R.H., and Balashov, V.N., 2005, Electrical conductances of aqueous Na₂SO₄, H₂SO₄, and their mixtures: Limiting equivalent ion conductances, dissociation constants, and speciation to 673 K and 28 MPa: *Physical Chemistry B*, v. 109, p. 9034–9046.
- Holland, H.D., 1959, Stability relations among the oxides, sulfides, sulfates and carbonates of ore and gangue metals. Part I: Some applications of thermochemical data to problems of ore deposits: *Economic Geology*, v. 54, p. 184–233.
- Horton, D.G., 1985, Mixed-layer illite/smectite as a paleotemperature indicator in the Amethyst vein system, Creede district, Colorado, USA: *Contributions to Mineralogy and Petrology*, v. 91, p. 171–179.
- Hudson, D.M., 2003, Epithermal alteration and mineralization in the Comstock district, Nevada: *Economic Geology*, v. 98, p. 367–385.
- Hudson, D.M., Castor, S.B., Garside, L.J., and Henry, C.D., 2009, Geologic map of the Virginia City Quadrangle, Washoe, Storey and Lyon Counties and Carson City, Nevada: Nevada Bureau of Mines and Geology Map 165, scale 1:24,000, www.nbmng.unr.edu/dox/m165.pdf.
- Hurwitz, S., Lowenstern, J.B., and Heasler, H., 2007, Spatial and temporal geochemical trends in the hydrothermal system of Yellowstone National Park: Inferences from river solute fluxes: *Journal of Volcanology and Geothermal Research*, v. 162, p. 149–171.
- Illanes, J.L., Peralta, C., and Fuentes, M., 2005, Purén discovery: A high sulfidation system in the Maricunga belt, Northern Chile: *NewGenGold 2005: Case Histories of Discovery*, Perth, Australia, November 2005, Proceedings, p. 135–150.
- Inan, E.E., and Einaudi, M.T., 2002, Nukundamite (Cu_{3.38}Fe_{0.62}S₄)-bearing copper ore in the Bingham porphyry deposit, Utah: Result of upflow through quartzite: *Economic Geology*, v. 97, p. 499–515.
- Iwasaki, I., and Ozawa, T., 1960, Genesis of sulfate in acid hot spring: *Bulletin of the Chemical Society of Japan*, v. 33, p. 1018–1019.
- Jannas, R.R., Bowers, T.S., Petersen, U., and Beane, R.E., 1999, High-sulfidation deposit types in the El Indio district, Chile: *Society of Economic Geologists Special Publication* 7, p. 219–266.
- John, D.A., Lee, R.G., Breit, G.N., Dilles, J.H., Calvert, A.T., Muffler, L.J.P., and Clynne, M.A., 2019, Pleistocene hydrothermal activity on Brokeoff volcano and in the Maidu volcanic center, Lassen Peak area, northeast California: Evolution of magmatic-hydrothermal systems on stratovolcanoes: *Geosphere*, v. 15, p. 946–982.
- Jones, D., Barreno, J.E., Pérez, P., Naranjo, G., Viera, F., and Camino, M., 2005, The high sulphidation Quimsacocha deposit, Ecuador: *NewGenGold 2005: Case Histories of Discovery*, Perth, Australia, November 2005, Proceedings, p. 117–134.
- Khashgerel, B.-E., Rye, R.O., Hedenquist, J.W., and Kavalieris, I., 2006, Geology and reconnaissance stable isotope study of the Oyu Tolgoi porphyry Cu-Au system, South Gobi, Mongolia: *Economic Geology*, v. 101, p. 503–522.
- Khashgerel, B.-E., Rye, R.O., Kavalieris, I., and Hayashi, K.-I., 2009, The sericitic to advanced argillic transition: Stable isotope and mineralogical characteristics from the Hugo Dummett porphyry Cu-Au deposit, Oyu Tolgoi district, Mongolia: *Economic Geology*, v. 104, p. 1087–1110.
- King, J., Williams-Jones, A.E., van Hinsberg, V., and Williams-Jones, G., 2014, High-sulfidation epithermal pyrite-hosted Au (Ag-Cu) ore formation by condensed magmatic vapors on Sangihe Island, Indonesia: *Economic Geology*, v. 109, p. 1705–1733.

- Kinross Gold Corporation, 2020, Kinross provides update on development projects and full-year 2019 exploration results: News Release, February 12, 2020, 22 p., https://s2.q4cdn.com/496390694/files/doc_financials/2019/q4/KGC-2019-LC-Projects-Exploration-ReservesResources-Final.pdf.
- Klein, T., Barreda, J., and Harvey, B., 1997, Sur Jose Sur high-sulfidation gold deposit, Yanacocha district, northern Peru, in Macharé, J., Cánepa, C., and Injoke, J., eds., IX Congreso Peruano de Geología, Resúmenes Extendidos [ext. abs.]: Lima, Sociedad Geológica del Perú, Vol. Especial 1, p. 57–60.
- Kreiner, D.C., and Barton, M.D., 2017, Sulfur-poor intense acid hydrothermal alteration: A distinctive hydrothermal environment: *Ore Geology Reviews*, v. 88, p. 174–187.
- Kusakabe, M., and Komoda, Y., 1992, Sulfur isotopic effects in the disproportionation reaction of sulfur dioxide at hydrothermal temperatures: *Geological Survey of Japan Report* 279, p. 93–96.
- Kusakabe, M., Hayashi, N., and Kobayashi, T., 1986, Genetic environments of the banded sulfur sediments at the Tateyama volcano, Japan: *Journal of Geophysical Research*, v. 91, p. 12,159–12,166.
- Kusakabe, M., Komoda, Y., Takano, B., and Abiko, T., 2000, Sulfur isotopic effects in the disproportionation reaction of sulfur dioxide in hydrothermal fluids: Implications for the $\delta^{34}\text{S}$ variations of dissolved bisulfate and elemental sulfur from active crater lakes: *Journal of Volcanology and Geothermal Research*, v. 97, p. 287–307.
- Larson, P.B., Phillips, A., John, D., Cosca, M., Pritchard, C., Andersen, A., and Manion, J., 2009, Older hot spring alteration in Sevenmile Hole, Grand Canyon of the Yellowstone River, Yellowstone caldera, Wyoming: *Journal of Volcanology and Geothermal Research*, v. 188, p. 225–236.
- Leary, S., Sillitoe, R.H., Stewart, P.W., Roa, K.J., and Nicolson, B.E., 2016, Discovery, geology, and origin of the Fruta del Norte epithermal gold-silver deposit, southeastern Ecuador: *Economic Geology*, v. 111, p. 1043–1072.
- Leys, C., Schwarz, A., Cloos, M., Widodo, S., Kyle, J.R., and Sirait, J., 2019, Grasberg copper-gold-(molybdenum) deposit: Product of two overlapping porphyry systems: *Society of Economic Geologists Special Publication* 23, p. 599–620.
- Lipske, J.L., 2002, Advanced argillic and sericitic alteration in the subvolcanic environment of the Yerington porphyry copper system, Buckskin Range, Nevada: M.Sc. thesis, Oregon State University, 124 p. plus 3 plates.
- Longo, A.A., Dilles, J.H., Grunder, A.L., and Duncan, R., 2010, Evolution of calco-alkaline volcanism and associated hydrothermal gold deposits at Yanacocha, Peru: *Economic Geology*, v. 105, p. 1191–1241.
- Mars, J.C., Robinson, G.R., Hammarstrom, J.M., Zürcher, L., Whitney, H., Solano, F., Gettings, M., and Ludington, S., 2019, Porphyry copper potential of the United States Southern Basin and Range using ASTER data integrated with geochemical and geologic datasets to assess potential near-surface deposits in well-explored permissive tracts: *Economic Geology*, v. 114, p. 1095–1121.
- Marumo, K., 1989, Genesis of kaolin minerals and pyrophyllite in Kuroko deposits of Japan: Implications for the origin of the hydrothermal fluids from mineralogical and stable isotope data: *Geochimica et Cosmochimica Acta*, v. 53, p. 2915–2924.
- Marumo, K., and Hattori, K., 1999, Seafloor hydrothermal clay alteration at Jade in the back-arc Okinawa trough: *Mineralogy, geochemistry and isotope characteristics: Geochimica et Cosmochimica Acta*, v. 63, p. 2785–2803.
- Matos, J.X., Barriga, F.J.A.S., and Oliveira, V.M.J., 2003, Alunite veins versus supergene kaolinite/halloysite alteration in the Lagoa Salgada, Algaesand S. João (Aljustrel) and S. Domingo massive sulphide deposits, Iberian pyrite belt, Portugal: *Ciências da Terra (UNL)*, Lisboa, v. 5, p. B56–B59.
- Megaw, P.K.M., 2010, Discovery of the silver-rich Juanicipio-Valdecañas vein zone, western Fresnillo district, Zacatecas, Mexico: *Society of Economic Geologists, Special Publication* 15, p. 119–132.
- Mercier-Langevin, P., Hannington, M.D., Dubé, B., and Bécu, V., 2011, The gold content of volcanogenic massive sulphide deposits: *Mineralium Deposita*, v. 46, p. 509–539.
- Mercier-Langevin, P., Hannington, M.D., Dubé, B., Piercey, S.J., Peter, J.M., and Pehrsson, S.J., 2015, Precious metal enrichment processes in volcanogenic massive sulphide deposits—a summary of key features, with an emphasis on TIGI-4 research contributions: *Geological Survey of Canada, Open File* 7853, p. 117–130.
- Merriman, R.J., and Frey, M., 1999, Patterns of very low-grade metamorphism in metapelitic rocks, in Frey, M., and Robinson, D., eds., *Low-grade metamorphism*: Oxford, Blackwell Science Ltd., 313 p.
- Meyer, C., and Hemley, J.J., 1967, Wallrock alteration, in Barnes, H.L., ed., *Geochemistry of hydrothermal ore deposits*: New York, Holt, Rinehart and Wilson, p. 166–235.
- Mielke, R.E., Pace, D.L., Porter, T., and Southam, G., 2003, A critical stage in the formation of acid mine drainage: Colonization of pyrite by *Acidithiobacillus ferrooxidans* under pH-neutral conditions: *Geobiology*, v. 1, p. 81–90.
- Montoya, J.W., and Hemley, J.J., 1975, Activity relations and stabilities in alkali feldspar and mica alteration reactions: *Economic Geology*, v. 70, p. 577–583.
- Nakovnik, N.I., 1934, Kounrad and its secondary quartzites: *Problemy sovetskoy geologii*, N4, p. 29–42 (in Russian).
- 1968, Secondary quartzites of the USSR and associated mineral deposits, 2nd ed.: Moscow, Nedra, 335 p. (in Russian).
- Nash, J.T., Utterback, W.C., and Trudel, W.S., 1995, Geology and geochemistry of Tertiary volcanic host rocks, Sleeper gold-silver deposit, Humboldt County, Nevada: *U.S. Geological Survey Bulletin* 2090, 63 p.
- Nordstrom, D.K., and Southam, G., 1997, Geomicrobiology of sulfide mineral oxidation: *Reviews in Mineralogy*, v. 35, p. 361–390.
- Nordstrom, D.K., McCleskey, R., and Ball, J.W., 2009, Sulfur geochemistry of hydrothermal waters in Yellowstone National Park: IV acid-sulfate waters: *Applied Geochemistry*, v. 24, p. 191–207.
- Oana, S., and Ishikawa, H., 1966, Sulfur isotopic fractionations between sulfur and sulfuric acid in the hydrothermal solutions of sulfur dioxide: *Geochemical Journal*, v. 1, p. 45–50.
- Ossandón, C.G., Fréaut, R.C., Gustafson, L.B., Lindsay, D.D., and Zentilli, M., 2001, Geology of the Chuquicamata mine: A progress report: *Economic Geology*, v. 96, p. 249–270.
- Padilla Garza, R.A., Titley, S.R., and Pimentel, F., 2001, Geology of the Escondida porphyry copper deposit, Antofagasta region, Chile: *Economic Geology*, v. 96, p. 307–324.
- Padilla-Garza, R.A., Titley, S.R., and Eastoe, C.J., 2004, Hypogene evolution of the Escondida porphyry copper deposit, Chile: *Society of Economic Geologists Special Publication* 11, p. 141–165.
- Penrose, R.A.F., Jr., 1894, The superficial alteration of ore deposits: *Journal of Geology*, v. 2, p. 288–317.
- Petersen, S., Herzig, P., Hannington, M., Jonhasson, I., and Arribas, A., 2002, Submarine gold mineralization near Lihir Island, New Ireland fore-arc, Papua New Guinea: *Economic Geology*, v. 97, p. 1795–1813.
- Pilco, R., and McCann, S., 2020, Gold deposits of the Yanacocha district, Cajamarca, Peru: *Society of Economic Geologist Special Publication* 23, p. 451–465.
- Pinto, R.M., 2002, Transición de un sistema de alta sulfuración a un sistema porfirítico de alto nivel en Kupfertal, Distrito Minero de Yanacocha, Cajamarca, Perú: Unpublished thesis, Ingeniero Geólogo de Perú, Universidad Nacional Mayor de San Marcos, 46 p.
- Poblete, J.A., Bissig, T., Mortensen, J.K., Gabites, J., Friedman, R., and Rodriguez, M., 2014, The Cerro Bayo district, Chilean Patagonia: Late Jurassic to Cretaceous magmatism and protracted history of epithermal Ag-Au mineralization: *Economic Geology*, v. 109, p. 487–502.
- Polyak, V.J., McIntosh, W.C., Provencio, P., and Güven, N., 1998, Age and origin of Carlsbad Caverns and related caves from $^{40}\text{Ar}/^{39}\text{Ar}$ of alunite: *Science*, v. 279, p. 1919–1922.
- Pope, J.G., McConchie, D., Clark, M.W., and Brown, K.L., 2004, Diurnal variations in the chemistry of geothermal fluids after discharge, Champagne Pool, Waiotapu, New Zealand: *Chemical Geology*, v. 203, p. 253–272.
- Power, J.F., Carere, C.R., Lee, C.K., Wakerley, G.L.J., Evans, D.W., Button, M., White, D., Climo, M.D., Hinze, A.M., Morgan, X.C., McDonald, I.R., Cary, S.C., and Stott, M.B., 2018, Microbial biogeography of 925 geothermal springs in New Zealand: *Nature Communications*, v. 9, article 2876, doi: 10.1038/s41467-018-05020-y.
- Quang, C.X., Clark, A.H., Lee, J.K.W., and Guillén, J., 2003, $^{40}\text{Ar}/^{39}\text{Ar}$ ages of hypogene and supergene mineralization in the Cerro Verde-Santa Rosa porphyry Cu-Mo cluster, Arequipa, Peru: *Economic Geology*, v. 98, p. 1683–1696.
- Rainbow, A., Clark, A.H., Kyser, T.K., Gaboury, F., and Hodgson, C.J., 2005, The Pierina epithermal Au-Ag deposit, Ancash, Peru: Paragenetic relationships, alunite textures, and stable-isotope geochemistry: *Chemical Geology*, v. 215, p. 235–252.
- Ransome, F.L., 1907, The association of alunite with gold in the Goldfield district, Nevada: *Economic Geology*, v. 2, p. 667–692.
- 1909, The geology and ore deposits of Goldfield, Nevada: *U.S. Geological Survey Professional Paper* 66, 259 p.
- Reyes, A.G., 1990, Petrology of Philippine geothermal systems and the application of alteration mineralogy to their assessment: *Journal of Volcanology and Geothermal Research*, v. 43, p. 279–309.

- Reyes, A.G., Giggenbach, W.F., Saleras, J.R.M., Salonga, N.D., and Vergara, M.C., 1993, Petrology and geochemistry of Alto Peak, a vapor-cored hydrothermal system, Leyte province, Philippines: *Geothermics*, v. 22, p. 479–519.
- Roedder, E., 1977, Changes in ore fluid with time, from fluid inclusion studies at Creede, Colorado: International Association on the Genesis of Ore Deposits (IAGOD) Symposium, 4th, Varna, Bulgaria, 1974, Proceedings, v. 2, p. 179–185.
- Ruggieri, G., Lattanzi, P., Luxoro, S.S., Dessi, R., Benvenuti, M., and Tanelli, G., 1997, Geology, mineralogy, and fluid inclusion data of the Furtei high-sulfidation gold deposit, Sardinia, Italy: *Economic Geology*, v. 92, p. 1–19.
- Rye, R.O., 2005, A review of the stable-isotope geochemistry of sulfate minerals in selected igneous environments and related hydrothermal systems: *Chemical Geology*, v. 215, p. 5–36.
- Rye, R.O., and Alpers, C.N., 1997, The stable isotope geochemistry of jarosite: U.S. Geological Survey Open-File 88–97, 28 p.
- Rye, R.O., Bethke, P.M., and Wasserman, M.D., 1992, The stable isotope geochemistry of acid sulfate alteration: *Economic Geology*, v. 87, p. 225–262.
- Sahlström, F., Dirks, P., Chang, Z., Arribas, A., Corral, I., Obiri-Yeboah, M., and Hall, C., 2018, The Paleozoic Mount Carlton deposit, Bowen basin, northeast Australia: Shallow high-sulfidation epithermal Au-Ag-Cu mineralization formed during rifting: *Economic Geology*, v. 113, p. 1733–1767.
- Sahlström, F., Chang, Z., Arribas, A., Dirks, P., Johnson, C.A., Huizenga, J.M., and Corral, I., 2020, Reconstruction of an early Permian, sublacustrine magmatic-hydrothermal system: Mount Carlton epithermal Au-Ag-Cu deposit, northeastern Australia: *Economic Geology*, v. 115, p. 129–152.
- Sakai, H., Gamo, T., Kim, E.S., Tsutsumi, M., Tanaka, T., Ishibashi, J., Wakita, H., Yamano, M., and Oomori, T., 1990, Venting of carbon dioxide-rich fluid and hydrate formation in Mid-Okinawa trough backarc basin: *Science*, v. 248, p. 1093–1096.
- Sales, R.H., and Meyer, C., 1949, Results from preliminary studies of vein formation at Butte, Montana: *Economic Geology*, v. 44, p. 465–484.
- Scher, S., Williams-Jones, A.E., and Williams-Jones, G., 2013, Fumarolic activity, acid-sulfate alteration, and high sulfidation epithermal precious metal mineralization in the crater of Kawah Ijen volcano, Java, Indonesia: *Economic Geology*, v. 108, p. 1099–1118.
- Schoen, R., 1969, Rate of sulfuric acid formation in Yellowstone National Park: *Geological Society of America Bulletin*, v. 80, p. 643–650.
- Schoen, R., White, D.E., and Hemley, J.J., 1974, Argillization by descending acid at Steamboat Springs, Nevada: *Clays and Clay Minerals*, v. 22, p. 1–22.
- Scotney, P.M., Roberts, S., Herrington, R.J., Boyce, A.J., and Burgess, R., 2005, The development of volcanic hosted massive sulfide and barite-gold orebodies on Wetar Island, Indonesia: *Mineralium Deposita*, v. 40, p. 76–99.
- Seedorf, E., Dilles, J.H., Proffett, J.M., Jr., Einaudi, M.T., Zurcher, L., Stavast, W.J.A., Johnson, D.A., and Barton, M.D., 2005, Porphyry deposits: Characteristics and origin of hypogene features: *Economic Geology* 100th Anniversary Volume, p. 251–298.
- Seewald, J.S., Reeves, E.P., Bach, W., Saccoccia, P.J., Craddock, P.R., Walsh, E., Shanks III, W.C., Sylva, S.P., Pichler, T., and Rosner, M., 2019, Geochemistry of hot-springs at the SuSu Knolls hydrothermal field, Eastern Manus basin: Advanced argillic alteration and vent fluid acidity: *Geochimica et Cosmochimica Acta*, v. 255, p. 25–48.
- Sherlock, R.L., Tosdal, R.M., Lehrman, N.J., Graney, J.R., Losh, S., Jowett, E.G., and Kesler, S.E., 1995, Origin of the McLaughlin mine sheeted vein complex: Metal zoning, fluid inclusion, and isotopic evidence: *Economic Geology*, v. 90, p. 2156–2181.
- Shinohara, H., Giggenbach, W.F., Kazahaya, K., Hedenquist, J.W., and Kusakabe, M., 1993, Geochemistry of volcanic gases and hot springs of Satsuma-Iwojima, Japan: *Following Matsuo: Geochemical Journal*, v. 27, p. 271–285.
- Shinohara, H., Kazahaya, K., Saito, G., Matsushima, N., and Kawanabe, Y., 2002, Satsuma-Iwojima volcano, Japan: Formation of a new degassing vent, 1990–1999: *Earth Planets Space*, v. 54, p. 175–185.
- Shinohara, H., Saito, G., Matsushima, G., Kawanabe, Y., Kazahaya, K., Urai, M., Nishi, Y., Saito, E., Hamasaki, S., Tomiya, A., Morikawa, N., Komazawa, M., and Yasuhara, M., 2008, Research on active volcanoes: Satsuma-Iwojima: Geological Survey of Japan, https://gbank.gsj.jp/volcano/Act_Vol/satsuma-iwojima/vr/index.html.
- Sillitoe, R.H., 1983, Enargite-bearing massive sulfide deposits high in porphyry copper systems: *Economic Geology*, v. 78, p. 348–352.
- 1993, Epithermal models: Genetic types, geometrical controls and shallow features: *Geological Association of Canada Special Paper* 40, p. 403–417.
- 1995a, Exploration of porphyry copper lithocaps: Pacrim Congress, Australasian Institute of Mining and Metallurgy, Auckland, 1995, Proceedings, p. 527–532.
- 1995b, Exploration and discovery of base- and precious metal deposits in the circum-Pacific region during the last 25 years: *Resource Geology Special Issue*, v. 19, 119 p.
- 1999, Styles of high-sulphidation gold, silver and copper mineralization in the porphyry and epithermal environments: Pacrim '99 Congress, Australasian Institute of Mining and Metallurgy, Bali, Indonesia, 1999, Proceedings, p. 29–44.
- 2005, Supergene oxidized and enriched porphyry copper and related deposits: *Economic Geology* 100th Anniversary Volume, p. 723–768.
- 2009, Supergene silver enrichment reassessed: *Society of Economic Geologists Special Publication* 14, p. 15–32.
- 2010, Porphyry copper systems: *Economic Geology*, v. 105, p. 3–41.
- 2015, Epithermal paleosurfaces: *Mineralium Deposita*, v. 50, p. 767–793.
- Sillitoe, R.H., and Hedenquist, J.W., 2003, Linkages between volcanotectonic settings, ore-fluid compositions, and epithermal precious metal deposits: *Society of Economic Geologists Special Publication* 10, p. 315–343.
- Sillitoe, R.H., and Lorson, R.C., 1994, Epithermal gold-silver-mercury deposits at Paradise Peak, Nevada: Ore controls, porphyry gold association, detachment faulting, and supergene oxidation: *Economic Geology*, v. 89, p. 1228–1248.
- Sillitoe, R.H., and McKee, E.H., 1996, Age of supergene oxidation and enrichment in the Chilean porphyry copper province: *Economic Geology*, v. 91, p. 164–179.
- Sillitoe, R.H., Hannington, M.D., and Thompson, J.F.H., 1996, High sulfidation deposits in the volcanogenic massive sulfide environment: *Economic Geology*, v. 91, p. 204–212.
- Sillitoe, R.H., Tolman, J., and Van Kerkvoort, G., 2013, Geology of the Caspi-ché porphyry gold-copper deposit, Maricunga belt, northern Chile: *Economic Geology*, v. 108, p. 585–604.
- Sillitoe, R.H., Burgoa, C., and Hopper, D.R., 2016, Porphyry copper discovery beneath the Valeriano lithocap, Chile: *Society of Economic Geologists, SEG Newsletter*, no. 106, p. 15–20.
- Simmons, S.F., 1991, Hydrologic implications of alteration and fluid inclusion studies in the Fresnillo district, Mexico: Evidence for a brine reservoir and a descending water table during the formation of hydrothermal Ag-Pb-Zn orebodies: *Economic Geology*, v. 86, p. 1579–1601.
- 2017, Proximal to distal hydrothermal alteration patterns around epithermal low-intermediate sulfidation vein deposits and their implications for precious metal exploration: *GNS Science Report* 2017/28, 38 p., doi: 10.21420/G2FW6C.
- Simmons, S.F., and Browne, P.R.L., 2000, Hydrothermal minerals and precious metals in the Broadlands-Ohaaki geothermal system: Implications for understanding low-sulfidation epithermal environments: *Economic Geology*, v. 95, p. 971–999.
- Simmons, S.F., Browne, P.R.L., and Scott, B.J., 2004, Geothermal systems, field trip 2: *Geological Society of New Zealand Miscellaneous Publication* 117B, 40 p.
- Simpson, M.P., and Christie, A.B., 2016, Exploration of New Zealand mineral deposits and geothermal systems using X-ray diffraction (XRD) and reflectance spectrometry (SWIR): A comparison of techniques: *GNS Science Report* 2016/61, 45 p., doi: 10.21420/G2NP4D.
- Simpson, M.P., and Rae, A.J., 2018, Short-wave infrared (SWIR) reflectance spectrometric characterisation of clays from geothermal systems of the Taupō Volcanic Zone, New Zealand: *Geothermics*, v. 73, p. 74–90.
- Singer, P.C., and Stumm, W., 1970, Acidic mine drainage: The rate-determining step: *Science*, v. 167, no. 3921, p. 1121–1123.
- Steiner, A., 1953, Hydrothermal rock alteration at Wairakei, New Zealand: *Economic Geology*, v. 48, p. 1–13.
- Steiner, A., and Rafter, T.A., 1966, Sulfur isotopes in pyrite, pyrrhotite, alunite and anhydrite from steam wells in the Taupo Volcanic Zone, New Zealand: *Economic Geology*, v. 61, p. 1115–1129.
- Steven, T.A., and Ratté, J.C., 1960, Geology and ore deposits of the Summitville district, San Juan Mountains, Colorado: U.S. Geological Survey Professional Paper 343, 70 p.
- Stoffregen, R., 1986, Observations on the behavior of gold during supergene oxidation at Summitville, Colorado, USA, and implications for electrum

- stability in the weathering environment: *Applied Geochemistry*, v. 1, p. 549–558.
- Stoffregen, R.E., 1987, Genesis of acid-sulfate alteration and Au-Cu-Ag mineralization at Summitville, Colorado: *Economic Geology*, v. 82, p. 1575–1591.
- 1993, Stability relations of jarosite and natrojarosite at 100–250°C: *Geochimica et Cosmochimica Acta*, v. 57, p. 2417–2429.
- Stoffregen, R.E., and Alpers, C.N., 1987, Woodhouseite and svanbergite in hydrothermal ore deposits: Products of apatite destruction during advanced argillic alteration: *The Canadian Mineralogist*, v. 25, p. 201–211.
- Stoffregen, R.E., and Cygan, G., 1990, An experimental study of Na-K exchange between alunite and aqueous sulfate solutions: *American Mineralogist*, v. 75, p. 209–220.
- Sverjensky, D.A., Hemley, J.J., and D'Angelo, W.M., 1991, Thermodynamic assessment of hydrothermal alkali feldspar-mica-aluminosilicate equilibria: *Geochimica et Cosmochimica Acta*, v. 55, p. 989–1004.
- Symonds, R.B., 1992, Getting the gold from the gas: How recent advances in volcanic-gas research have provided new insight on metal transport in magmatic fluids: *Geological Survey of Japan Report 279*, p. 170–175.
- Takano, B., Koshida, M., Fujiwara, Y., Sugimori, K., and Takayanagi, S., 1997, Influence of sulfur-oxidizing bacteria on the budget of sulfate in Yugama crater lake, Kusatsu-Shirane volcano, Japan: *Biogeochemistry*, v. 38, p. 227–253.
- Taran, Y.A., Hedenquist, J.W., Korzhinsky, M.A., Tkachenko, S.I., and Shmulovich, K.I., 1995, Geochemistry of magmatic gases from Kudryavsky volcano, Iturup, Kuril Islands: *Geochimica et Cosmochimica Acta*, v. 59, p. 1749–1761.
- Taran, Y.A., Zelenski, M., Chaplygin, I., Malik, N., Campion, R., Inguaggiato, S., Pokrovsky, B., Kalacheva, E., Melnikov, D., Kazahaya, R., and Fischer, T., 2018, Gas emissions from volcanoes of the Kuril island arc (NW Pacific): Geochemistry and fluxes: *Geochemistry, Geophysics, Geosystems*, doi: 10.1029/2018GC007477.
- Taylor, B.E., 1992, Degassing of H₂O from rhyolite magma during eruption and shallow intrusion, and the isotopic composition of magmatic water in hydrothermal systems: *Geological Survey of Japan Report 279*, p. 190–194.
- Thompson, A.J.B., Hauff, P.L., and Robitaille, A.J., 1999, Alteration mapping in exploration: Application of short-wave infrared (SWIR) spectroscopy: *Society of Economic Geologists, SEG Newsletter*, no. 39, p. 1, 16–27.
- Tornos, F., Velasco, F., Slack, J.F., Delgado, A., Gomez-Miguel, N., Escobar, J.M., and Gomez, C., 2017, The high-grade Las Cruces copper deposit, Spain: A product of secondary enrichment in an evolving basin: *Mineralium Deposita*, v. 52, p. 1–34.
- Turner, S.J., 1997, The Yanacocha epithermal gold deposits, northern Peru: High-sulfidation mineralization in a flow dome setting: Ph.D. thesis, Golden, Colorado, Colorado School of Mines, 341 p.
- Urashima, Y., Saito, M., and Sato, E., 1981, The Iwato gold ore deposits, Kagoshima Prefecture, Japan: *Society of Mining Geologists of Japan Special Issue 10*, p. 1–14 (in Japanese with English abs.).
- van de Kamp, P.C., 2008, Smectite-illite-muscovite transformations, quartz dissolution, and silica release in shales: *Clays and Clay Minerals*, v. 56, p. 66–81.
- Van Leeuwen, T.M., Leach, T., Hawke, A.A., and Hawke, M.M., 1990, The Kelian disseminated gold deposit, East Kalimantan, Indonesia: *Journal of Geochemical Exploration*, v. 15, p. 1–61.
- Wallace, A.B., 1987, Geology of the Sulphur district, southwestern Humboldt County, Nevada, in Johnson, J.L., ed., Bulk mineable precious metal mineralization of the western United States. Guidebook for field trips: Reno, Geological Society of Nevada, p. 165–171.
- Wallace, A.R., 2003, Geology of the Ivanhoe Hg-Au district, northern Nevada: Influence of Miocene volcanism, lakes, and active faulting on epithermal mineralization: *Economic Geology*, v. 98, p. 409–424.
- Warren, I., Archibald, D.A., and Simmons, S.F., 2008, Geochronology of epithermal Au-Ag mineralization, magmatic-hydrothermal alteration, and supergene weathering in the El Peñon district, northern Chile: *Economic Geology*, v. 103, p. 851–864.
- Wasserman, M.D., Rye, R.O., Bethke, P.M., and Arribas, A., Jr., 1992, Methods for separation and total stable isotope analysis of alunite: U.S. Geological Survey Open-File Report 92-9, 20 p.
- Watanabe, Y., and Hedenquist, J.W., 2001, Mineralogic and stable isotope zonation at the surface over the El Salvador porphyry copper deposit, Chile: *Economic Geology*, v. 96, p. 1775–1797.
- Webster, J.G., and Mann, A.W., 1984, The influence of climate, geomorphology and primary geology on the supergene migration of gold and silver: *Journal of Geochemical Exploration*, v. 22, p. 21–42.
- White, D.E., 1957, Thermal waters of volcanic origin: *Geological Society of America Bulletin*, v. 68, p. 1637–1658.
- Wilson, M.J., 2014, The structure of opal-CT revisited: *Journal of Non-Crystalline Solids*, v. 405, p. 68–75.
- Wood, C.P., 1983, Petrological logs of drillholes BR26 to BR40, Broadlands geothermal field: New Zealand Geological Survey Report 108, 49 p.
- Yakich, T.Yu., Ananyev, Y.S., Ruban, A.S., Gavrilov, R.Yu., Lesnyak, D.L., Levochskaya, D.V., Savinova, O.V., and Rudmin, M.A., 2021, Mineralogy of the Svetloye epithermal district, Okhotsk-Chukotka volcanic belt, and its insights for exploration: *Ore Geology Reviews*, v. 136, article 104257.
- Yildiz, B., Sillitoe, R., Foster, B., Hall, D., and Stallman, M., 2017, Öksüt: A high-sulphidation epithermal gold discovery in Turkey: *NewGenGold 2017: Case histories of discovery*, Perth, 2017, Proceedings, p. 273–287.
- Zelenski, M., Malik, N., and Taran, Y., 2014, Emissions of trace elements during the 2012–2013 effusive eruption of Tolbachik volcano, Kamchatka: Enrichment factors, partition coefficients and aerosol contribution: *Journal of Volcanology and Geothermal Research*, v. 285, p. 136–149.
- Zelenski, M., Kamenetsky, V.S., and Hedenquist, J.W., 2016, Gold recycling and enrichment beneath volcanoes: A case study of Tolbachik, Kamchatka: *Earth and Planetary Science Letters*, v. 437, p. 35–46.
- Zotov, A., Mukhamet-Galeev, A., and Schott, J., 1998, An experimental study of kaolinite and dickite relative stability at 150–300°C and the thermodynamic properties of dickite: *American Mineralogist*, v. 83, p. 516–524.



Antonio Arribas teaches at the Department of Earth, Environmental and Resource Sciences of The University of Texas at El Paso, where he is the inaugural holder of the Kenneth F. and Patricia Clark Distinguished Chair. Previously he taught at Akita University (Japan) and worked for two decades with the mineral exploration industry, including Vice President Geoscience (BHP), Senior Manager Geosciences (Newmont), and Exploration Manager South America (Placer Dome). Antonio conducts research in geology and geochemistry of mineral deposits and is also interested in the history and teaching of economic geology and exploration. His education includes the University of Salamanca, Spain (B.Sc., M.Sc.) and University of Michigan (Ph.D.).



Jeffrey Hedenquist conducted research with the Department of Scientific and Industrial Research—Chemistry Division in New Zealand and the Geological Survey of Japan for 10 years each on geothermal energy development and volcanic discharges, respectively, as well as the formation of epithermal gold and porphyry copper deposits. Since 1999 he has been an independent advisor to the mineral industry, governmental agencies, and the World Bank, providing assessments of hydrothermal gold and copper projects as well as training related to mineral exploration in over 40 countries. His education includes Macalester College (B.A.), The Johns Hopkins University (M.A.), and the University of Auckland (Ph.D.).

